Prediction of Energies of Spin States for First Row Transition Metal Complexes: DFT vs Ligand Field Theory

Samuel Mace, Ben Grace, Alister Goodfellow, Martin A. Bates, Maclolm A. Halcrow, Paul H. Walton,* Yingjian Xu, Bao N. Nguyen*

E-mail: paul.walton@york.ac.uk;b.nguyen@leeds.ac.uk

Electronic supporting information

Contents

1 Datasets

1.1 Spin state dataset (*base_spin_dataset*)

1.1.1 Cr(II) Complexes

Table S1: Geometries and experimental spin states Cr(II) crystal structures.

CCDC Identifier	Coordination Number	Closest Point Group	Multiplicity
CAMVER[1]	6	O_h	3
CIDVOA[2]	6	O_h	5
DUYZII[3]	4	D_{4h}	5
GENZII[4]	6	O_h	3
HIZNEJ[5]	2×η-5	D_5	3
HUYWOO[6]	4	D_{4h}	5
KAPPEW[7]	4	D_{4h}	5
LESMAX[8]	2×η-5	D_{5h}	3
OKIJUQ[9]	4	D_{4h}	5
OWUTIL[10]	3, η-5	C_s	3
PIXXEE[11]	2×η-5	D_{5h}	3
SEBQIB[12]	2	$D_{\infty h}$	5
JARJOC[13]	2	$D_{\infty h}$	5
SOFXAM[14]	4	D_{4h}	5
SOFXIU[14]	6	O_h	5
UDURUJ[15]	4	D_{4h}	5
VAZWAU[16]	6	O_h	5
YALPEG[17]	2×η-5	D_5	3

1.1.2 Mn(II) Complexes

Table S2: Geometries and experimental spin states Mn(II) crystal structures.

CCDC Identifier	Coordination Number	Closest Point Group	Multiplicity
AXUMEL[18]	7	C_s	2
AZULIQ[19]	6	O_h	6
BIKZUQ[20]	6	O_h	6
BUBGEL[21]	2×η-5	D_{5h}	6
BUBGUB[21]	2×η-5	D_5	6
BUSMOR[22]	4	T_d	6
CAZZUY[23]	4	T_d	6
CEBBAM[23]	6	O_h	2
EQEGEN[24]	6	O_h	6
GIQMUO[25]	6	O_h	6
HEVCEQ[26]	6	O_h	6
IKEQUK[27]	6	O_h	6
IMAFEH[28]	6	O_h	4
KASNUQ[29]	6	O_h	6
KEYPIT[30]	6	O_h	6
MNPHCY[31]	4	D_{4h}	4
NUYZIS[32]	4	T_d	6
ODIZEG[33]	2×η-5	D_5	2
OKUXUO[34]	5	C_{4v}	6
QABBAA[35]	4	T_d	6
SEWMUC[36]	6	O_h	6
SUTWOT[37]	6	O_h	6
TAWFUT[38]	6	O_h	6
TOGPEK[39]	4	D_{4h}	6
TUSBIT[40]	7	C_s	6
VAQDUM[41]	6	O_h	6
VEBJOB[42]	2×η-5	D_5	6
XAKDOE[24]	6	O_h	6
XAMWEP[43]	4	T_d	6
ZIMGIL[44]	6	O_h	6

1.1.3 Fe(III) Complexes

Table S3: Geometries and experimental spin states Fe(III) crystal structures.

CCDC Identifier	Coordination Number	Closest Point Group	Multiplicity
CALGAX[45]	6	C_{4v}	6
CELVEU[46]	5	C_{4v}	6
CEQPOF[47]	1, η-3, η-5	S	2
ELIRUN[48]	5	C_{4v}	6
EXUBIK[49]	6	O_h	6
FEACAC[50]	6	O_h	6
FONNAZ[51]	6	O_h	6
GEDTUE[52]	5	C_{4v}	4
KANYUT[53,54]	5	C_{4v}	6
KIKBOV[55]	4	T_d	6
LUJNOV[56]	5	C_{4v}	6
MOPDUQ[57]	6	O_h	6
OETPFE[58]	5	C_{4v}	4
OQODEE[59]	6	O_h	6
POGXEQ[60]	6	O_h	6
QOXVUW[61]	5	C_{4v}	6
SAVHIG[62]	5	C_{4v}	6
SELQIJ[63]	5	C_{4v}	4
SIDVIL[64]	6	O_h	6
TISDUU[65]	5	C_{4v}	4
TOQZEH[66]	6	O_h	2
UJAZOX[67]	6	O_h	6
UHEZOX[68]	6	O_h	6
UHIBAP[68]	6	O_h	2
UWIQIB[69]	6	O_h	6
VEFGIW[70]	6	O_h	6
VOFZEV[71]	4	T_d	6
WUQBAN[72]	5	C_{4v}	6

1.1.4 Fe(II) Complexes

Table S4: Geometries and experimental spin states Fe(II) crystal structures. [a]Structures used in the Fe(II) SCO benchmarking. [b]CCDC identifier for ferrocene.

CCDC Identifier	Coordination Number	Closest Point Group	Multiplicity
[a]HPZBFE[73]	6	O_h	1
[a]KEKVIF[74]	6	O_h	1
[a]BAXFIS[75]	6	O_h	1
[a]NEFSUM[76]	6	O_h	1
[a]WAHKEX[77]	6	O_h	1
BOYDOI[78]	6	O_h	5
CAGROU[79]	6	O_h	1
DAGLUU[80]	4	T_d	5
DEDWUE[81]	4	D_{4h}	3
FEGVOE[82]	2	$D_{\infty h}$	5
FEPHCY[83,84]	4	D_{4h}	5
[b]FEROCE	2×η-5	D_5	1
GORKIJ[85]	4	T_d	5
HAZQAD[86]	6	O_h	1
HMPBFE[73]	6	O_h	5
IBUVUW[87]	6	O_h	1
IKIJIX[88]	4	T_d	5
JIRSUB[89]	4	D_{4h}	3
OCAHAE[80]	6	O_h	5
OCAHEI[80]	6	O_h	5
POGXUG[60]	6	O_h	5
QAHVIE[90]	6	O_h	1
QOPBIH[91]	6	O_h	5
RUWZUF[92]	4	T_d	5
SAKWIM[93]	3	D_{3h}	5
SUVROS[94]	4	T_d	5
YIMHOT[95]	3	D_{3h}	5
YUMVUX[96]	4	T_d	5

[a]Structures used in the Fe(II) SCO benchmarking. [b]CCDC identifier for ferrocene

1.1.5 Co(II) Complexes

Table S5: Geometries and experimental spin states Co(II) crystal structures. [a]Structures not deposited on the CSD.

CCDC Identifier	Coordination Number	Closest Point Group	Multiplicity
BIHGEE[97]	4	T_d	4
BIHGII[98]	4	T_d	4
BUQVOY[99]	4	T_d	2
CETBOV[100]	4	T_d	4
CETBUB[100]	4	T_d	4
CTPYCO[101]	5	C_{4v}	4
DAHROU[102]	6	O_h	4
FUFVUX[103]	4	T_d	4
JAWJAT[104]	6	O_h	4
JUWPIA[105]	4	D_{4h}	2
LEGWAW[106,107]	4	T_d	4
KIQREL[108]	5	C_{4v}	4
KIQRIP[108]	6	O_h	4
KIQROV[108]	6	O_h	4
OZIMIV[109]	6	O_h	4
PEBSEW[104]	6	O_h	4
PEBSOG[104]	6	O_h	4
PEBSUM[104]	6	O_h	4
RIPSEO[105]	4	D_{4h}	2
RIPSIS[105]	4	D_{4h}	2
SAPBIV[103]	4	T_d	4
SEQFIE[103]	4	T_d	4
TPORCP[110,111]	4	D_{4h}	2
TUBTIT[112]	2, η-5	C_s	2
UKUJUG[113]	4	T_d	4
VIYGIU[114]	6	O_h	4
XIZLUO[115]	6	O_h	4
YUDGUA[100]	4	T_d	4

1.2 Spin-crossover dataset (*T_SCO_dataset*)

1.2.1 Fe(II) complexes with T_{SCO}

Table S6: Fe(II) structures with their experimental T_{SCO} values[116]

Identifier	**Complex Structure**	T_{SCO} (K)
HACL-1	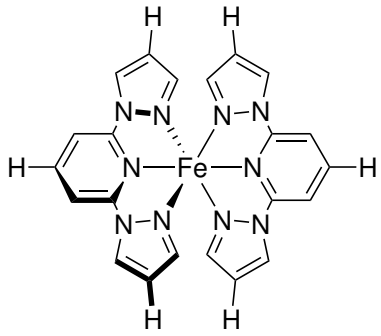	248
HALC-2	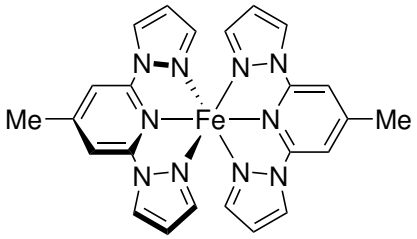	216
HALC-3	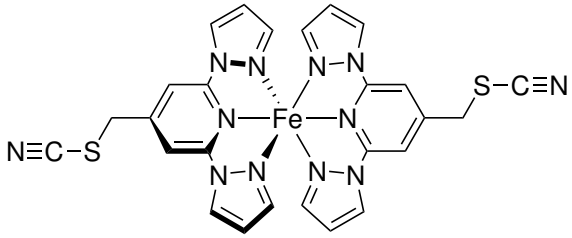	213
HALC-4	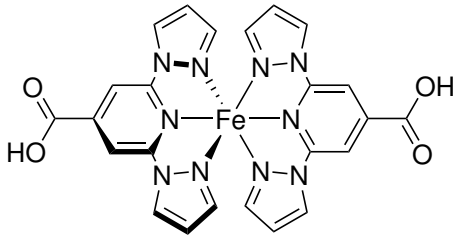	281
HALC-5[a]	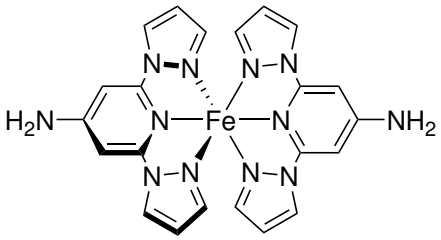	

Continued on next page...

Identifier	**Complex Structure**	T_{SCO} (K)
HALC-6[a]	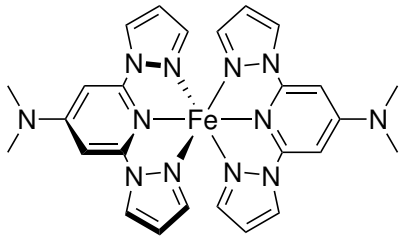	
HALC-7	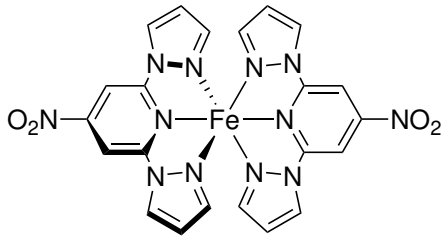	309
HALC-8	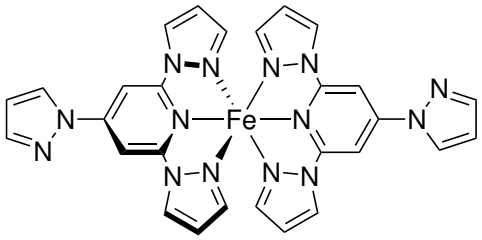	215
HALC-9	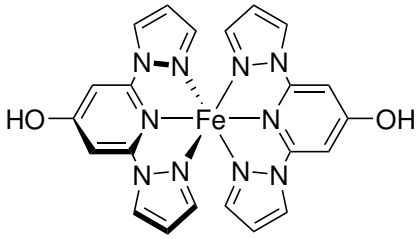	164
HALC-10	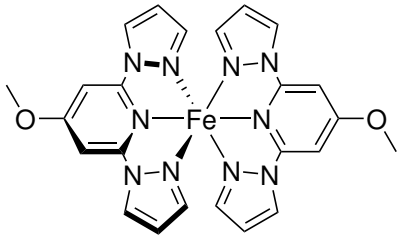	158
HALC-11	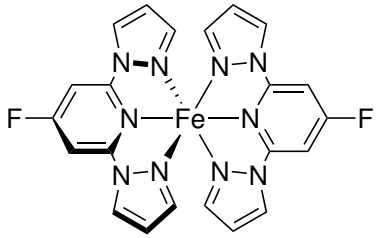	215

Continued on next page...

Identifier	**Complex Structure**	T_{SCO} (K)
HALC-12	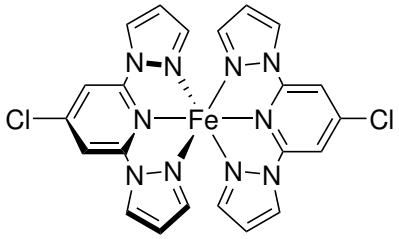	226
HALC-13	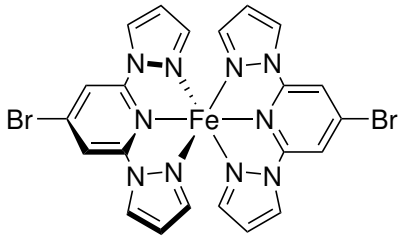	234
HALC-14	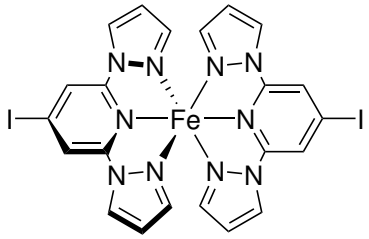	236
HALC-15	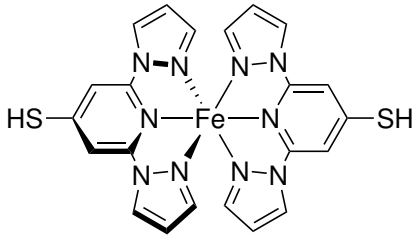	215
HALC-16	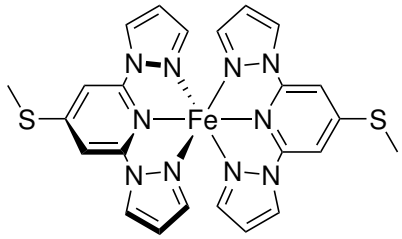	194
HALC-17	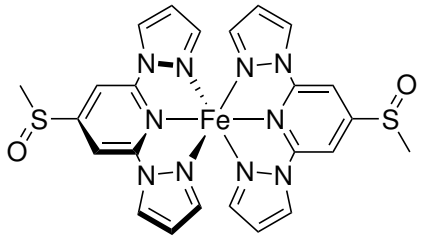	284

Continued on next page...

Identifier	**Complex Structure**	T_{SCO} (K)
HALC-18	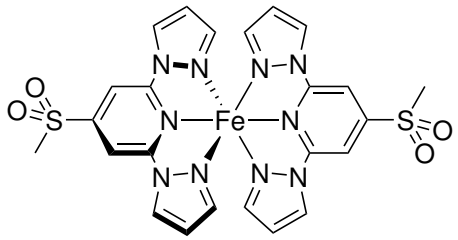	294
HALC-19	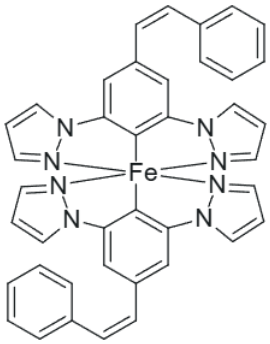	245
HALC-20	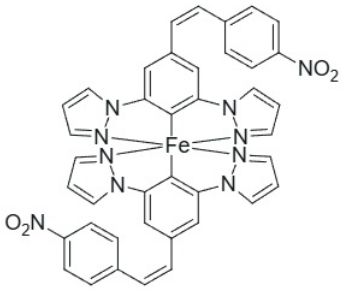	259
HALC-21	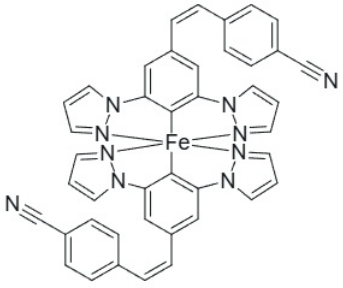	261

Continued on next page...

Identifier	**Complex Structure**	T_{SCO} (K)
HALC-22	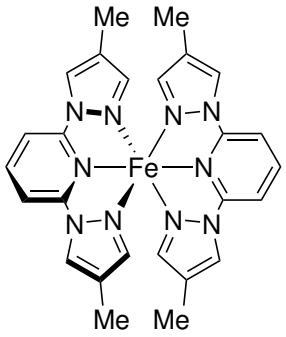	273
HALC-23	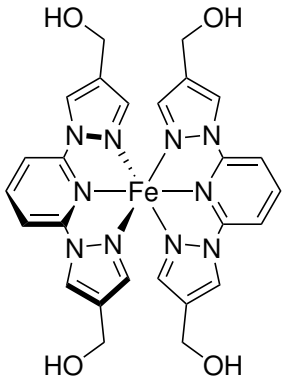	259
HALC-24	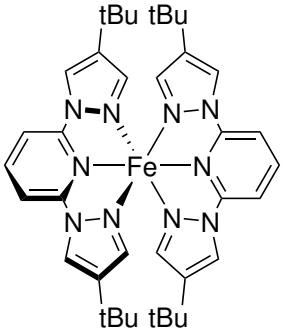	251
HALC-25	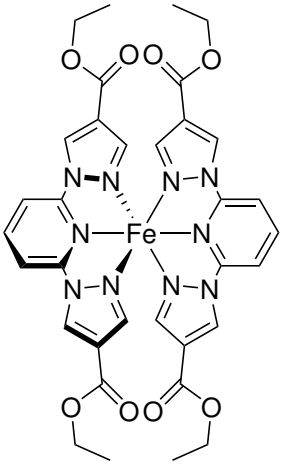	256

Continued on next page...

Identifier	**Complex Structure**	T_{SCO} (K)
HALC-26	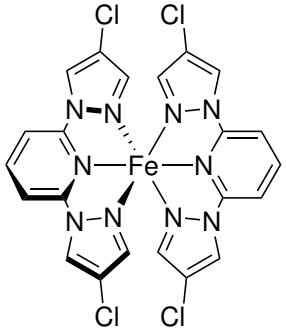	231
HALC-27	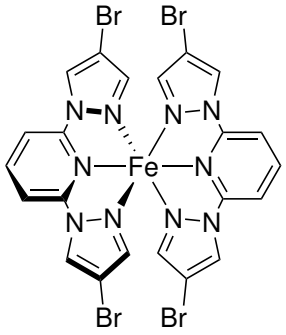	238
HALC-28	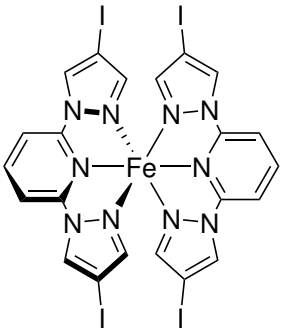	237
ZUCROE	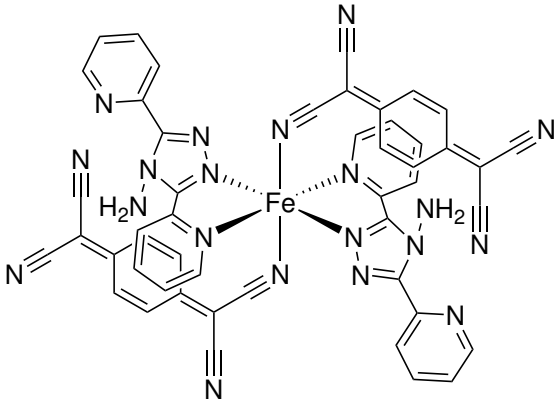	280

Continued on next page...

Identifier	**Complex Structure**	T_{SCO} (K)
WAHKEX	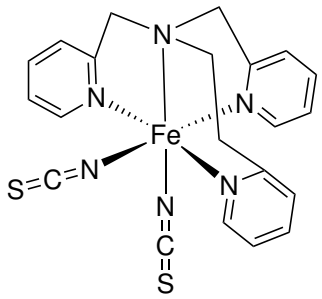	184
KEKVIF03	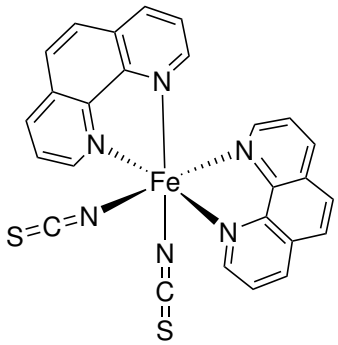	176
NEFSUM02	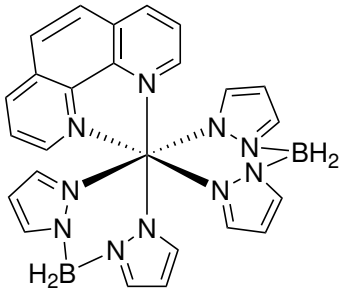	160
HPZBFE	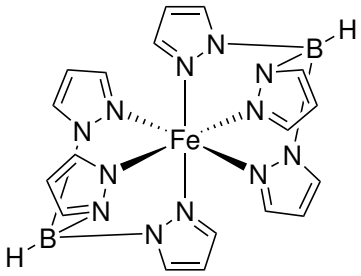	393
BAXFIS02	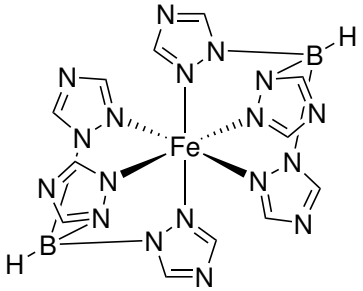	333

[a]Structures were not included in analysis as they were high spin at all temperatures

2 Prediction of Spin States with DFT

2.1 General method

Cr(II) and Fe(II) complexes were optimised with their three different possible multiplicities (2S+1 = 1, 3, 5). While low spin Cr(II) complexes are very rare, they are still possible, so their low spin structures was calculated.[117] Based on the known experimental values, Mn(II), Fe(III) complexes were optimised with their three different possible multiplicities (2S+1 = 2, 4, 6) while cobalt(II) complexes were only optimised with two different multiplicities (2S+1 = 2, 4). All jobs were initially allocated 16 CPU cores, 64 GB of RAM and 48 hours of time to optimise and calculate frequencies of all complexes. Jobs were considered successful when all frequencies of all multiplicities were not imaginary. Multiplicity was assigned to the complex when all separate calculations were successful. The success rate of optimisation for the four methods are 97%, 96%, 97% and 82% for B3LYP, PBE0, TPSSh and M06-L, respectively.

2.1.1 Energies of spin states

Table S7: PBE0/def2-TZVP electronic energy results for Cr(II) complexes.

Identifier	Singlet energy (Hartrees)	Triplet energy (Hartrees)	Quintet energy (Hartrees)
CAMVER	−2965.092932	−2965.140629	−2965.126319
CIDVOA	−2221.698167	−2221.766320	−2221.817251
DUYZII	−3286.132177	−3286.204451	−3286.252610
GENZII	−3141.196005	−3141.265337	−3141.254985
HIZNEJ	−2138.006931	−2138.048869	−2138.047217
HUYWOO	−2544.174370	−2544.237276	−2544.275266
KAPPEW	−3122.017862	−3122.065362	−3122.113358
LESMAX	−1509.555159	−1509.598970	−1509.592819
OKIJUQ	−1892.726337	−1892.787287	−1892.834370
OWUTIL	−2769.186569	−2769.273296	−2769.272154
PIXXEE	−1755.270218	−1755.292042	−1755.296914
SOFXAM	−2711.399755	−2711.460294	−2711.507869
SOFXIU	−2414.591332	−2414.646099	−2414.683056
UDURUJ	−2676.964756	−2677.023887	−2677.071209
VAZWAU	−3795.168837	−3795.218455	−3795.227779
YALPEG	−2287.916178	−2287.952998	−2287.966292

Table S8: B3LYP/def2-TZVP electronic energy results for Cr(II) complexes

Identifier	Singlet energy (Hartrees)	Triplet energy (Hartrees)	Quintet energy (Hartrees)
CAMVER	−2965.850956	−2965.895588	−2965.890569
CIDVOA	−2222.550111	−2222.610120	−2222.659546
DUYZII	−3287.223558	−3287.285307	−3287.329271
GENZII	−3142.217595	−3142.277885	−3142.267819
HIZNEJ	−2138.713336	−2138.748455	−2138.747049
HUYWOO	−2545.008954	−2545.061365	−2545.099364
KAPPEW	−3122.826954	−3122.864440	−3122.908072
LESMAX	−1509.940415	−1509.976981	−1509.971217
OKIJUQ	−1893.343841	−1893.393863	−1893.436394
OWUTIL	−2770.128157	−2770.205962	−2770.204359
PIXXEE	−1755.781921	−1755.803217	−1755.808444
SOFXAM	−2712.244234	−2712.293758	−2712.336746
SOFXIU	−2415.506516	−2415.554729	−2415.587350
UDURUJ	−2677.843303	−2677.891602	−2677.934686
VAZWAU	−3796.008592	−3796.053486	−3796.065537
YALPEG	−2288.704012	−2288.734496	−2288.747242

Table S9: TPSSh/def2-TZVP electronic energy results for Cr(II) complexes

Identifier	Singlet energy (Hartrees)	Triplet energy (Hartrees)	Quintet energy (Hartrees)
CAMVER	−2966.689759	−2966.728898	−2966.704192
CIDVOA	−2223.281576	−2223.339917	−2223.371204
DUYZII	−3288.344569	−3288.406051	−3288.445049
GENZII	−3143.258472	−3143.304562	−3143.287898
HIZNEJ	−2139.692777	−2139.730614	−2139.714070
HUYWOO	−2545.880463	−2545.921734	−2545.956842
KAPPEW	−3123.461816	−3123.496443	−3123.534966
LESMAX	−1510.413407	−1510.453244	−1510.431722
OKIJUQ	−1894.064406	−1894.116822	−1894.155176
OWUTIL	−2771.172953	−2771.238458	−2771.236078
PIXXEE	−1756.431909	−1756.440551	−1756.428672
SOFXAM	−2713.026238	−2713.074904	−2713.113518
SOFXIU	−2416.519341	−2416.567290	−2416.591877
UDURUJ	−2678.830154	−2678.878591	−2678.917139
VAZWAU	−3796.851995	−3796.894926	−3796.889647
YALPEG	−2289.779735	−2289.811440	−2289.812760

Table S10: M06-L/def2-TZVP electronic energy results for Cr(II) complexes

Identifier	Singlet energy (Hartrees)	Triplet energy (Hartrees)	Quintet energy (Hartrees)
CAMVER	−2966.424417	−2966.464060	−2966.446668
CIDVOA	−2223.038263	−2223.103967	−2223.129405
DUYZII	−3288.013007	−3288.071759	−3288.121688
GENZII	−3142.945357	−3142.999176	−3142.982334
HIZNEJ	−2139.408577	−2139.458313	−2139.442479
HUYWOO	−2545.602587	−2545.650785	−2545.687974
KAPPEW	−3123.235127	−3123.275629	−3123.326832
LESMAX	−1510.243840	−1510.295625	−1510.277461
OKIJUQ	−1893.832128	−1893.825098	−1893.931754
OWUTIL	−2770.862794	−2770.935537	−2770.934115
PIXXEE	−1756.230064	−1756.235896	−1756.227837
SOFXAM	−2712.742279	−2712.818890	−2712.868670
UDURUJ	−2678.505551	−2678.577261	−2678.628215
VAZWAU	−3797.060497	−3797.108735	−3797.109290
YALPEG	−2289.486743	−2289.527214	−2289.527805

Table S11: Spin state predictions for Cr(II). Green coloured boxes denote correctly predicted spin state, red coloured boxes denote incorrectly predicted spin state, white coloured box denote failed calculation.

Identifier	Multiplicity	B3LYP	PBE0	TPSSh	M06-L
CAMVER	3	3	3	3	3
CIDVOA	5	5	5	5	5
DUYZII	5	5	5	5	5
GENZII	3	3	3	3	3
HIZNEJ	3	3	3	3	3
HUYWOO	5	5	5	5	5
KAPPEW	5	5	5	5	5
LESMAX	3	3	3	3	3
OKIJUQ	5	5	5	5	5
OWUTIL	3	3	3	3	3
PIXXEE	3	5	5	3	3
SOFXAM	5	5	5	5	5
SOFXIU	5	5	5	5	
UDURUJ	5	5	5	5	5
VAZWAU	5	5	5	3	5
YALPEG	3	5	5	5	5

Table S12: PBE0/def2-TZVP electronic energy results for Mn(II) complexes

Identifier	Doublet energy (Hartrees)	Quartet energy (Hartrees)	Sextet energy (Hartrees)
AXUMEL	−5689.827701	−5689.827407	−5689.798238
AZULIQ	−3142.375404	−3142.394715	−3142.454367
BIKZUQ	−3036.773722	−3036.780734	−3036.832685
BUBGEL	−3988.293672	−3988.286892	−3988.323546
BUBGUB	−2480.175131	−2480.164115	−2480.200363
BUSMOR	−3043.948272	−3043.990661	−3044.034276
CAZZUY	−2849.592096	−2849.624671	−2849.667822
CEBBAM	−3301.316589	−3301.296535	−3301.309972
EQEGEN	−3282.087405	−3282.095149	−3282.146144
GIQMUO	−3371.637413	−3371.660175	−3371.696749
HEVCEQ	−2840.912344	−2840.930373	−2840.995535
IKEQUK	−3727.283639	−3727.308770	−3727.354370
IMAFEH	−3312.893977	−3312.908420	−3312.832174
KASNUQ	−7902.326978	−7902.345564	−7902.405283
KEYPIT	−2321.993623	−2322.019297	−2322.064903
MNPHCY	−2816.683511	−2816.720057	−2816.701836
NUYZIS	−2967.956027	−2967.982660	−2968.033581
ODIZEG	−2771.158887	−2771.137623	−2771.159830
OKUXUO	−3007.140965	−3007.171396	−3007.216753
QABBAA	−3654.031158	−3654.060789	−3654.126767
TAWFUT	−4531.704351	−4531.719415	−4531.776204
TOGPEK	−6015.594281	−6015.629354	−6015.620619
TUSBIT	−2437.264948	−2437.287263	−2437.346614
VAQDUM	−4021.100406	−4021.111760	−4021.155296
VEBJOB	−2480.199408	−2480.189597	−2480.222637
XAKDOE	−2857.660016	−2857.684963	−2857.738385
XAMWEP	−2879.815971	−2879.849287	−2879.906217
ZIMGIL	−2966.538775	−2966.536346	−2966.589897

Table S13: B3LYP/def2-TZVP electronic energy results for Mn(II) complexes

Identifier	Doublet energy (Hartrees)	Quartet energy (Hartrees)	Sextet energy (Hartrees)
AXUMEL	−5690.916321	−5690.913110	−5690.881994
AZULIQ	−3143.328967	−3143.347574	−3143.398637
BIKZUQ	−3037.738839	−3037.742654	−3037.788385
BUBGEL	−3989.515314	−3989.507080	−3989.537506
BUBGUB	−2481.000042	−2480.987904	−2481.017679
BUSMOR	−3044.707661	−3044.747032	−3044.784221
CAZZUY	−2850.463970	−2850.490918	−2850.530520
CEBBAM	−3302.200252	−3302.198372	−3302.208924
EQEGEN	−3283.203102	−3283.203721	−3283.254283
GIQMUO	−3373.090899	−3373.108481	−3373.138211
HEVCEQ	−2841.652998	−2841.668454	−2841.727574
IKEQUK	−3728.679326	−3728.691948	−3728.741240
IMAFEH	−3314.258748	−3314.269493	−3314.256440
KASNUQ	−7903.736658	−7903.753491	−7903.806337
KEYPIT	−2322.835236	−2322.865659	−2322.895527
MNPHCY	−2817.769209	−2817.796786	−2817.774087
NUYZIS	−2968.732875	−2968.756680	−2968.803478
OKUXUO	−3008.086051	−3008.109934	−3008.152055
QABBAA	−3655.263321	−3655.286914	−3655.348669
SUTWOT	−4317.995075	−4317.998415	−4318.034634
TAWFUT	−4533.236389	−4533.248455	−4533.296690
TOGPEK	−6017.365109	−6017.401100	−6017.389514
TUSBIT	−2438.161703	−2438.181146	−2438.232575
VAQDUM	−4022.922429	−4022.927307	−4022.966341
VEBJOB	−2481.027103	−2481.016515	−2481.043941
XAKDOE	−2858.535062	−2858.542975	−2858.603455
XAMWEP	−2880.919105	−2880.949331	−2880.999015
ZIMGIL	−2967.724919	−2967.720354	−2967.766065

Table S14: TPSSh/def2-TZVP electronic energy results for Mn(II) complexes

Identifier	Doublet energy (Hartrees)	Quartet energy (Hartrees)	Sextet energy (Hartrees)
AXUMEL	−5691.851890	−5691.839414	−5691.796412
AZULIQ	−3144.287023	−3144.291517	−3144.331646
BIKZUQ	−3038.662031	−3038.653100	−3038.688900
BUBGEL	−3990.848169	−3990.827947	−3990.845048
BUBGUB	−2482.179777	−2482.154353	−2482.171783
BUSMOR	−3045.520537	−3045.554397	−3045.579422
CAZZUY	−2851.484889	−2851.507938	−2851.534931
CEBBAM	−3303.203506	−3303.169674	−3303.168008
EQEGEN	−3284.345425	−3284.335546	−3284.368028
GIQMUO	−3374.137952	−3374.147473	−3374.159832
HEVCEQ	−2842.471280	−2842.474339	−2842.524753
IKEQUK	−3730.032141	−3730.047665	−3730.069944
IMAFEH	−3315.815926	−3315.789670	−3315.794362
KASNUQ	−7904.935276	−7904.939264	−7904.979340
KEYPIT	−2323.566508	−2323.578357	−2323.608155
MNPHCY	−2818.968685	−2818.998813	−2818.974757
NUYZIS	−2969.542038	−2969.559045	−2969.590225
ODIZEG	−2772.940014	−2772.904879	−2772.909208
OKUXUO	−3009.018865	−3009.035104	−3009.060803
QABBAA	−3656.645526	−3656.663221	−3656.718800
SUTWOT	−4319.676873	−4319.673970	−4319.688404
TAWFUT	−4534.705980	−4534.704804	−4534.744039
TOGPEK	−6019.162275	−6019.197917	−6019.185493
TUSBIT	−2438.994803	−2439.001277	−2439.041944
VAQDUM	−4024.436369	−4024.429724	−4024.451690
VEBJOB	−2482.204285	−2482.180070	−2482.195112
XAKDOE	−2859.331324	−2859.322328	−2859.377369
XAMWEP	−2882.258783	−2882.285165	−2882.324819
ZIMGIL	−2968.927499	−2968.908886	−2968.942942

Table S15: M06-L/def2-TZVP electronic energy results for Mn(II) complexes

Identifier	Doublet energy (Hartrees)	Quartet energy (Hartrees)	Sextet energy (Hartrees)
AXUMEL	−5691.507722	−5691.494000	−5691.453317
AZULIQ	−3143.972183	−3143.990239	−3144.041582
BIKZUQ	−3038.360100	−3038.363754	−3038.414392
BUBGEL	−3990.438758	−3990.426943	−3990.449138
BUBGUB	−2481.862834	−2481.846192	−2481.870197
BUSMOR	−3045.251203	−3045.294322	−3045.332317
CAZZUY	−2851.163869	−2851.190078	−2851.227474
CEBBAM	−3302.887492	−3302.861109	−3302.869434
EQEGEN	−3283.987664	−3283.994573	−3284.036106
GIQMUO	−3373.775833	−3373.794640	−3373.817830
HEVCEQ	−2842.209565	−2842.223575	−2842.295373
IMAFEH	−3315.353475	−3315.354709	−3315.342704
KASNUQ	−7904.559297	−7904.578096	−7904.628630
MNPHCY	−2818.604515	−2818.632057	−2818.614206
NUYZIS	−2969.271830	−2969.293800	−2969.332076
OKUXUO	−3008.723987	−3008.758568	−3008.789325
QABBAA	−3656.246044	−3656.279700	−3656.342074
SUTWOT	−4319.149281	−4319.155354	−4319.179957
TAWFUT	−4534.235379	−4534.248297	−4534.302656
TOGPEK	−6018.602080	−6018.649331	−6018.640411
TUSBIT	−2438.726083	−2438.752703	−2438.795279
VEBJOB	−2481.892736	−2481.875557	−2481.894576
XAKDOE	−2859.069895	−2859.085476	−2859.143242
XAMWEP	−2881.860062	−2881.896680	−2881.949440
ZIMGIL	−2968.554775	−2968.561517	−2968.595151

Table S16: Spin state predictions for Mn(II). Green coloured boxes denote correctly predicted spin state, red coloured boxes denote incorrectly predicted spin state, white coloured box denote failed calculation. The experimental ground spin states are shown in Tabel S2.

Identifier	Multiplicity	B3LYP	PBE0	TPSSh	M06-L
AXUMEL	2	2	2	2	2
AZULIQ	6	6	6	6	6
BIKZUQ	6	6	6	6	6
BUBGEL	6	6	6	2	6
BUBGUB	6	6	6	2	6
BUSMOR	6	6	6	6	6
CAZZUY	6	6	6	6	6
CEBBAM	2	6	2	2	2
EQEGEN	6	6	6	6	6
GIQMUO	6	6	6	6	6
HEVCEQ	6	6	6	6	6
IKEQUK	6	6	6	6	
IMAFEH	4	4	4	2	4
KASNUQ	6	6	6	6	6
KEYPIT	6	6	6	6	
MNPHCY	4	4	4	4	4
NUYZIS	6	6	6	6	6
OKUXUO	6	6	6	6	6
QABBAA	6	6	6	6	6
SUTWOT	6	6		6	6
TAWFUT	6	6	6	6	6
TOGPEK	6	4	4	4	4
TUSBIT	6	6	6	6	6
VAQDUM	6	6	6	6	
VEBJOB	6	6	6	2	6
XAKDOE	6	6	6	6	6
XAMWEP	6	6	6	6	6
ZIMGIL	6	6	6	6	6
ODIZEG	2		6	2	

Table S17: PBE0/def2-TZVP electronic energy results for Fe(III) complexes.

Identifier	Doublet energy (Hartrees)	Quartet energy (Hartrees)	Sextet energy (Hartrees)
CALGAX	−3454.701242	−3454.721395	−3454.728100
CELVEU	−3398.310726	−3398.332964	−3398.345798
CEQPOF	−2338.394240	−2338.390600	−2338.380045
ELIRUN	−3598.547838	−3598.566883	−3598.586441
EXUBIK	−2928.542788	−2928.501825	−2928.459310
FEACAC	−2298.434320	−2298.430609	−2298.460360
FONNAZ	−3112.438508	−3112.427864	−3112.448885
GEDTUE	−3812.930927	−3812.959693	−3812.958029
KANYUT	−3634.651886	−3634.672979	−3634.681740
KIKBOV	−4784.606395	−4784.633550	−4784.689208
LUJNOV	−3317.081340	−3317.098518	−3317.122075
MOPDUQ	−2921.268658	−2921.265283	−2921.293750
OETPFE	−3638.829696	−3638.855869	−3638.860140
OQODEE	−3366.234706	−3366.248325	−3366.273300
POGXEQ	−3205.094958	−3205.089939	−3205.121407
QOXVUW	−5299.438683	−5299.465129	−5299.483357
SAVHIG	−4715.030285	−4715.062844	−4715.073348
SELQIJ	−4094.112998	−4094.136719	−4094.137715
SIDVIL	−2227.089750	−2227.099435	−2227.128990
TISDUU	−6549.112546	−6549.134943	−6549.095078
TOQZEH	−3212.329715	−3212.326484	−3212.358244
UHEZOX	−2774.226066	−2774.216403	−2774.239405
UHIBAP	−2406.893633	−2406.881869	−2406.890233
UJAZOX	−4612.091274	−4612.080946	−4612.103768
UWIQIB	−2945.603283	−2945.613848	−2945.635810
VEFGIW	−3827.481806	−3827.491676	−3827.521959
VOFZEV	−3255.731874	−3255.763698	−3255.813000
WUQBAN	−3116.797654	−3116.816612	−3116.844414

Table S18: B3LYP/def2-TZVP electronic energy results for Fe(III) complexes

Identifier	Doublet energy (Hartrees)	Quartet energy (Hartrees)	Sextet energy (Hartrees)
CALGAX	−3456.095089	−3456.111631	−3456.110799
CELVEU	−3399.255246	−3399.275050	−3399.282344
CEQPOF	−2338.948194	−2338.954598	−2338.935909
ELIRUN	−3599.543878	−3599.559879	−3599.574095
EXUBIK	−2929.662133	−2929.621073	−2929.578261
FEACAC	−2299.209721	−2299.202383	−2299.225670
FONNAZ	−3113.517751	−3113.503563	−3113.521010
GEDTUE	−3813.786988	−3813.812959	−3813.808651
KANYUT	−3635.977133	−3635.995310	−3635.997457
KIKBOV	−4786.181901	−4786.205765	−4786.256624
LUJNOV	−3317.951608	−3317.965384	−3317.984012
MOPDUQ	−2922.370835	−2922.365219	−2922.388113
OETPFE	−3640.143095	−3640.158915	−3640.159974
OQODEE	−3367.102555	−3367.113128	−3367.132693
POGXEQ	−3206.089646	−3206.081587	−3206.106558
QOXVUW	−5301.577527	−5301.600893	−5301.614689
SAVHIG	−4716.434873	−4716.464177	−4716.474712
SELQIJ	−4095.420788	−4095.440600	−4095.439177
SIDVIL	−2227.827418	−2227.833938	−2227.857073
TISDUU	−6550.978386	−6550.998140	−6550.956714
TOQZEH	−3213.608430	−3213.601574	−3213.626935
UHEZOX	−2775.077887	−2775.065819	−2775.083288
UHIBAP	−2407.709384	−2407.695631	−2407.698873
UJAZOX	−4613.325008	−4613.312328	−4613.329771
UWIQIB	−2946.565284	−2946.573912	−2946.589752
VEFGIW	−3828.610568	−3828.617586	−3828.642367
VOFZEV	−3256.484540	−3256.510841	−3256.557490
WUQBAN	−3117.690502	−3117.706579	−3117.729266

Table S19: TPSSh/def2-TZVP electronic energy results for Fe(III) complexes

Identifier	Doublet energy (Hartrees)	Quartet energy (Hartrees)	Sextet energy (Hartrees)
CALGAX	−3457.651182	−3457.653784	−3457.653112
CELVEU	−3400.132887	−3400.144764	−3400.143402
CEQPOF	−2339.577339	−2339.555893	−2339.538454
ELIRUN	−3600.478419	−3600.484946	−3600.490473
EXUBIK	−2930.749188	−2930.707200	−2930.711071
FEACAC	−2299.932707	−2299.914898	−2299.929220
FONNAZ	−3114.624733	−3114.600116	−3114.608141
GEDTUE	−3814.570168	−3814.587326	−3814.575813
KANYUT	−3637.477154	−3637.486920	−3637.481996
KIKBOV	−4787.637450	−4787.653177	−4787.696437
LUJNOV	−3318.731730	−3318.737854	−3318.747967
MOPDUQ	−2923.513402	−2923.497001	−2923.512007
OETPFE	−3641.622691	−3641.628126	−3641.620088
OQODEE	−3367.889693	−3367.888067	−3367.901876
POGXEQ	−3207.001596	−3206.983005	−3207.000394
QOXVUW	−5303.456830	−5303.471959	−5303.479169
SAVHIG	−4717.864492	−4717.884741	−4717.887152
SELQIJ	−4096.847256	−4096.856019	−4096.847032
SIDVIL	−2228.383316	−2228.380476	−2228.396939
TISDUU	−6552.818155	−6552.829753	−6552.787489
TOQZEH	−3214.948250	−3214.930727	−3214.946727
UHEZOX	−2775.949728	−2775.925956	−2775.935450
UHIBAP	−2408.565735	−2408.540023	−2408.534307
UJAZOX	−4614.456177	−4614.431796	−4614.441197
UWIQIB	−2947.495668	−2947.492782	−2947.501366
VEFGIW	−3829.715473	−3829.709905	−3829.728753
VOFZEV	−3257.105083	−3257.123797	−3257.159692
WUQBAN	−3118.547334	−3118.554239	−3118.568705

Table S20: M06-L/def2-TZVP electronic energy results for Fe(III) complexes

Identifier	Doublet energy (Hartrees)	Quartet energy (Hartrees)	Sextet energy (Hartrees)
CALGAX	−3457.166907	−3457.182256	−3457.201483
CELVEU	−3399.825329	−3399.845862	−3399.863691
CEQPOF	−2339.617019	−2339.603408	−2339.591626
EXUBIK	−2930.425897	−2930.381441	−2930.412307
FEACAC	−2299.698414	−2299.691462	−2299.724374
KANYUT	−3637.005417	−3637.024628	−3637.040641
LUJNOV	−3318.468922	−3318.491120	−3318.510193
MOPDUQ	−2923.148052	−2923.144658	−2923.178035
OQODEE	−3367.628191	−3367.637411	−3367.670132
POGXEQ	−3206.693616	−3206.684086	−3206.723749
SAVHIG	−4717.399709	−4717.435471	−4717.449976
TISDUU	−6552.243728	−6552.263786	−6552.270730
TOQZEH	−3214.530563	−3214.525676	−3214.558649
UHEZOX	−2775.661800	−2775.649612	−2775.678350
UHIBAP	−2408.281638	−2408.268226	−2408.279777
UJAZOX	−4614.091518	−4614.081678	−4614.106695
UWIQIB	−2947.189681	−2947.196647	−2947.226336
VEFGIW	−3829.369214	−3829.374163	−3829.413339
WUQBAN	−3118.253379	−3118.271583	−3118.308039

Table S21: Spin state predictions for Fe(III). Green coloured boxes denote correctly predicted spin state, red coloured boxes denote incorrectly predicted spin state, white coloured box denote failed calculation. The experimental ground spin states are shown in Tabel S3.

Identifier	Multiplicity	B3LYP	PBE0	TPSSh	M06-L
CALGAX	6	4	6	4	6
CELVEU	6	6	6	4	6
CEQPOF	2	4	2	2	2
ELIRUN	6	6	6	6	
EXUBIK	6	2	2	2	2
FEACAC	6	6	6	2	6
FONNAZ	6	6	6	2	
GEDTUE	4	4	4	4	
KANYUT	6	6	6	4	6
KIKBOV	6	6	6	6	
LUJNOV	6	6	6	6	6
MOPDUQ	6	6	6	2	6
OETPFE	4	6	6	4	
OQODEE	6	6	6	6	6
POGXEQ	6	6	6	2	6
QOXVUW	6	6	6	6	
SAVHIG	6	6	6	6	6
SELQIJ	4	4	6	4	
SIDVIL	6	6	6	6	
TISDUU	4	4	4	4	6
TOQZEH	2	6	6	2	6
UHEZOX	6	6	6	2	6
UHIBAP	2	2	2	2	2
UJAZOX	6	6	6	2	6
UWIQIB	6	6	6	6	6
VEFGIW	6	6	6	6	6
VOFZEV	6	6	6	6	
WUQBAN	6	6	6	6	6

Table S22: PBE0/def2-TZVP electronic energy results for Fe(II) complexes

Identifier	Singlet energy (Hartrees)	Triplet energy (Hartrees)	Quintet energy (Hartrees)
BOYDOI	−3199.306998	−3199.317488	−3199.344528
CAGROU	−3203.535637	−3203.508592	−3203.538500
DAGLUU	−2833.451712	−2833.477196	−2833.529109
DEDWUE	−2879.593694	−2879.652354	−2879.650839
FEGVOE	−3125.257485	−3125.302078	−3125.346789
FEROCE	−1650.275667	−1650.245908	−1650.254782
GORKIJ	−2845.837721	−2845.866317	−2845.902655
HAZQAD	−3025.816502	−3025.777578	−3025.780959
HMPBFE	−3138.697198	−3138.683995	−3138.715576
IBUVUW	−3326.410073	−3326.403371	−3326.427241
IKIJIX	−7915.483515	−7915.512074	−7915.563288
JIRSUB	−3485.419602	−3485.474339	−3485.457717
OCAHAE	−2726.611143	−2726.616578	−2726.652468
OCAHEI	−2979.617881	−2979.628995	−2979.663994
POGXUG	−7993.790139	−7993.778728	−7993.810008
QAHVIE	−3827.623474	−3827.582059	−3827.652775
QOPBIH	−2601.188807	−2601.204845	−2601.219580
RUWZUF	−2457.009222	−2457.054128	−2457.059356
SAKWIM	−4055.636935	−4055.699825	−4055.743653
SUVROS	−3312.630312	−3312.664142	−3312.714342
YIMHOT	−3121.043090	−3121.096462	−3121.129878
YUMVUX	−3470.825127	−3470.865999	−3470.880764

Table S23: B3LYP/def2-TZVP electronic energy results for Fe(II) complexes

Identifier	Singlet energy (Hartrees)	Triplet energy (Hartrees)	Quintet energy (Hartrees)
BOYDOI	−3200.334791	−3200.343280	−3200.365222
CAGROU	−3204.797991	−3204.766785	−3204.792703
DAGLUU	−2834.177639	−2834.196408	−2834.243771
DEDWUE	−2880.630672	−2880.686333	−2880.618672
FEGVOE	−3126.279644	−3126.324524	−3126.361248
FEPHCY	−2930.461909	−2930.515131	−2930.473686
FEROCE	−1650.629276	−1650.602463	−1650.607502
GORKIJ	−2846.857013	−2846.883073	−2846.914155
HAZQAD	−3026.960660	−3026.923479	−3026.922442
HMPBFE	−3139.881342	−3139.867648	−3139.893741
IBUVUW	−3327.775246	−3327.766876	−3327.784938
IKIJIX	−7916.837121	−7916.858798	−7916.905117
JIRSUB	−3486.548080	−3486.594355	−3486.580394
OCAHAE	−2727.620256	−2727.622555	−2727.651152
OCAHEI	−2980.776815	−2980.785660	−2980.812498
POGXUG	−7995.143837	−7995.129425	−7995.156508
QAHVIE	−3828.985655	−3828.943960	−3828.997182
QOPBIH	−2602.129196	−2602.142798	−2602.150851
RUWZUF	−2457.839132	−2457.878475	−2457.882145
SAKWIM	−4056.887313	−4056.942223	−4056.981598
SUVROS	−3313.478973	−3313.506695	−3313.552827
YIMHOT	−3122.218572	−3122.265594	−3122.292798
YUMVUX	−3471.880537	−3471.924140	−3471.931527

Table S24: TPSSh/def2-TZVP electronic energy results for Fe(II) complexes

Identifier	Singlet energy (Hartrees)	Triplet energy (Hartrees)	Quintet energy (Hartrees)
BOYDOI	−3201.238199	−3201.240284	−3201.250054
CAGROU	−3206.187711	−3206.157902	−3206.157853
DAGLUU	−2834.862888	−2834.873419	−2834.913272
FEGVOE	−3127.473355	−3127.503911	−3127.534932
FEPHCY	−2931.662247	−2931.716234	−2931.672698
FEROCE	−1651.054682	−1651.009928	−1651.000501
GORKIJ	−2848.120078	−2848.137621	−2848.158781
HAZQAD	−3028.326042	−3028.273217	−3028.259364
HMPBFE	−3141.295362	−3141.270864	−3141.286390
IBUVUW	−3329.174447	−3329.136136	−3329.167633
IKIJIX	−7918.095234	−7918.120331	−7918.144218
JIRSUB	−3487.975237	−3488.019461	−3487.990412
OCAHAE	−2728.603671	−2728.597227	−2728.613245
OCAHEI	−2981.939506	−2981.939410	−2981.954202
POGXUG	−7996.172046	−7996.148384	−7996.163603
QAHVIE	−3830.335654	−3830.302912	−3830.333854
QOPBIH	−2603.048322	−2603.056988	−2603.054056
RUWZUF	−2458.812254	−2458.843580	−2458.834284
SAKWIM	−4058.295595	−4058.348058	−4058.378655
SUVROS	−3314.287078	−3314.312248	−3314.350369
YIMHOT	−3123.702764	−3123.746311	−3123.763570
YUMVUX	−3473.011405	−3473.041367	−3473.038683

Table S25: M06-L/def2-TZVP electronic energy results for Fe(II) complexes

Identifier	Singlet energy (Hartrees)	Triplet energy (Hartrees)	Quintet energy (Hartrees)
CAGROU	−3205.758264	−3205.725740	−3205.744264
DAGLUU	−2834.633301	−2834.641774	−2834.690720
DEDWUE	−2881.520616	−2881.568016	−2881.564568
FEGVOE	−3127.114955	−3127.149556	−3127.193057
FEPHCY	−2931.283377	−2931.330274	−2931.311231
FEROCE	−1650.903525	−1650.853661	−1650.854632
GORKIJ	−2847.754079	−2847.764398	−2847.798429
HAZQAD	−3027.912122	−3027.870053	−3027.868824
HMPBFE	−3140.901632	−3140.872755	−3140.893980
IBUVUW	−3328.775462	−3328.724211	−3328.779670
IKIJIX	−7917.724773	−7917.749425	−7917.787497
OCAHAE	−2728.300332	−2728.292646	−2728.318056
OCAHEI	−2981.586631	−2981.570767	−2981.609173
POGXUG	−7995.851698	−7995.828534	−7995.855514
QAHVIE	−3829.929613	−3829.916832	−3829.921834
QOPBIH	−2602.760009	−2602.762746	−2602.777875
RUWZUF	−2458.506357	−2458.543688	−2458.538229
SAKWIM	−4057.892553	−4057.937529	−4057.978570
SUVROS	−3314.007171	−3314.026275	−3314.077196

Table S26: Spin state predictions for Fe(II). Green coloured boxes denote correctly predicted spin state, red coloured boxes denote incorrectly predicted spin state, white coloured box denote failed calculation. The experimental ground spin states are shown in Tabel S4.

Identifier	Multiplicity	B3LYP	PBE0	TPSSh	M06-L
BOYDOI	5	5	5	5	
CAGROU	1	1	5	1	1
DAGLUU	5	5	5	5	5
DEDWUE	3	3	3		3
FEGVOE	5	5	5	5	5
FEPHCY	3	3		3	3
FEROCE	1	1	1	1	1
GORKIJ	5	5	5	5	5
HAZQAD	1	1	1	1	1
HMPBFE	5	5	5	1	1
IBUVUW	5	5	5	1	5
IKIJIX	5	5	5	5	5
JIRSUB	3	3	3	3	
OCAHAE	5	5	5	5	5
OCAHEI	5	5	5	5	5
POGXUG	5	5	5	1	5
QAHVIE	5	5	5	1	1
QOPBIH	5	5	5	3	5
RUWZUF	5	5	5	3	3
SAKWIM	5	5	5	5	5
SUVROS	5	5	5	5	5
YIMHOT	5	5	5	5	
YUMVUX	5	5	5	3	

Table S27: PBE0/def2-TZVP electronic energy results for Co(II) complexes

Identifier	Doublet energy (Hartrees)	Quartet energy (Hartrees)
BIHGEE	−4374.008609	−4374.040674
BIHGII	−8601.606037	−8601.638169
BUQVOY	−4466.950895	−4466.968942
CETBOV	−8792.233980	−8792.266324
CETBUB	−4626.171810	−4626.200653
CTPYCO	−3044.705150	−3044.726221
DAHROU	−2740.210809	−2740.226574
FUFVUX	−2912.038439	−2912.076079
JAWJAT	−2795.313029	−2795.334804
JUWPIA	−3589.927816	−3589.922239
KIQREL	−7919.828171	−7919.855364
KIQRIP	−8812.578296	−8812.603265
KIQROV	−3213.622953	−3213.642647
LEGWAW	−4545.450535	−4545.479350
OZIMIV	−2544.192475	−2544.196677
PEBSEW	−3097.983121	−3098.006277
PEBSOG	−3591.768735	−3591.790562
PEBSUM	−3367.643195	−3367.663862
RIPSEO	−3234.718368	−3234.704993
RIPSIS	−3080.047243	−3080.036231
SAPBIV	−3061.965062	−3062.002649
SEQFIE	−2941.737624	−2941.776996
TPORCP	−3293.645562	−3293.636387
TUBTIT	−2117.332527	−2117.333589
UKUJUG	−2655.796293	−2655.826657
VIYGIU	−2871.433268	−2871.453672
XIZLUO	−3430.337247	−3430.363539
YUDGUA	−4564.636090	−4564.668109

Table S28: B3LYP/def2-TZVP electronic energy results for Co(II) complexes

Identifier	Doublet energy (Hartrees)	Quartet energy (Hartrees)
BIHGEE	−4375.322286	−4375.351554
BIHGII	−8603.088352	−8603.117851
BUQVOY	−4468.327349	−4468.344031
CETBOV	−8793.808530	−8793.838258
CETBUB	−4627.685944	−4627.712272
CTPYCO	−3045.493087	−3045.508803
DAHROU	−2741.171779	−2741.181054
FUFVUX	−2912.738493	−2912.772732
JAWJAT	−2796.306629	−2796.325568
JUWPIA	−3590.994788	−3590.982633
KIQREL	−7921.150132	−7921.172946
KIQRIP	−8814.390261	−8814.412890
KIQROV	−3214.840584	−3214.855064
LEGWAW	−4546.925659	−4546.950171
OZIMIV	−2545.024892	−2545.023414
PEBSEW	−3099.142660	−3099.160833
PEBSOG	−3593.207764	−3593.223682
PEBSUM	−3368.957093	−3368.972012
RIPSEO	−3235.754756	−3235.736397
RIPSIS	−3080.995479	−3080.979904
SAPBIV	−3062.753988	−3062.788336
SEQFIE	−2942.467730	−2942.504342
TPORCP	−3294.876579	−3294.861289
TUBTIT	−2117.904852	−2117.901644
UKUJUG	−2656.677760	−2656.704508
VIYGIU	−2872.466502	−2872.480201
XIZLUO	−3431.411782	−3431.434173
YUDGUA	−4566.041891	−4566.071191

Table S29: TPSSh/def2-TZVP electronic energy results for Co(II) complexes

Identifier	Doublet energy (Hartrees)	Quartet energy (Hartrees)
BIHGEE	−4376.670529	−4376.694584
BIHGII	−8604.358647	−8604.382809
BUQVOY	−4469.813744	−4469.819282
CETBOV	−8795.197264	−8795.222077
CETBUB	−4629.251741	−4629.271217
CTPYCO	−3046.229604	−3046.233029
DAHROU	−2741.945779	−2741.950636
FUFVUX	−2913.379996	−2913.412475
JAWJAT	−2797.248289	−2797.258356
JUWPIA	−3592.107658	−3592.089334
KIQREL	−7922.222978	−7922.238147
KIQRIP	−8816.081896	−8816.091012
KIQROV	−3216.113497	−3216.120132
LEGWAW	−4548.331725	−4548.351078
OZIMIV	−2545.808724	−2545.799288
PEBSEW	−3100.252908	−3100.265081
PEBSOG	−3594.644999	−3594.654519
PEBSUM	−3370.289215	−3370.299338
RIPSEO	−3236.890818	−3236.864707
RIPSIS	−3082.018234	−3082.013132
SAPBIV	−3063.483155	−3063.515836
SEQFIE	−2943.087821	−2943.122789
TPORCP	−3296.297799	−3296.277535
TUBTIT	−2118.521627	−2118.506614
UKUJUG	−2657.706219	−2657.721446
VIYGIU	−2873.467365	−2873.475724
XIZLUO	−3432.275344	−3432.292549
YUDGUA	−4567.508782	−4567.533137

Table S30: M06-L/def2-TZVP electronic energy results for Co(II) complexes

Identifier	Doublet energy (Hartrees)	Quartet energy (Hartrees)
BIHGEE	−4376.235283	−4376.256165
BIHGII	−8603.945869	−8603.966155
BUQVOY	−4469.585359	−4469.582554
CETBOV	−8794.756805	−8794.775540
CETBUB	−4628.775674	−4628.783668
CTPYCO	−3045.980892	−3045.982206
DAHROU	−2741.687819	−2741.688313
FUFVUX	−2913.153563	−2913.182321
JAWJAT	−2796.943801	−2796.948432
JUWPIA	−3591.760035	−3591.741398
KIQREL	−7921.878568	−7921.891493
KIQRIP	−8815.590321	−8815.596632
KIQROV	−3215.729292	−3215.731477
LEGWAW	−4547.878947	−4547.890622
OZIMIV	−2545.546288	−2545.535952
PEBSEW	−3099.899465	−3099.904402
PEBSOG	−3594.203984	−3594.209128
PEBSUM	−3369.862083	−3369.866621
RIPSEO	−3236.531708	−3236.511047
SAPBIV	−3063.226836	−3063.255697
SEQFIE	−2942.864639	−2942.898425
TPORCP	−3295.850305	−3295.826071
TUBTIT	−2118.319333	−2118.303953
UKUJUG	−2657.382470	−2657.399285
VIYGIU	−2873.143943	−2873.147298
YUDGUA	−4567.046276	−4567.064725

Table S31: Spin state predictions for Co(II). Green coloured boxes denote correctly predicted spin state, red coloured boxes denote incorrectly predicted spin state, white coloured box denote failed calculation.

Identifier	Multiplicity	B3LYP	PBE0	TPSSh	M06-L
BIHGEE	4	4	4	4	4
BIHGII	4	4	4	4	4
BUQVOY	2	4	4	4	2
CETBOV	4	4	4	4	4
CETBUB	4	4	4	4	4
CTPYCO	4	4	4	4	4
DAHROU	4	4	4	4	4
FUFVUX	4	4	4	4	4
JAWJAT	4	4	4	4	4
JUWPIA	2	2	2	2	2
KIQREL	4	4	4	4	4
KIQRIP	4	4	4	4	4
KIQROV	4	4	4	4	4
LEGWAW	4	4	4	4	4
OZIMIV	4	2	4	2	2
PEBSEW	4	4	4	4	4
PEBSOG	4	4	4	4	4
PEBSUM	4	4	4	4	4
RIPSEO	2	2	2	2	2
RIPSIS	2	2	2	2	
SAPBIV	4	4	4	4	4
SEQFIE	4	4	4	4	4
TPORCP	2	2	2	2	2
TUBTIT	2	2	4	2	2
UKUJUG	4	4	4	4	4
VIYGIU	4	4	4	4	4
XIZLUO	4	4	4	4	
YUDGUA	4	4	4	4	4

2.1.2 Analysis of optimised structures and their spin states

Table S32: Categorising the geometries of 5-coordinate complexes with Addison's τ index.[118]

Identifier	Metal Center	Multiplicity	Closest Point Group	Addison's τ index
CTPYCO	Co(II)	4	D_{3h}	0.50
MOL1DT	Co(II)	4	D_{3h}	0.88
CELVEU	Fe(III)	6	C_{4v}	0.58
ELIRUN	Fe(III)	6	C_{4v}	0.48
GEDTUE	Fe(III)	4	C_{4v}	0.57
IXUNIY	Fe(III)	4	C_{4v}	0.57
KANYUT	Fe(III)	6	C_{4v}	0.48
LUJNOV	Fe(III)	6	D_{3h}	0.93
OETPFE	Fe(III)	4	C_{4v}	0.25
QOXVUW	Fe(III)	6	D_{3h}	0.63
SAVHIG	Fe(III)	6	D_{3h}	0.97
SELQIJ	Fe(III)	4	C_{4v}	0.65
TISDUU	Fe(III)	4	C_{4v}	0.30
WUQBAN	Fe(III)	6	D_{3h}	0.58
OKUXUO	Mn(II)	6	D_{3h}	0.83

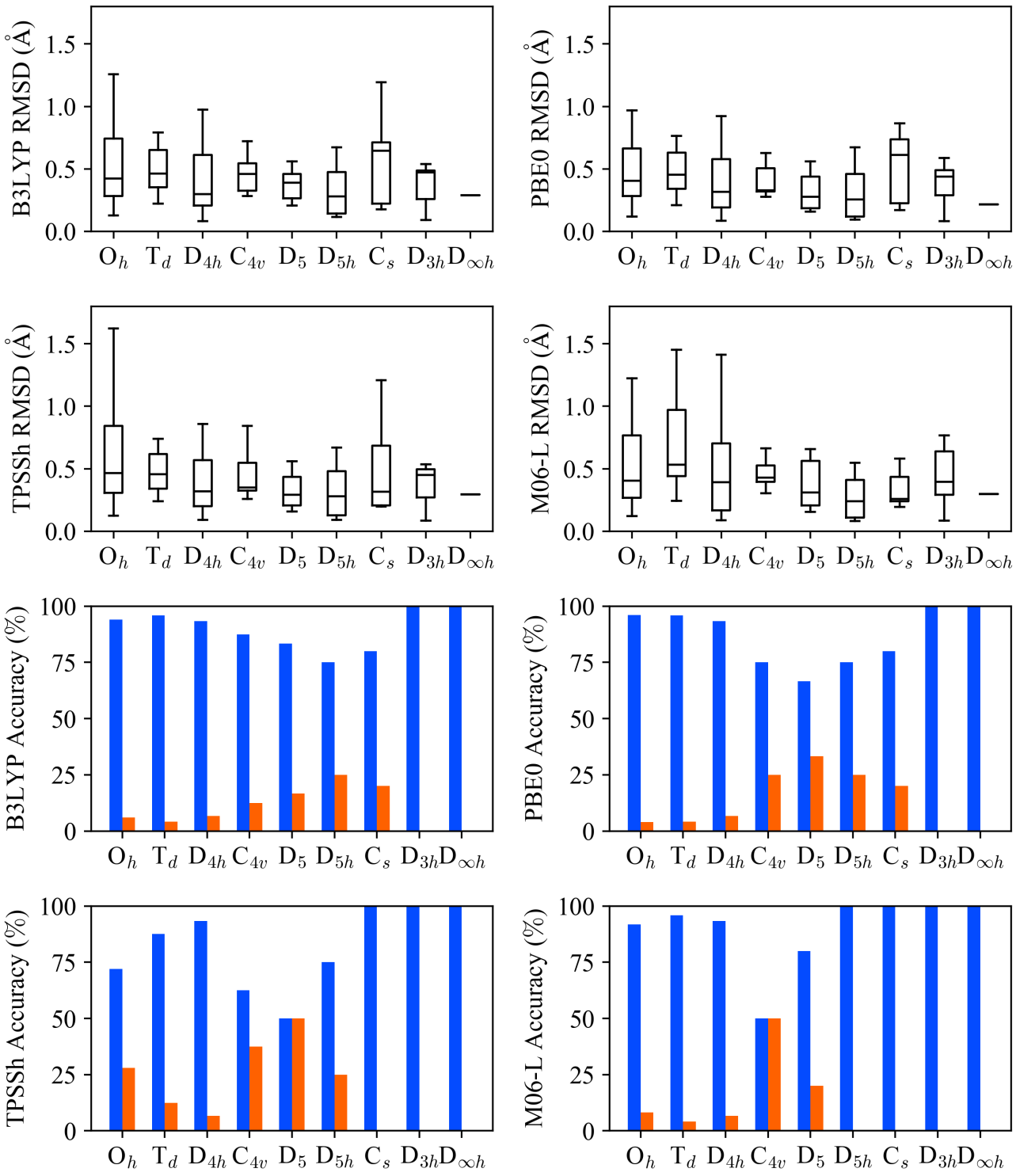

Figure S1: Top Half: Box plots showing the of RMSD values of DFT optimised geometries against XRD geometries across the different types of coordination environments and DFT methods. Bottom Half: Prediction accuracy of the various DFT methods across the different types of metal complex geometries, blue indicates correctly predicted ground state multiplicity and orange indicates incorrectly predicted ground state multiplicity.

2.1.3 ωB97X-D2/def2-TZVP Results

Table S33: Electronic energy (Hartrees) results for Cr(II) and predicted multiplicity. Green boxes denote correctly predicted spin state and red boxes denote incorrectly predicted spin state.

Identifier	Singlet Energy	Triplet Energy	Quintet Energy	Predicted Multiplicity
CAMVER	-2965.955172	-2965.999181	-2965.982692	3
CIDVOA	-2222.609919	-2222.654104	-2222.732286	5
KAPPEW	-3123.041583	-3123.101	-3123.160284	5
LESMAX	-1509.951327	-1510.042339	-1510.031809	3
OKIJUQ	-1893.307298	-1893.33705	-1893.399146	5
PIXXEE	-1755.8567	-1755.776269	-1755.850761	1
SOFXAM	-2712.377851	-2712.408296	-2712.476013	5

Table S34: Electronic energy (Hartrees) results for Mn(II) and predicted multiplicity. Green boxes denote correctly predicted spin state and red boxes denote incorrectly predicted spin state.

Identifier	Doublet Energy	Quartet Energy	Sextet Energy	Predicted Multiplicity
AXUMEL	-5691.314979	-5691.317417	-5691.291232	4
BIKZUQ	-3037.913493	-3037.922155	-3037.970841	6
NUYZIS	-2968.828331	-2968.856848	-2968.896004	6
ODIZEG	-2771.998506	-2771.999511	-2772.00754	6
TUSBIT	-2438.261703	-2438.279874	-2438.340206	6

Table S35: Electronic energy (Hartrees) results for Fe(III) and predicted multiplicity. Green boxes denote correctly predicted spin state and red boxes denote incorrectly predicted spin state.

Identifier	Doublet Energy	Quartet Energy	Sextet Energy	Predicted Multiplicity
CELVEU	-3399.44723	-3399.471247	-3399.483534	6
CEQPOF	-2339.066817	-2339.059844	-2339.049553	2
FEACAC	-2299.24961	-2299.244484	-2299.271302	6
GEDTUE	-3814.021912	-3814.059402	-3814.057749	4
LUJNOV	-3318.189184	-3318.205055	-3318.232842	6
OQODEE	-3367.306679	-3367.318894	-3367.341538	6
POGXEQ	-3206.262347	-3206.262063	-3206.295668	6
UHEZOX	-2775.169232	-2775.158965	-2775.179299	6
UHIBAP	-2407.758294	-2407.726603	-2407.753613	2
UWIQIB	-2946.658507	-2946.653437	-2946.686816	6

Table S36: Electronic energy (Hartrees) results for Fe(II) and predicted multiplicity. Green boxes denote correctly predicted spin state and red boxes denote incorrectly predicted spin state.

Identifier	Singlet Energy	Triplet Energy	Quintet Energy	Predicted Multiplicity
SUVROS	-3313.656935	-3313.675263	-3313.721674	5

Table S37: Electronic energy (Hartrees) results for Co(II) and predicted multiplicity. Green boxes denote correctly predicted spin state and red boxes denote incorrectly predicted spin state.

Identifier	Doublet Energy	Quartet Energy	Predicted Multiplicity
CTPYCO	-3045.686734	-3045.710095	4
SAPBIV	-3062.936451	-3062.991282	4
SEQFIE	-2942.659895	-2942.645093	2
TUBTIT	-2117.95646	-2117.952764	2
XIZLUO	-3431.60814	-3431.635269	4

Table S38: P1-score and calculation success rate of ωB97X-D2/def2-TZVP calculations.

Metal centre	Cr(II)	Mn(II)	Fe(III)	Fe(II)	Co(II)
P1-score (%)	71	60	100	100	80
Success rate (%)	39	13	36	4	18

2.1.4 Spin Contamination Analysis

Table S39: Proportion (%) of complexes with calculated spin deviation values exceeding 10% error of the spin expectation value.

Method	B3LYP	PBE0	TPSSh	M06-L
Cr(II)	26	31	29	31
Mn(II)	25	34	29	34
Fe(III)	21	24	23	14
Fe(II)	17	15	15	13
Co(II)	34	38	20	13
All Metals	25	29	23	21

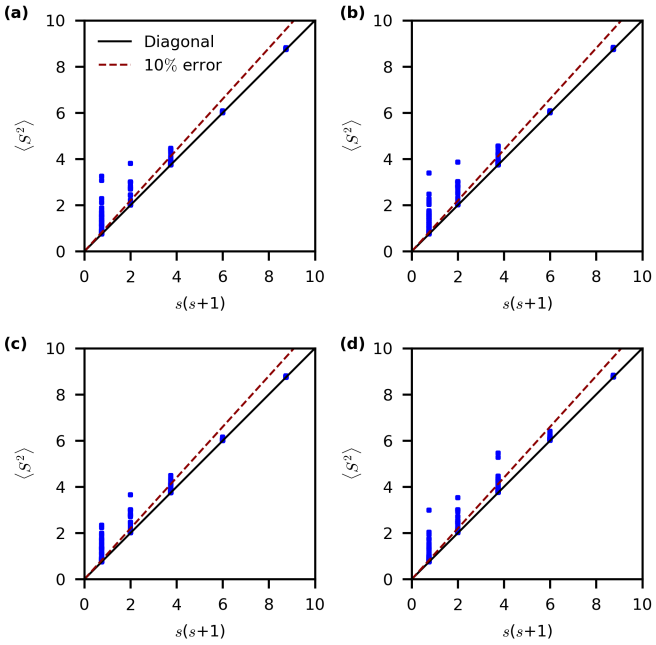

Figure S2: Scatter plot comparing $\langle S^2 \rangle$ deviations across four DFT methods as a function of ideal spin expectation values S(S+1). Red line represent the 10% spin deviation error tolerance for reference.

3 Prediction of T_{SCO} with DFT methods

3.1 Thermodynamic results

3.1.1 Results with B3LYP

Table S40: B3LYP/def2-TZVP calculated entropies, enthalpies ($J.mol^{-1}.K^{-1}$, $kJ.mol^{-1}$) and T_{SCO} (K) values.

Identifier	Exp ΔS	Comp ΔS	Exp ΔH	Comp ΔH	Exp T_{SCO}	Comp T_{SCO}
BAXFIS02		60		-7.6	333	-127
HALC-1	101.0	59	24.1	-18.8	248	-320
HALC-13	90.0	57	21.2	-21.0	234	-366
HALC-3		56		-19.9	213	-356
HALC-20	78.0	55	20.1	-21.4	259	-386
HALC-12	96.0	58	21.9	-21.4	226	-370
HALC-4	146.0	57	40.9	-18.1	281	-320
HALC-11		58		-22.7	215	-390
HALC-14	98.0	58	23.2	-20.4	236	-354
HALC-2		58		-20.1	216	-348
HALC-7	67.0	57	20.6	-20.0	309	-353
HALC-9		65		-23.2	164	-357
HALC-10		60		-22.5	158	-375
HALC-8		57		-23.4	215	-413
HALC-15		57		-22.9	246	-401
HALC-16		58		-23.3	194	-403
HALC-18	112.0	56	33.0	-19.1	294	-342
HALC-17	81.0	57	23.0	-19.6	284	-346
HALC-27		57		-20.4	238	-361
HALC-23	99.0	56	25.7	-18.0	259	-320
HALC-26		57		-20.7	231	-364
HALC-25	99.0	57	24.4	-15.8	246	-278
HALC-28	80.0	56	19.2	-19.5	237	-351
HALC-22	96.0	58	26.4	-17.7	273	-305
HALC-24	76.0	52	19.0	-16.9	251	-325
HPZBFE		60		-3.8	393	-64
KEKVIF03		61		-35.9	176	-593
NEFSUM02		62		-23.8	160	-382
WAHKEX		58		-48.9	184	-847

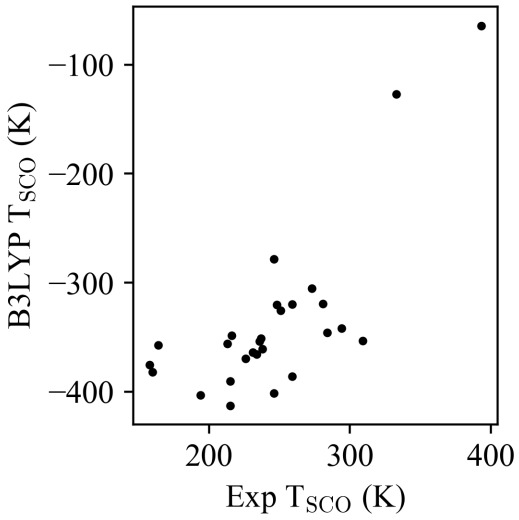

Figure S3: Predicted *vs* calculated T_{SCO} using B3LYP/def2-TZVP.

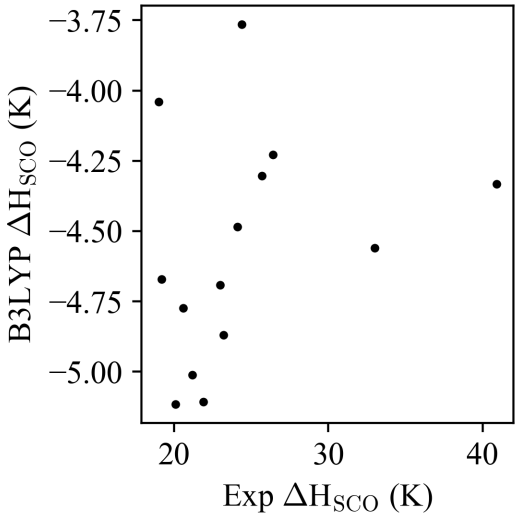

Figure S4: Predicted *vs* calculated ΔH_{SCO} using B3LYP/def2-TZVP.

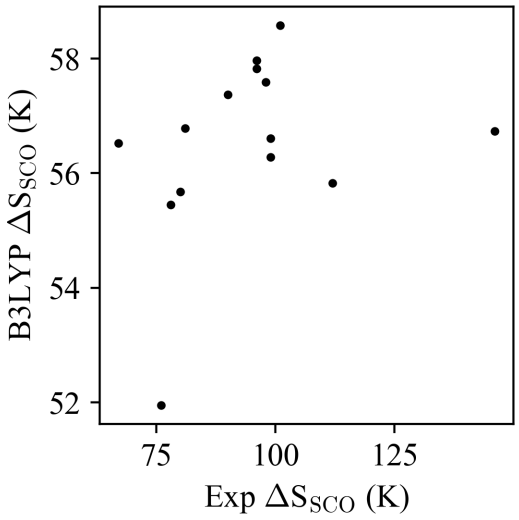

Figure S5: Predicted *vs* calculated ΔS_{SCO} using B3LYP/def2-TZVP.

3.1.2 Results with M06-L

Table S41: M06-L/def2-TZVP calculated entropies, enthalpies ($J.mol^{-1}.K^{-1}$, $kJ.mol^{-1}$) and T_{SCO} (K) values.

Identifier	Exp ΔS	Comp ΔS	Exp ΔH	Comp ΔH	Exp T_{SCO}	Comp T_{SCO}
BAXFIS02		59		31.9	333	544
HALC-1	101.0	51	24.1	9.8	248	190
HALC-13	90.0	50	21.2	7.2	234	143
HALC-3		49		7.1	213	144
HALC-12	96.0	51	21.9	6.8	226	133
HALC-11		51		5.4	215	106
HALC-14	98.0	50	23.2	7.7	236	156
HALC-2		46		8.3	216	180
HALC-9		59		2.1	164	35
HALC-10		49		3.6	158	72
HALC-8		51		6.2	215	120
HALC-16		53		3.6	194	68
HALC-18	112.0	55	33.0	7.4	294	135
HALC-17	81.0	52	23.0	9.0	284	174
HALC-27		50		8.1	238	163
HALC-23	99.0	47	25.7	11.5	259	243
HALC-26		50		7.3	231	148
HALC-25	99.0	49	24.4	13.6	246	279
HALC-28	80.0	48	19.2	9.3	237	196
HALC-22	96.0	53	26.4	11.5	273	219
HALC-24	76.0	56	19.0	15.1	251	271
HPZBFE		62		36.1	393	584
KEKVIF03		41		-20.8	176	-507
NEFSUM02		52		4.8	160	92
WAHKEX		55		-33.1	184	-597

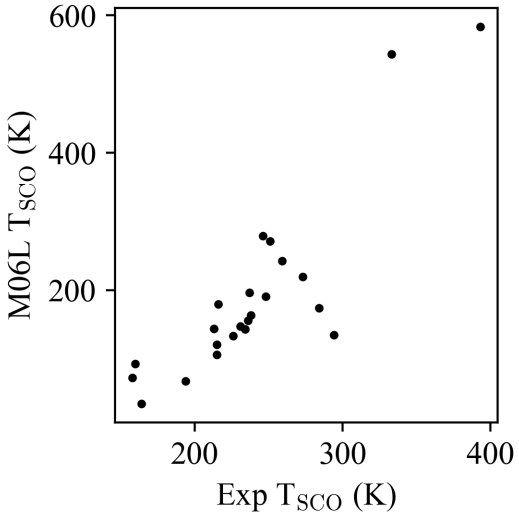

Figure S6: Predicted *vs* calculated T_{SCO} using M06-L/def2-TZVP.

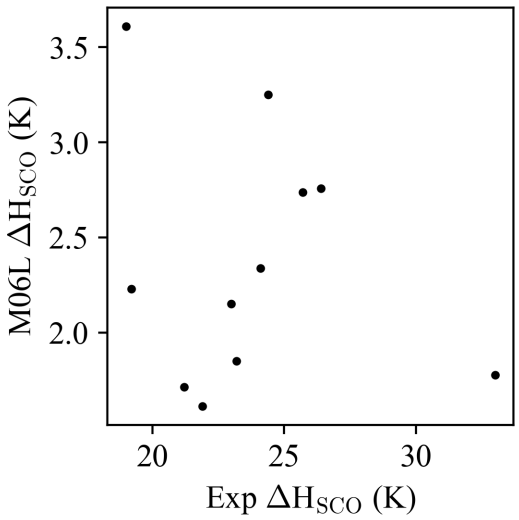

Figure S7: Predicted *vs* calculated ΔH_{SCO} using M06-L/def2-TZVP.

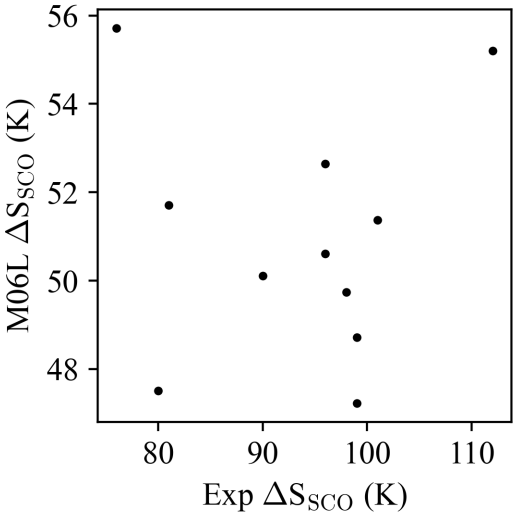

Figure S8: Predicted *vs* calculated ΔS_{SCO} using M06-L/def2-TZVP.

3.1.3 Results with PBE0

Table S42: PBE0/def2-TZVP calculated entropies, enthalpies ($J.mol^{-1}.K^{-1}$, $kJ.mol^{-1}$) and T_{SCO} (K) values.

Identifier	Exp ΔS	Comp ΔS	Exp ΔH	Comp ΔH	Exp T_{SCO}	Comp T_{SCO}
BAXFIS02		62		-25.6	333	-411
HALC-1	101.0	60	24.1	-39.7	248	-657
HALC-13	90.0	59	21.2	-42.1	234	-718
HALC-3		57		-41.0	213	-722
HALC-20	78.0	56	20.1	-42.3	259	-756
HALC-21	81.0	56	21.1	-41.8	261	-750
HALC-12	96.0	59	21.9	-42.5	226	-718
HALC-4	146.0	58	40.9	-38.9	281	-667
HALC-11		60		-43.9	215	-735
HALC-14	98.0	59	23.2	-41.4	236	-706
HALC-2		60		-41.2	216	-685
HALC-7	67.0	58	20.6	-40.9	309	-706
HALC-9		62		-44.6	164	-724
HALC-10		61		-43.9	158	-720
HALC-8		61		-43.2	215	-707
HALC-15		60		-43.0	246	-715
HALC-16		58		-44.1	194	-760
HALC-18	112.0	57	33.0	-40.0	294	-700
HALC-17	81.0	59	23.0	-40.6	284	-693
HALC-27		58		-41.3	238	-712
HALC-23	99.0	58	25.7	-38.9	259	-669
HALC-26		58		-41.7	231	-713
HALC-25	99.0	58	24.4	-36.6	246	-633
HALC-28	80.0	58	19.2	-40.3	237	-699
HALC-22	96.0	60	26.4	-38.5	273	-642
HALC-24	76.0	53	19.0	-37.7	251	-715
HPZBFE		63		-20.8	393	-332
KEKVIF03		66		-53.6	176	-810
NEFSUM02		64		-42.1	160	-655
WAHKEX		58		-66.8	184	-1145

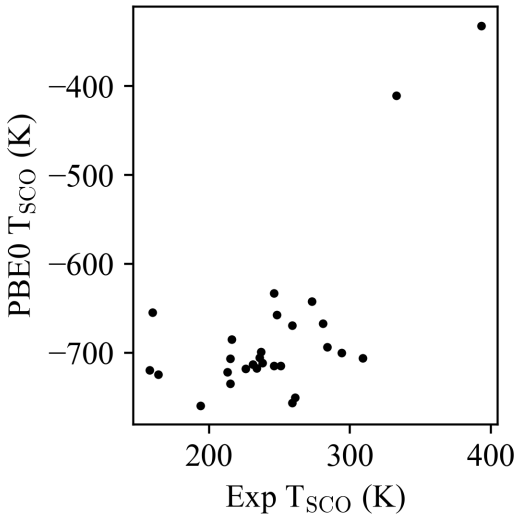

Figure S9: Predicted *vs* calculated T_{SCO} using PBE0/def2-TZVP.

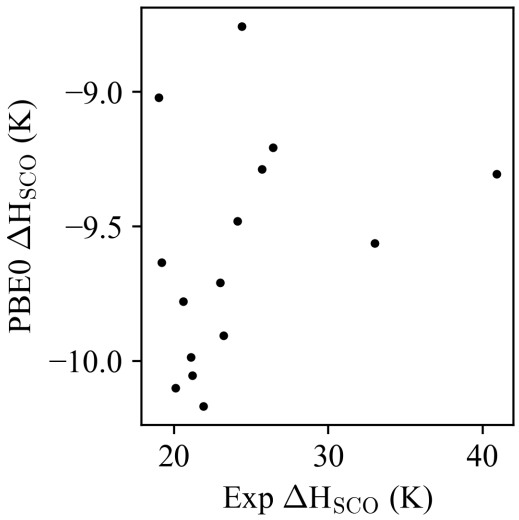

Figure S10: Predicted *vs* calculated ΔH_{SCO} using PBE0/def2-TZVP.

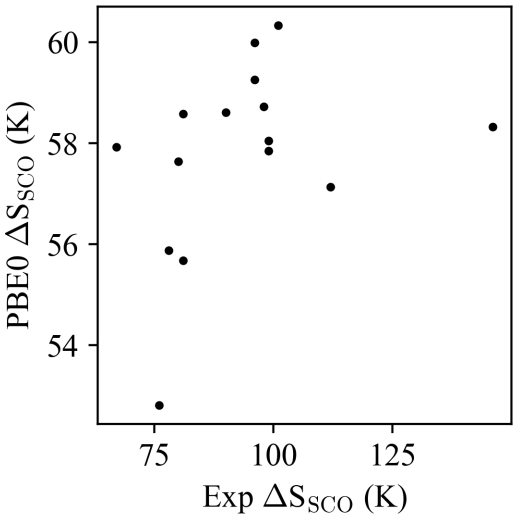

Figure S11: Predicted *vs* calculated ΔS_{SCO} using PBE0/def2-TZVP.

3.1.4 Results with PBE0-D4

Table S43: PBE0-D4/def2-TZVP calculated entropies, enthalpies ($J.mol^{-1}.K^{-1}$, $kJ.mol^{-1}$) and T_{SCO} (K) values.

Identifier	Exp ΔS	Comp ΔS	Exp ΔH	Comp ΔH	Exp T_{SCO}	Comp T_{SCO}
BAXFIS02		64		-6.3	333	-98
HALC-1	101.0	62	24.1	-20.6	248	-330
HALC-13	90.0	61	21.2	-22.9	234	-378
HALC-3		59		-22.2	213	-376
HALC-21	81.0	56	21.1	-23.2	261	-414
HALC-12	96.0	67	21.9	-23.5	226	-350
HALC-4	146.0	60	40.9	-19.7	281	-327
HALC-11		62		-25.1	215	-406
HALC-14	98.0	61	23.2	-22.2	236	-365
HALC-2		62		-22.1	216	-355
HALC-7	67.0	60	20.6	-21.7	309	-363
HALC-9		63		-25.7	164	-408
HALC-10		63		-24.9	158	-396
HALC-8		62		-24.0	215	-386
HALC-15		62		-23.9	246	-388
HALC-16		60		-24.6	194	-409
HALC-18	112.0	57	33.0	-21.2	294	-374
HALC-17	81.0	60	23.0	-21.3	284	-353
HALC-27		60		-21.3	238	-354
HALC-23	99.0	60	25.7	-19.1	259	-319
HALC-26		61		-22.1	231	-364
HALC-25	99.0	60	24.4	-16.4	246	-273
HALC-28	80.0	60	19.2	-19.7	237	-329
HALC-22	96.0	62	26.4	-18.8	273	-303
HALC-24	76.0	54	19.0	-16.3	251	-302
HPZBFE		65		-0.2	393	-3
KEKVIF03		46		-46.6	176	-1015
WAHKEX		58		-54.2	184	-928

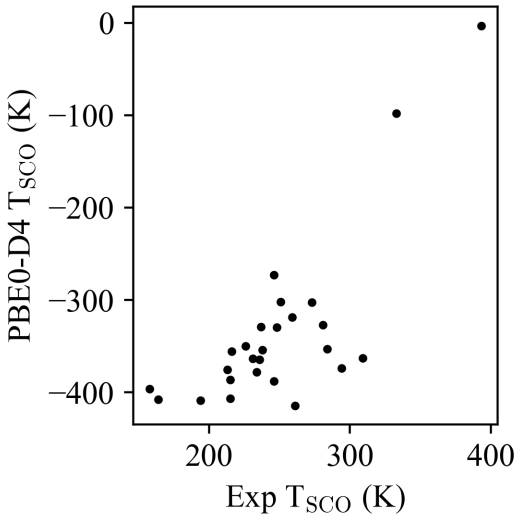

Figure S12: Predicted *vs* calculated T_{SCO} using PBE0-D4/def2-TZVP.

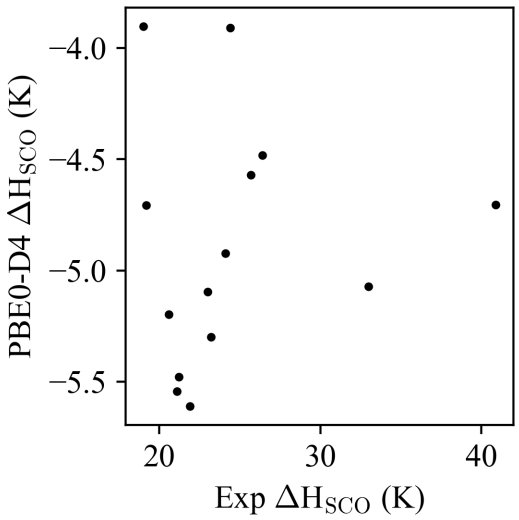

Figure S13: Predicted *vs* calculated H_{SCO} using PBE0-D4/def2-TZVP.

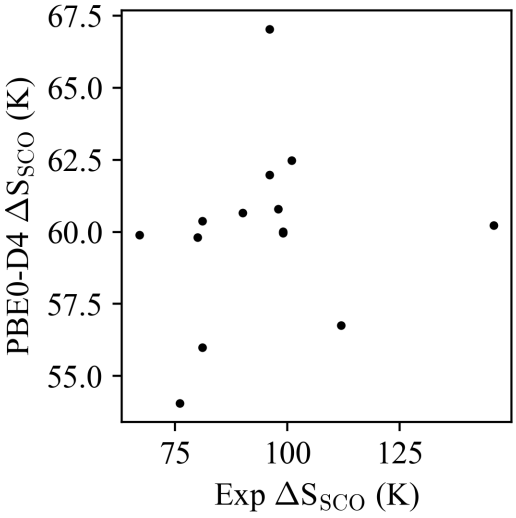

Figure S14: Predicted *vs* calculated ΔS_{SCO} using PBE0-D4/def2-TZVP.

3.1.5 Results with PBE0-D4 and acetone as solvent

Table S44: PBE0-D4/def2-TZVP with acetone SMD solvent model calculated entropies, enthalpies ($J.mol^{-1}.K^{-1}$, $kJ.mol^{-1}$) and T_{SCO} (K) values.

Identifier	Exp ΔS	Comp ΔS	Exp ΔH	Comp ΔH	Exp T_{SCO}	Comp T_{SCO}
HALC-1	101	69	24.1	−6.7	248	−407
HALC-12	96	68	21.9	−7.1	226	−434
HALC-13	90	65	21.2	−6.9	234	−445
HALC-14	98	66.1	23.2	−7	236	−441
HALC-16		58.1		−7.8	194	−560
HALC-17	81	69.3	23	−7.1	284	−430
HALC-19	79	57.8	19.4	−7.3	245	−527
HALC-25	99	71	24.4	−6.5	246	−381
HALC-28	80	53	19.2	−7.5	237	−589
HALC-4	146	65.6	40.9	−6.2	281	−396

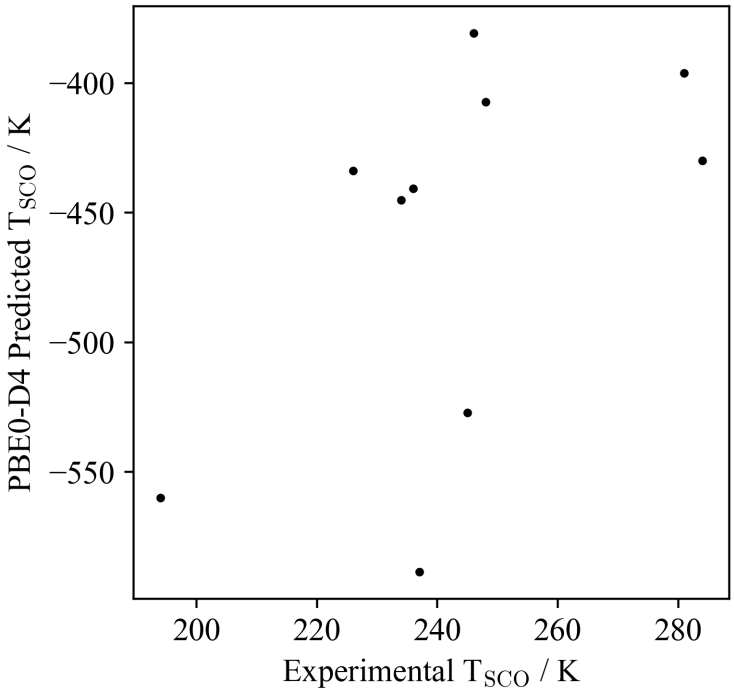

Figure S15: Predicted *vs* calculated T_{SCO} using PBE0-D4/def2-TZVP and acetone as solvent.

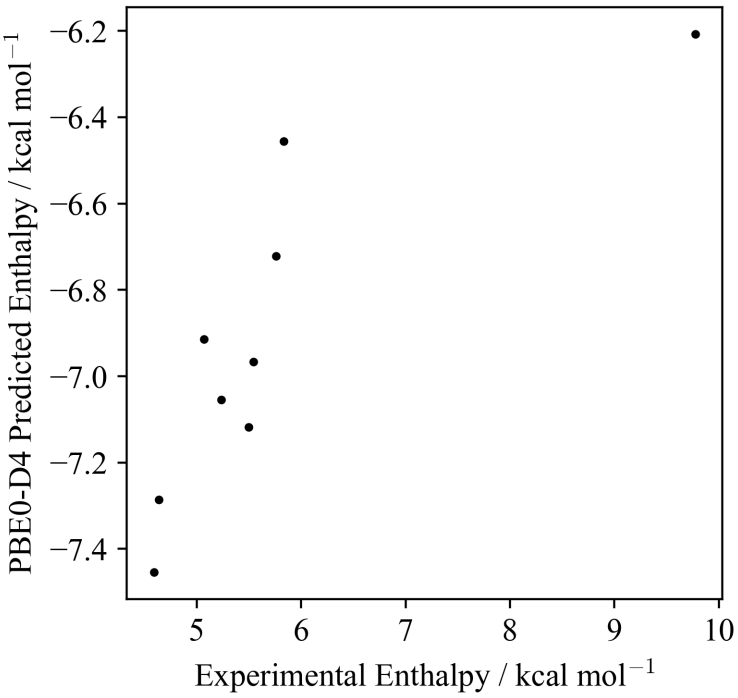

Figure S16: Predicted *vs* calculated ΔH_{SCO} using PBE0-D4/def2-TZVP and acetone as solvent.

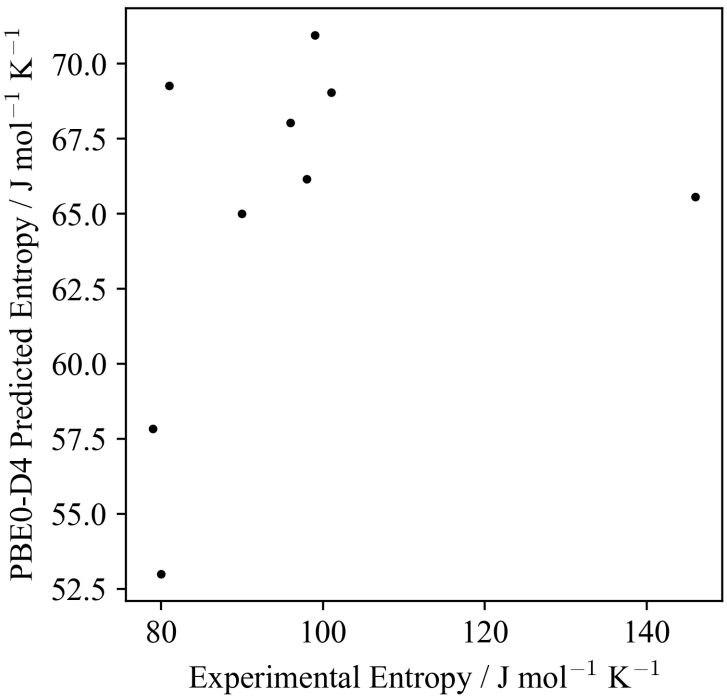

Figure S17: Predicted *vs* calculated ΔS_{SCO} using PBE0-D4/def2-TZVP and acetone as solvent.

3.1.6 Results with PBE0-D4 and nitromethane as solvent

Table S45: PBE0-D4/def2-TZVP with nitromethane SMD solvent model calculated entropies, enthalpies (J.mol^{-1}.K^{-1}, kJ.mol^{-1}) and T_{SCO} (K) values.

Identifier	Exp ΔS	Comp ΔS	Exp ΔH	Comp ΔH	Exp T_{SCO}	Comp T_{SCO}
HALC-11		77.8		−7.3	215	−392
HALC-15		63.9		−7.1	246	−464
HALC-18	112	56.6	33	−6.1	294	−452
HALC-22	96	68.8	26.4	−6.5	273	−398
HALC-26		68.5		−7.1	231	−434
HALC-27		66		−7.1	238	−448

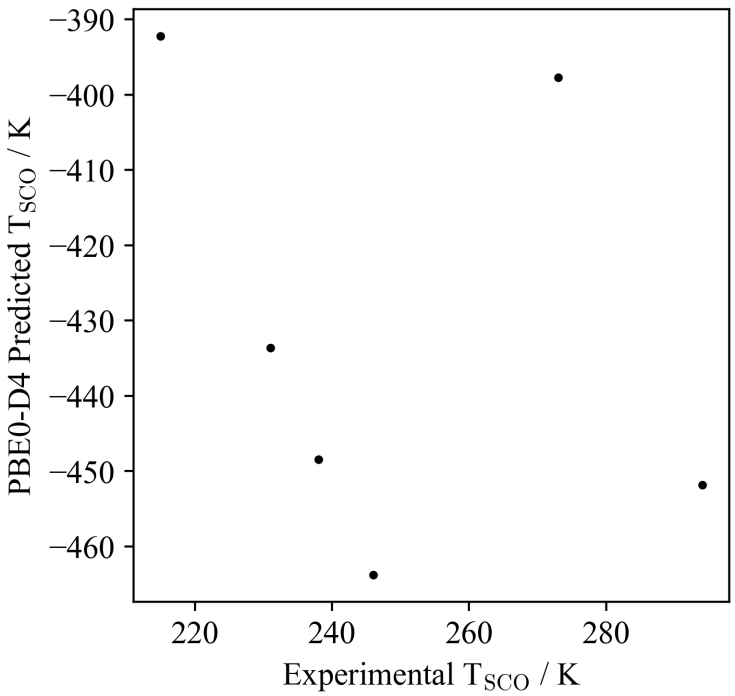

Figure S18: Predicted *vs* calculated T_{SCO} using PBE0-D4/def2-TZVP and nitromethane as solvent.

3.1.7 Results with TPSSh

Table S46: TPSSh/def2-TZVP calculated entropies, enthalpies ($J.mol^{-1}.K^{-1}$, $kJ.mol^{-1}$) and T_{SCO} (K) values.

Identifier	Exp ΔS	Comp ΔS	Exp ΔH	Comp ΔH	Exp T_{SCO}	Comp T_{SCO}
BAXFIS02		67		50.8	333	762
HALC-1	101.0	70	24.1	39.3	248	562
HALC-13	90.0	63	21.2	36.5	234	579
HALC-3		59		39.4	213	670
HALC-20	78.0	61	20.1	37.2	259	613
HALC-12	96.0	63	21.9	36.1	226	568
HALC-4	146.0	62	40.9	40.8	281	657
HALC-11		65		34.4	215	533
HALC-14	98.0	63	23.2	37.2	236	591
HALC-2		64		37.4	216	586
HALC-7	67.0	62	20.6	39.0	309	632
HALC-9		60		32.8	164	544
HALC-10		61		32.8	158	541
HALC-8		60		34.5	215	576
HALC-15		67		35.2	246	522
HALC-16		61		34.5	194	568
HALC-18	112.0	61	33.0	39.7	294	650
HALC-17	81.0	65	23.0	38.3	284	587
HALC-27		63		37.1	238	588
HALC-23	99.0	62	25.7	40.0	259	642
HALC-26		63		36.7	231	583
HALC-25	99.0	63	24.4	42.8	246	680
HALC-28	80.0	67	19.2	38.7	237	579
HALC-22	96.0	64	26.4	40.5	273	634
HALC-24	76.0	60	19.0	41.7	251	700
HPZBFE		67		54.8	393	824
KEKVIF03		64		25.0	176	392
NEFSUM02		64		34.7	160	542
WAHKEX		61		7.4	184	122

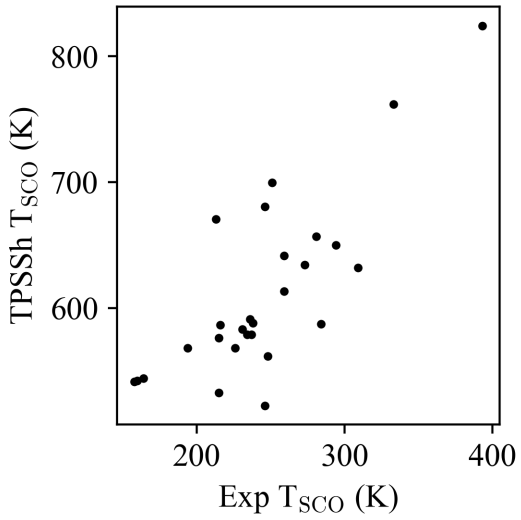

Figure S19: Predicted *vs* calculated T_{SCO} using TPSSh/def2-TZVP.

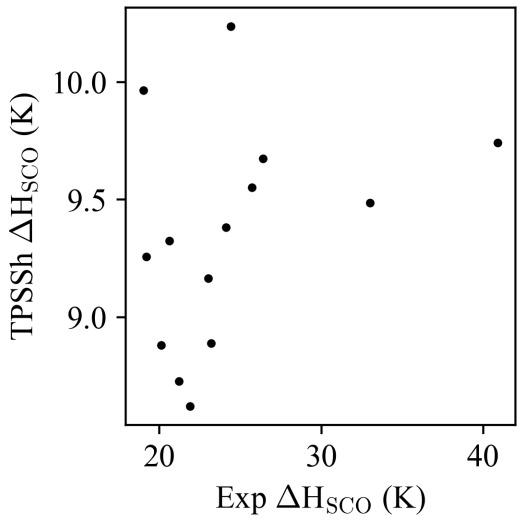

Figure S20: Predicted *vs* calculated ΔH_{SCO} using TPSSh/def2-TZVP.

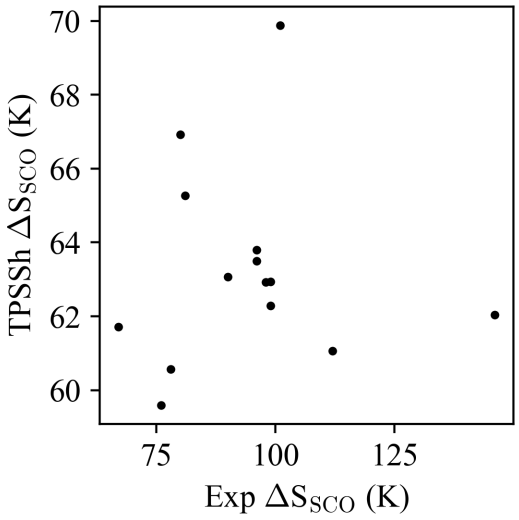

Figure S21: Predicted *vs* calculated ΔS_{SCO} using TPSSh/def2-TZVP.

3.1.8 Results with r^{2}SCAN

Table S47: r^{2}SCAN/def2-TZVP calculated entropies, enthalpies (J.mol^{-1}.K^{-1}, kJ.mol^{-1}) and T_{SCO} (K) values.

Identifier	Exp ΔS	Comp ΔS	Exp ΔH	Comp ΔH	Exp T_{SCO}	Comp T_{SCO}
BAXFIS02		70		57.2	333	823
HALC-1	101.0	59	24.1	39.4	248	666
HALC-13	90.0	58	21.2	36.1	234	620
HALC-3		54		38.4	213	717
HALC-20	78.0	57	20.1	36.6	259	642
HALC-21	81.0	57	21.1	36.2	261	637
HALC-12	96.0	64	21.9	35.7	226	557
HALC-4	146.0	57	40.9	40.7	281	708
HALC-11		58		34.1	215	586
HALC-14	98.0	58	23.2	36.8	236	632
HALC-2		58		37.2	216	645
HALC-7	67.0	57	20.6	38.5	309	675
HALC-9		59		32.9	164	558
HALC-10		59		33.5	158	571
HALC-8		59		34.7	215	593
HALC-15		58		34.5	246	596
HALC-16		58		34.8	194	600
HALC-18	112.0	56	33.0	39.0	294	701
HALC-17	81.0	58	23.0	38.0	284	650
HALC-27		57		37.0	238	653
HALC-23	99.0	57	25.7	40.5	259	713
HALC-26		57		36.7	231	642
HALC-25	99.0	57	24.4	43.6	246	768
HALC-28	80.0	57	19.2	38.0	237	670
HALC-22	96.0	58	26.4	41.0	273	703
HALC-24	76.0	56	19.0	42.7	251	769
HPZBFE		70		62.2	393	892
KEKVIF03		49		14.4	176	296
NEFSUM02		61		31.3	160	514
WAHKEX		58		-6.0	184	-104

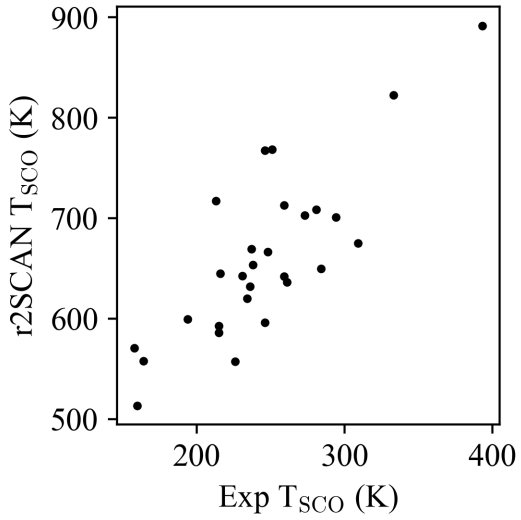

Figure S22: Predicted *vs* calculated T_{SCO} using r^2SCAN/def2-TZVP.

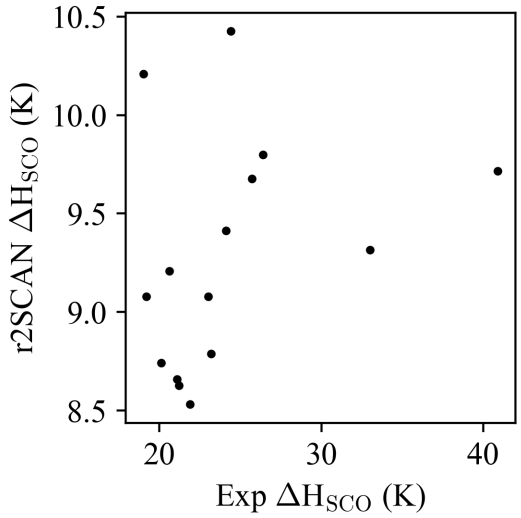

Figure S23: Predicted *vs* calculated ΔH_{SCO} using r^2SCAN/def2-TZVP.

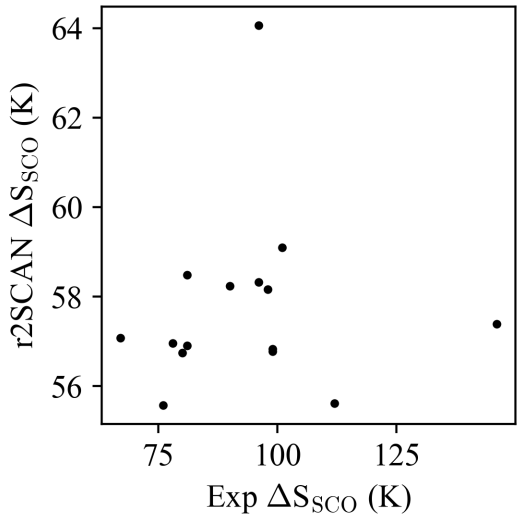

Figure S24: Predicted *vs* calculated ΔS_{SCO} using r^{2}SCAN/def2-TZVP.

3.2 Analysis of optimised structures and prediction metrics

Table S48: Performance of DFT and kestrel prediction of T_{SCO} of the Fe(II) SCO complexes from both Halcrow and non-Halcrow complexes. WAHKEX and KEKVIF complexes were excluded from this analysis since their T_{SCO} values are outliers from the general trend. [a]Comparison of change in entropy and enthalpy values are exclusively for the 16 Halcrow complexes with experimental entropy and enthalpy values. [b]SMD acetone solvent model used. [c]SMD nitromethane solvent model used.

Method	[a]MAE ΔH (kcal·mol^{-1})	[a]MAE ΔS (J·mol^{-1}·K^{-1})	MAE T_{SCO} (K)	StDev T_{SCO} (K)	T_{SCO} r^2
B3LYP	10.4	37.7	581	50	0.57
M06-L	3.3	42.5	88	91	0.75
PBE0-D4	10.8	34.4	584	63	0.59
PBE0	15.4	35.5	925	70	0.46
TPSSh	3.5	31.0	367	44	0.62
r^{2}SCAN	3.5	35.6	415	52	0.66
[b]PBE0-D4	31.1	31.7	704	62	0.29
[c]PBE0-D4	36.0	41.3	680	47	0.07

Table S49: Metrics for T_{SCO} prediction using DFT methods

Method	Slope	Intercept (K)	R^2
B3LYP	1.12	−611	0.57
M06-L	2.07	−312	0.71
PBE0-D4	1.44	−693	0.59
PBE0	1.25	−987	0.46
TPSSh	1.08	347	0.62
r^2SCAN	1.32	334	0.65

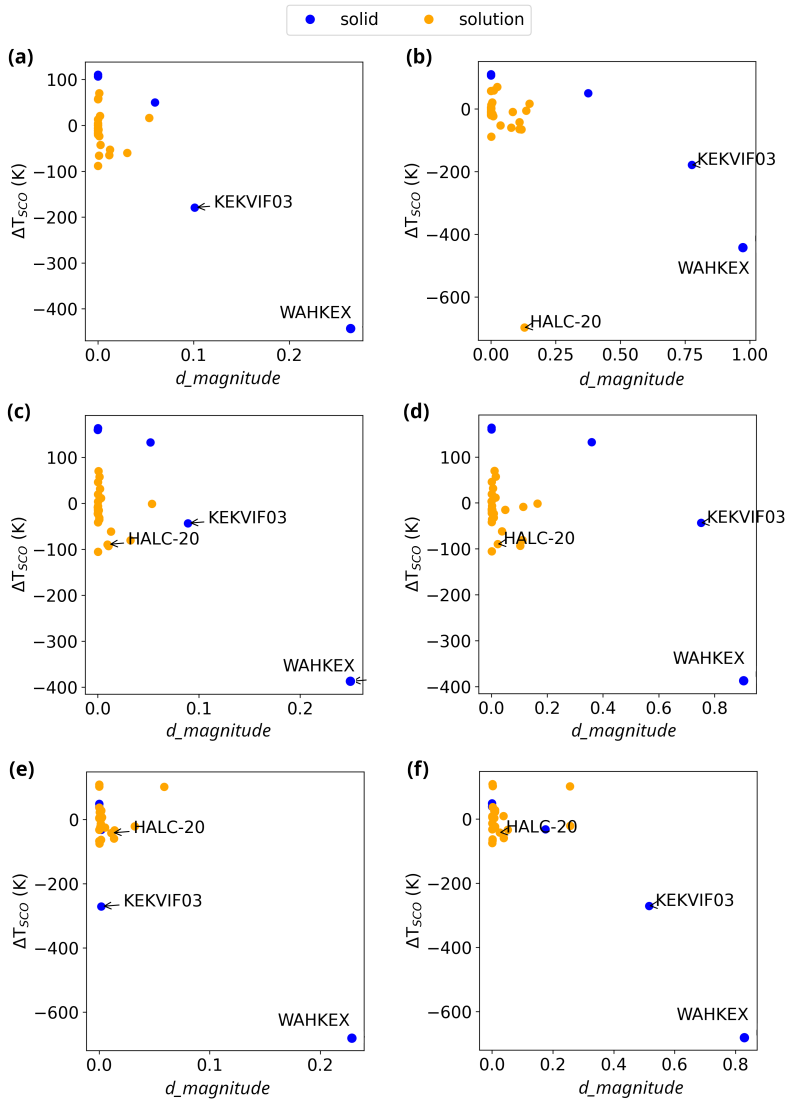

Figure S25: Plots of ΔT_{SCO} *vs d_magnitude* of optimised structures using (a) B3LYP/def2-TZVP and singlet; (b) B3LYP/def2-TZVP and quintet; (c) PBE0/def2-TZVP and singlet; (d) PBE0/def2-TZVP and quintet; (e) r^2SCAN/def2-TZVP and singlet; and (f) r^2SCAN/def2-TZVP and quintet. The outliers HALC-20, WAHKEX and KEKVIF03 are labelled for easy tracking

Table S50: Fe–N–C angles for the SCN– ligands in WAHKEK and KEFVIF03 complexes

Complex/DFT functionals	Singlet, Angle 1	Singlet, Angle 2	Quintet, Angle 1	Quintet, Angle 2
WAHKEK/B3LYP	163.5	170.2	158.3	172.6
WAHKEK/PBE0	160.7	169.1	151.8	168.9
WAHKEK/r^{2}SCAN	156.4	167.0	148.7	163.4
KEFVIF03/B3LYP	169.4	169.4	167.5	167.5
KEFVIF03/PBE0	168.3	168.4	160.5	160.4
KEFVIF03/r^{2}SCAN	147.9	147.9	147.9	147.9

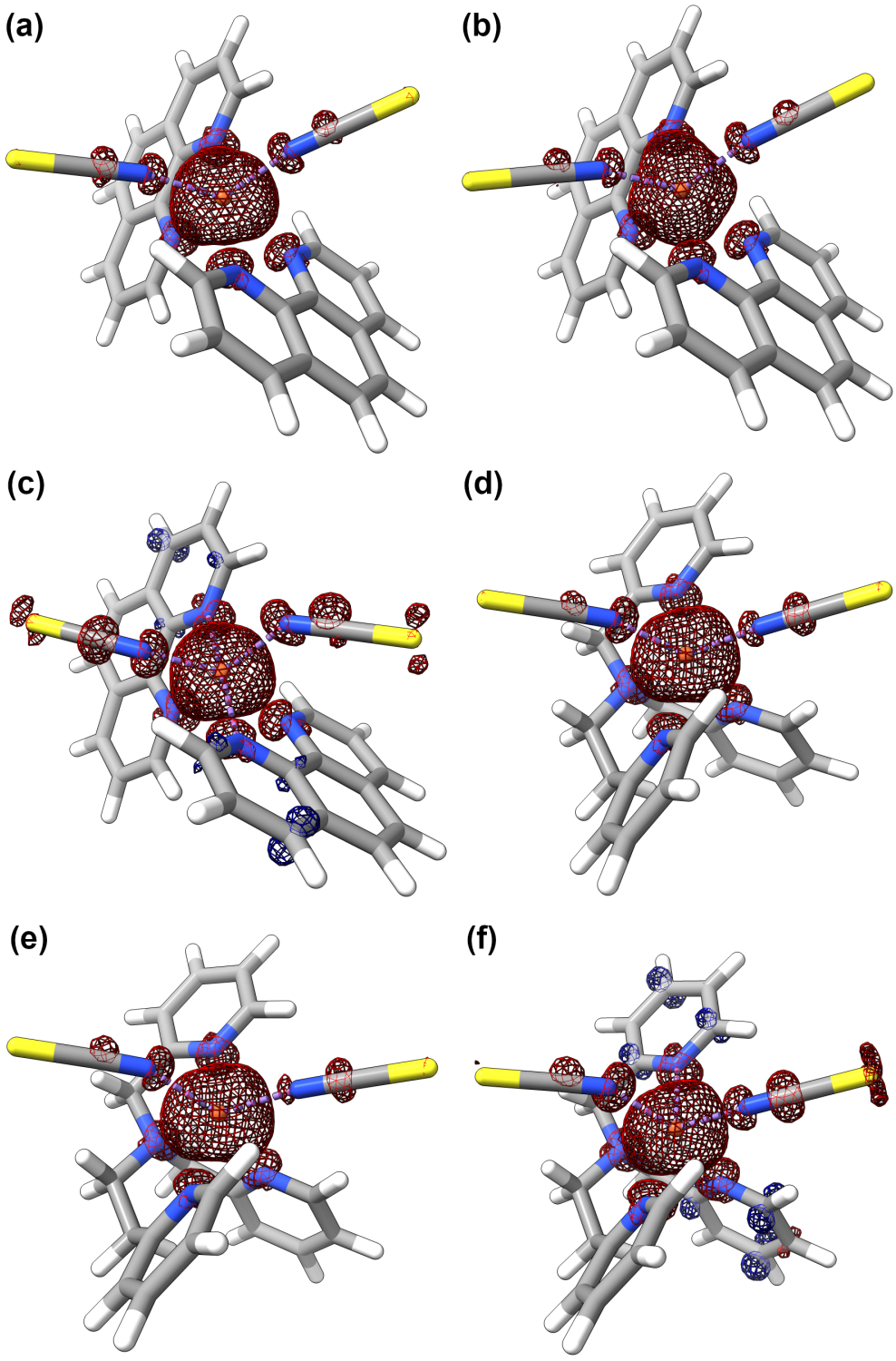

Figure S26: Optimised geometries and spin density analysis of WAHKEX and KEKVIF03 quintet complexes with (a) B3LYP/def2-TZVP for KEKVIF03, (b) PBE0/def2-TZVP for KEKVIF03, (c) r^{2}SCAN/def2-TZVP for KEKVIF03, (d) B3LYP/def2-TZVP for WAHKEX, (b) PBE0/def2-TZVP for WAHKEX, and (c) r^{2}SCAN/def2-TZVP for WAHKEX.

4 Prediction of T_{SCO} with *Kestrel*

4.1 *Kestrel* Software

Kestrel consists of a GUI and python package, *KestrelPy*, both of which calculate paramagnetic susceptibilities and electronic states, electron paramagnetic resonance (EPR) parameters and absorption spectra. Calculations consider only the angular coordination of the atoms directly ligating the metal centre, with the bonding of each ligand parameterised using e values. These are chemically meaningful and describe the strength and type of ligand bond (i.e. e_σ represents a σ bond).

Each e value contributes to the 5×5 ligand field matrix which describes the ligand field surrounding a metal centre. Its diagonalisation gives the d orbital splitting. Addition of spin-orbit coupling (SOC) and interelectronic repulsion parameters (Racah B and C) to the ligand field matrix give an effective Hamiltonian which provides the energy of each electronic state along with its configuration interaction. Using an effective Hamiltonian alongside ligand field parameters affords real-time calculation of electronic and magnetic properties.

	d_{xy}	d_{yz}	d_{z2}	d_{xz}	d_{x2-y2}
d_{xy}	0	0	0	0	0
d_{yz}	0	0	0	0	0
d_{z2}	0	0	7400	0	0
d_{xz}	0	0	0	0	0
d_{x2-y2}	0	0	0	0	22200

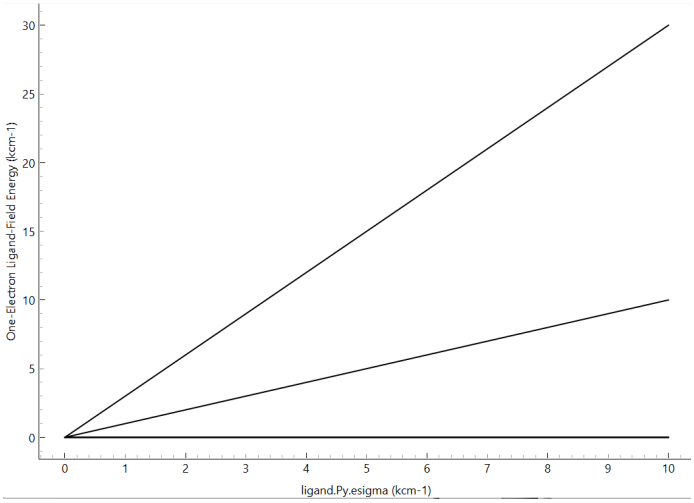

Left: 5×5 ligand field matrix for a square planar (D_{4h}) Cu^{2+} complex.
Right: Variation of d orbital energies with increasing e_σ parameter value

4.1.1 Calculating T_{SCO} with *Kestrel*

For the following analysis, optimised DFT structures (PBE0 and PBE0-D4) were imported from .xyz files. The metal centre (Fe^{II}) was assigned and the coordinating atoms of each ligand were defined, with an extra atom used to orient the ligand x/y directions (Fig. S27). Common e values were then assigned to each pyridine and pyrazolyl ligand and Racah B/C and spin-orbit coupling parameters were used to describe the Fe^{II} metal centre.

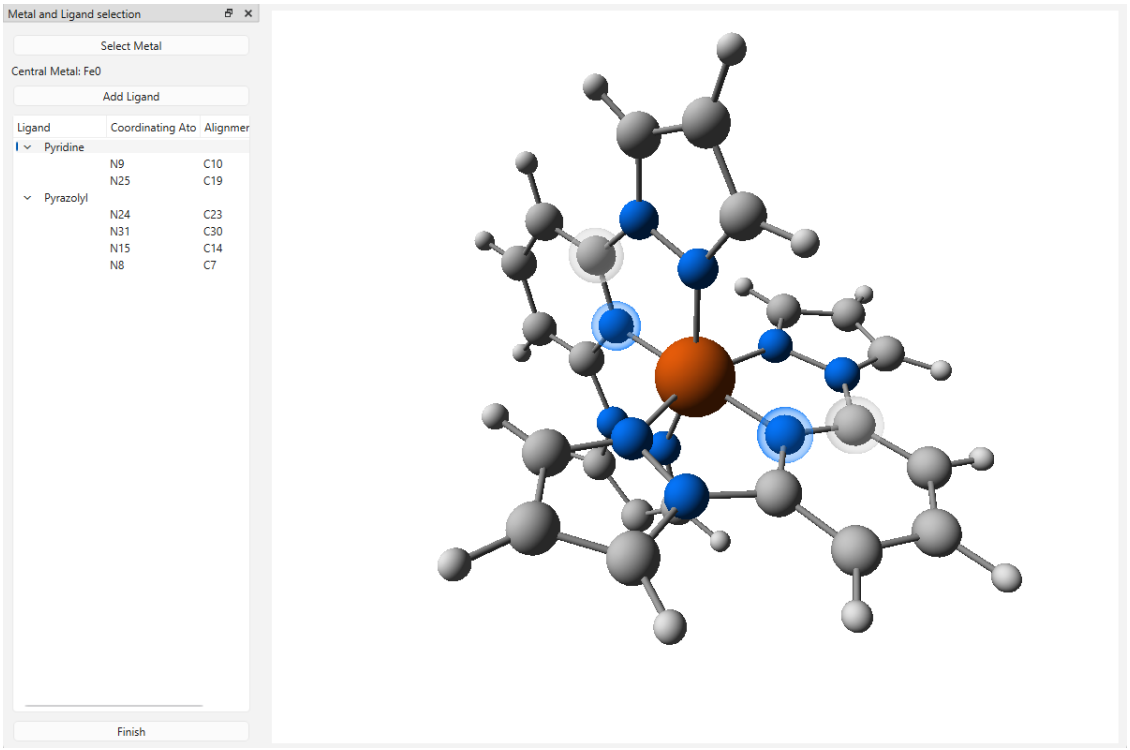

Figure S27: Assignment of the metal centre and ligating atoms after importing a .xyz file in *Kestrel*'s GUI. The pyridine coordinating nitrogen's have been highlighted and the assigned ligand atoms can be seen in the left panel.

From the e parameters, *Kestrel* constructs the 5×5 ligand field matrix to which spin-orbit coupling and inter-electronic repulsion are added to form an effective Hamiltonian. This describes the energy of each Russell-Saunders state and permits the calculation of magnetic properties such as the paramagnetic susceptibility. Full details of this process are given in the workflow on the page 72.

Paramagnetic susceptibilities were then calculated at 5 K intervals, averaged over each orientation and plotted against the temperature (Fig. S29). The midpoint of each plot, where the LS and HS states are equally occupied (at approx. 1.5 cm^3 K mol^{-1}), gave T_{SCO} for a single complex. Comparison with other complexes in ***T_SCO_dataset*** showed this be sensitive to both e value (Fig. S40) and ligand bite angle (Fig. S35).

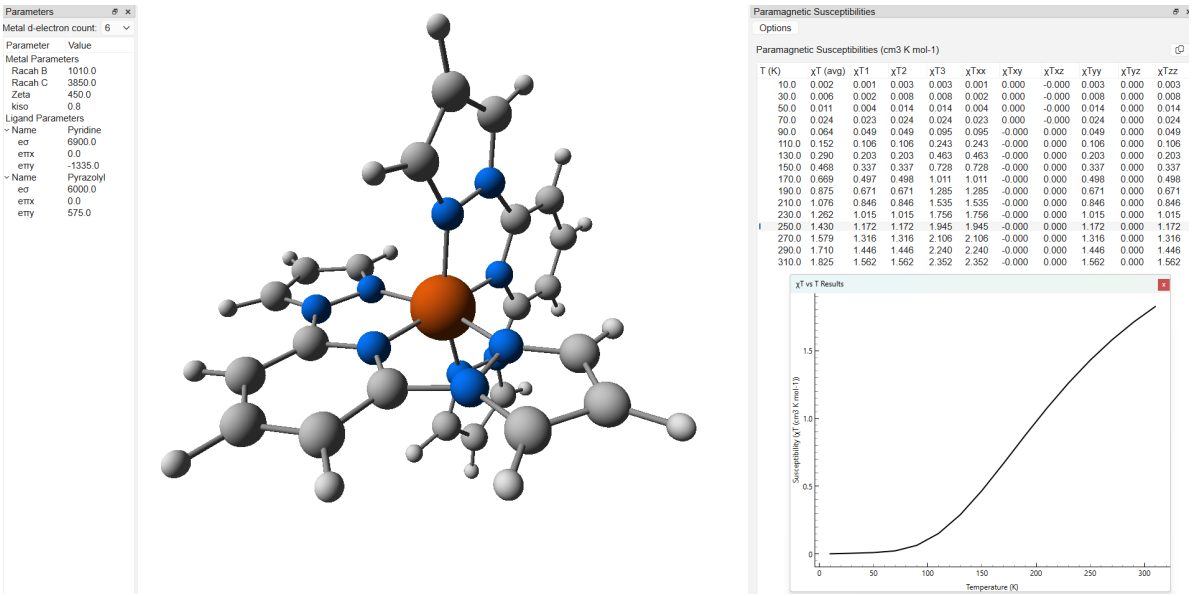

Figure S28: Molecular structure of HALC-1 along with input parameters (left panel) and the calculated paramagnetic susceptibility curve (right panel) in *Kestrel*'s GUI. The plot will update in real-time as parameter inputs are changed.

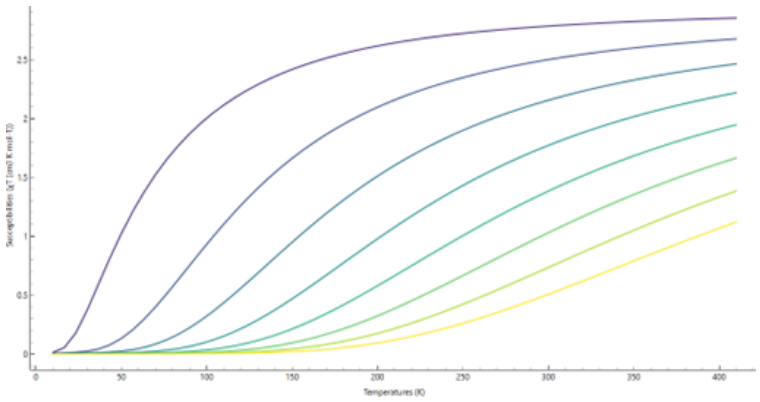

Figure S29: Variation of calculated paramagnetic susceptibility curves with pyridine e_σ value. e_σ was varied (step = 50 cm^{-1}) between 6750 cm^{-1} (dark purple, lowest T_{SCO}) and 7100 cm^{-1} (yellow, highest T_{SCO}) for HALC-1.

The computational workflow below details how T_{SCO} for a single complex is calculated in *Kestrel* from a set of parameter values. For the user, this calculation runs in real-time requiring no further input beyond the entry of parameter values.

Start

Construct the 5×5 ligand field matrix from e parameters

Construct an effective Hamiltonian in the d^n basis from the 5×5 ligand field matrix, interelectronic repulsion (Racah) and spin-orbit coupling parameters (ζ).

$$\mathcal{H}_{LF} = T + \sum_{i<j}^{N} U(i,j) + \sum_{i}^{N} V_{LF}(\mathbf{r}_i) + \xi \sum_{i}^{N} \mathbf{l}_i \cdot \mathbf{s}_i$$

Apply the effective Hamiltonian to a Russell-Saunders basis matrix. Solve to obtain the energy and spin multiplicity of each electronic state

Calculate the paramagnetic susceptibility, χ(T), using the Van Vleck equation to sum over the Boltzmann-populated electronic states[119]

$$\chi_{\alpha\beta} = \sum_{i} Z_i \left(\frac{\sum_j \langle i|\mu_\alpha|j\rangle\langle j|\mu_\beta|i\rangle}{k_B T} + \frac{2\sum_{k\neq i}\langle i|\mu_\alpha|k\rangle\langle k|\mu_\beta|i\rangle}{E_k - E_i} \right)$$

Plot χ(T) vs temperature. The midpoint, where the LS and HS states are equally occupied, gives T_{SCO} for a single complex.

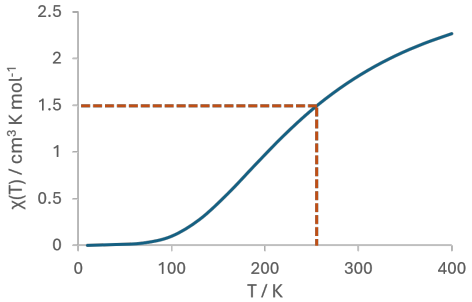

Stop

4.2 Calculated T_{SCO} using fixed ligand field parameters

Initially, the effect of geometric differences between each HALC-X complex in ***T_SCO_dataset*** were analysed using the same parameter values for each complex. This allowed the sensitivity of T_{SCO} to variations in geometry to be explored.

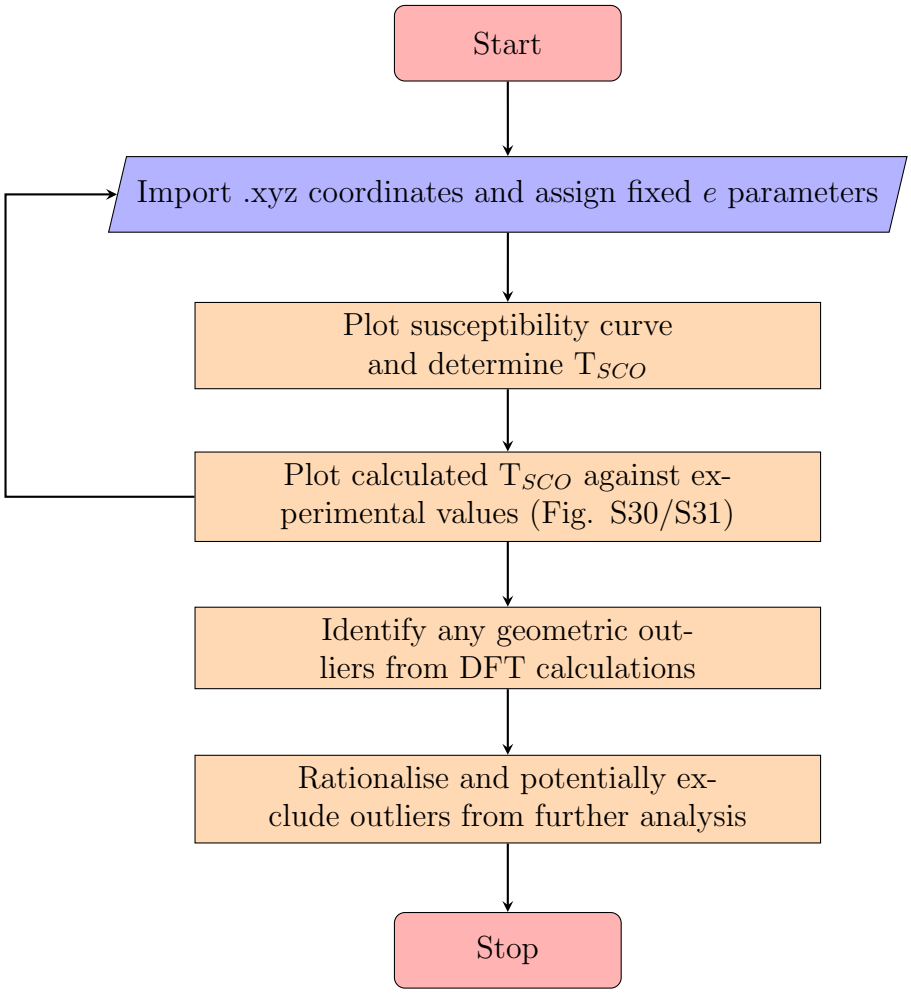

Table S51: Tabulation of Experimental T_{SCO} from NMR studies by M. Halcrow,[116] *Kestrel*-calculated T_{SCO} and the energy gap between the singlet ground state and quintet state to which SCO occurs. DFT optimised geometries (PBE0/def2-TZVP or PBE0-D4/def2-TZVP) were used for each complex. Parameter values were fixed at: $p_y(e_\sigma) = 6900$ cm^{-1}; $p_y(e_\pi) = -1335$ cm^{-1}; $p_z(e_\sigma) = 6000$ cm^{-1}; p_z $(e_\pi) = 575$ cm^{-1}; Racah B = 1010 cm^{-1}, Racah C = 3850 cm^{-1}, SOC = 450 cm^{-1}.

Complex	Experimental T_{SCO} (K)	*Kestrel* T_{SCO} (PBE0) (K)	LS-HS Energy (PBE0) (cm^{-1})	*Kestrel* T_{SCO} (PBE0-D4) (K)	LS-HS Energy (PBE0-D4) (cm^{-1})
HALC-1	248	248	333	348	500
HALC-2	216	187	235	292	404
HALC-3	213	196	241	302	402
HALC-4	281	255	343	358	515
HALC-5*	<145	104	112	215	281
HALC-6*	<190	75	74	195	249
HALC-7	309	257	346	362	523
HALC-8	215	144	169	256	346
HALC-9	164	150	178	260	352
HALC-10	158	145	171	254	344
HALC-11	215	203	260	306	429
HALC-12	226	197	251	305	427
HALC-13	234	201	257	308	433
HALC-14	236	202	258	310	436
HALC-15	246	159	191	270	368
HALC-16	194	153	183	261	354
HALC-17	284	232	306	351	504
HALC-18	294	248	328	353	498
HALC-19	245	154	184	289	396
HALC-20	259	160	192	298	411
HALC-21	261	162	195	295	407
HALC-22	273	241	321	340	485
HALC-23	259	243	323	344	492
HALC-24	251	248	332	354	510
HALC-25	246	282	388	379	553
HALC-26	231	214	277	320	451
HALC-27	238	219	286	325	461
HALC-28	237	229	302	333	474

*For HALC-5 and HALC-6, Experimental T_{SCO} values were unavailable due to the complexes remaining high spin over the liquid range of the solvent.

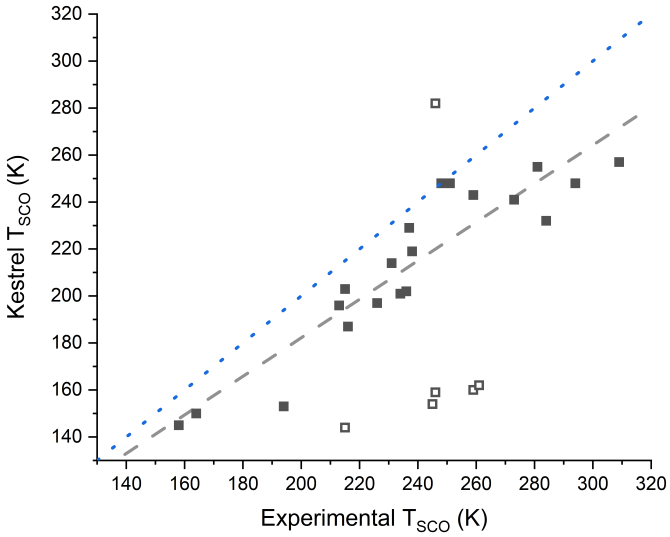

Figure S30: Experimental T_{SCO} against *Kestrel*-calculated T_{SCO} for HALCROW complexes (n = 26, $R^2 = 0.42$) using PBE0/def2-TZVP, *e* parameters were fixed at $p_y(e_\sigma) = 6900$ cm^{-1}; $p_y(e_\pi) = -1335$ cm^{-1}; $p_z(e_\sigma) = 6000$ cm^{-1}; p_z $(e_\pi) = 575$ cm^{-1}; Racah B = 1010 cm^{-1}, Racah C = 3850 cm^{-1}, SOC = 450 cm^{-1}. Outliers are represented with white squares. Dotted line (blue) shows the experimental trend ($y = x$).

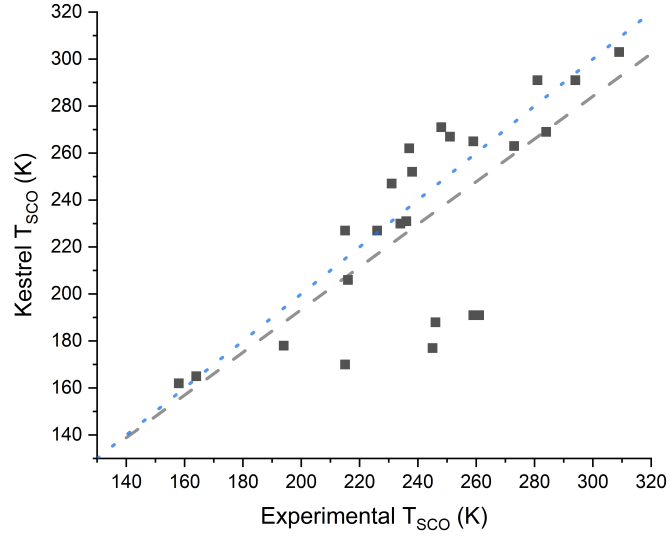

Figure S31: Experimental T_{SCO} against *Kestrel*-calculated T_{SCO} for HALCROW complexes (n = 26, $R^2 = 0.57$) using PBE0-D4/def2-TZVP. *e* parameters were fixed at $p_y(e_\sigma) = 6900$ cm^{-1}; $p_y(e_\pi) = -1335$ cm^{-1}; $p_z(e_\sigma) = 6000$ cm^{-1}; p_z $(e_\pi) = 575$ cm^{-1}; Racah B = 1010 cm^{-1}, Racah C = 3850 cm^{-1}, SOC = 450 cm^{-1}. Dotted line (blue) shows the experimental trend ($y = x$).

4.3 Geometric dependence of calculated T_{SCO}

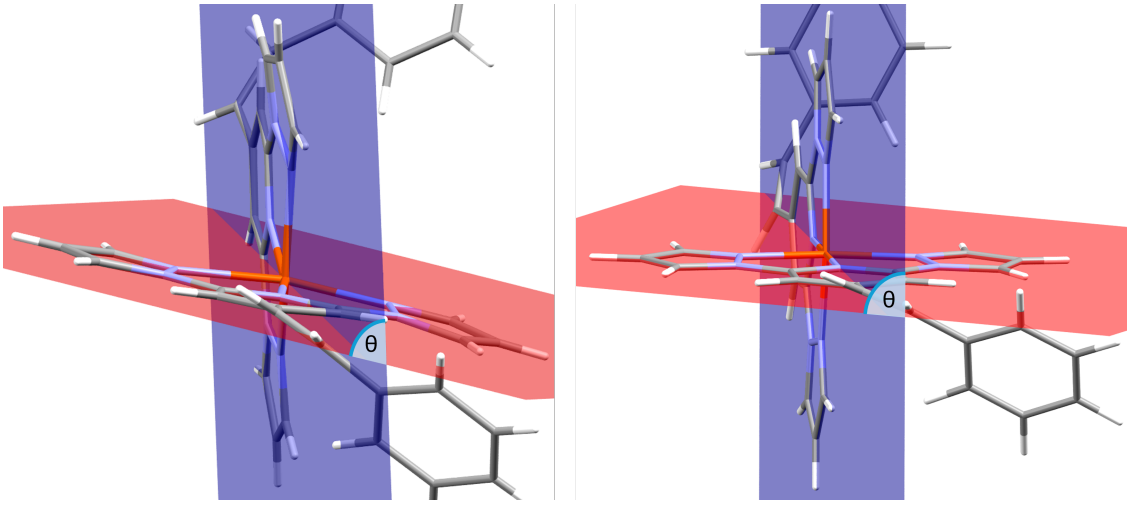

Figure S32: Crystal structure (left) and DFT-calculated structure (PBE0/def2-TZVP) (right) for HALC-19. The interplanar angle between the least-squares planes of the two tridentate ligands is shown. For DFT, $\theta = 90.0°$ and for the crystal structure, $\theta = 80.2°$

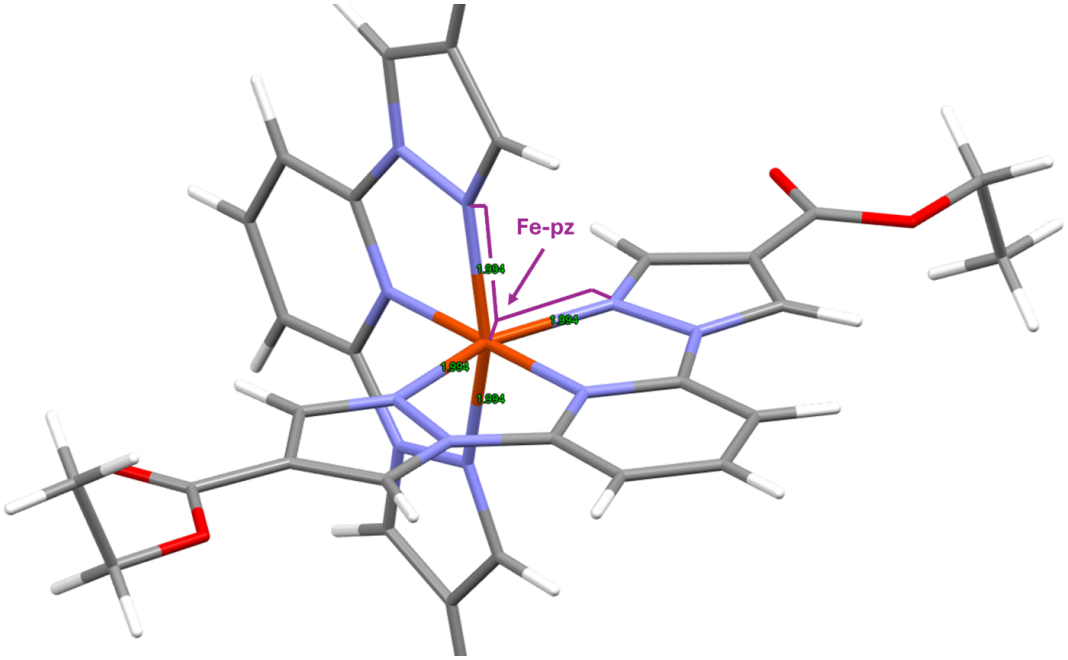

Figure S33: DFT optimised structure of HALC-25 (PBE0/def2-TZVP) showing the reduced Fe-N(p_z) bond length.

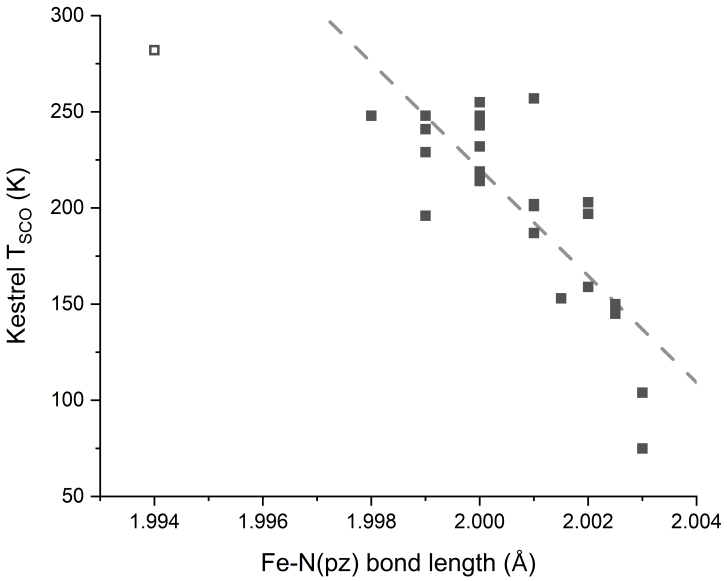

Figure S34: Correlation between Fe-N(p_z) bond length (PBE0/def2-TZVP) and *Kestrel*-calculated T_{SCO} (n = 23, R^2 = 0.64). HALC-25 is represented by a white square and is ommitted from the correlation.

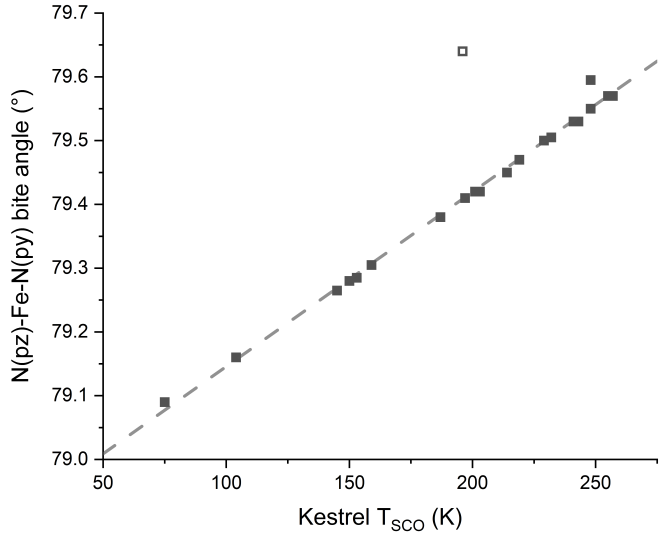

Figure S35: Variation of *Kestrel*-calculated T_{SCO} with the smallest N(p_z)-Fe-N(p_y) angle for each complex (PBE0/def2-TZVP). HALC-3 is represented by a white square. (n = 22, $R^2 > 0.99$ in the absence of HALC-3).

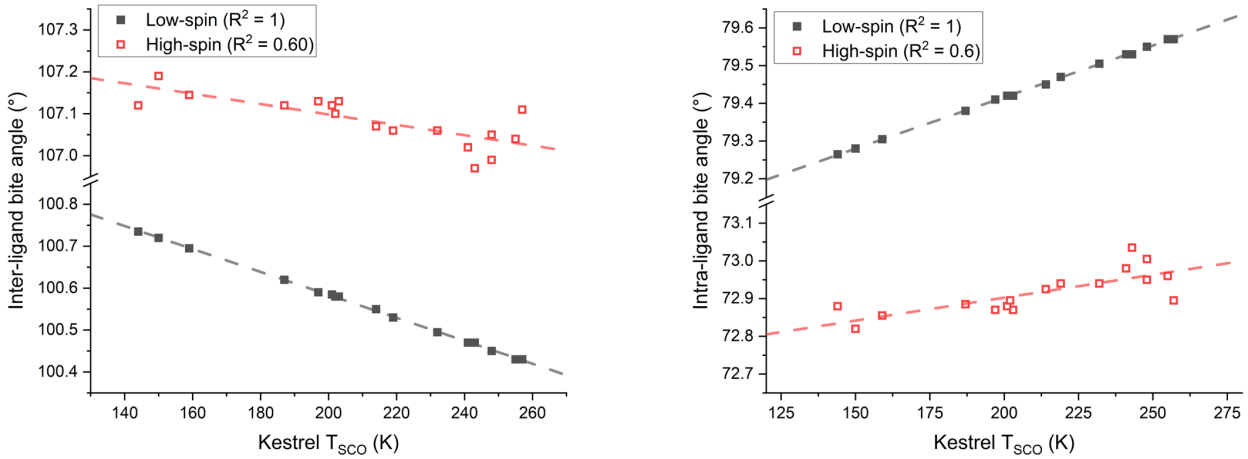

Figure S36: Variation of inter-ligand bite angle (left) and intra-ligand bite angle (right) with calculated T_{SCO} for low-spin (black, squares) and high-spin (red, empty squares) geometries. All geometries were optimised with PBE0/def2-TZVP.

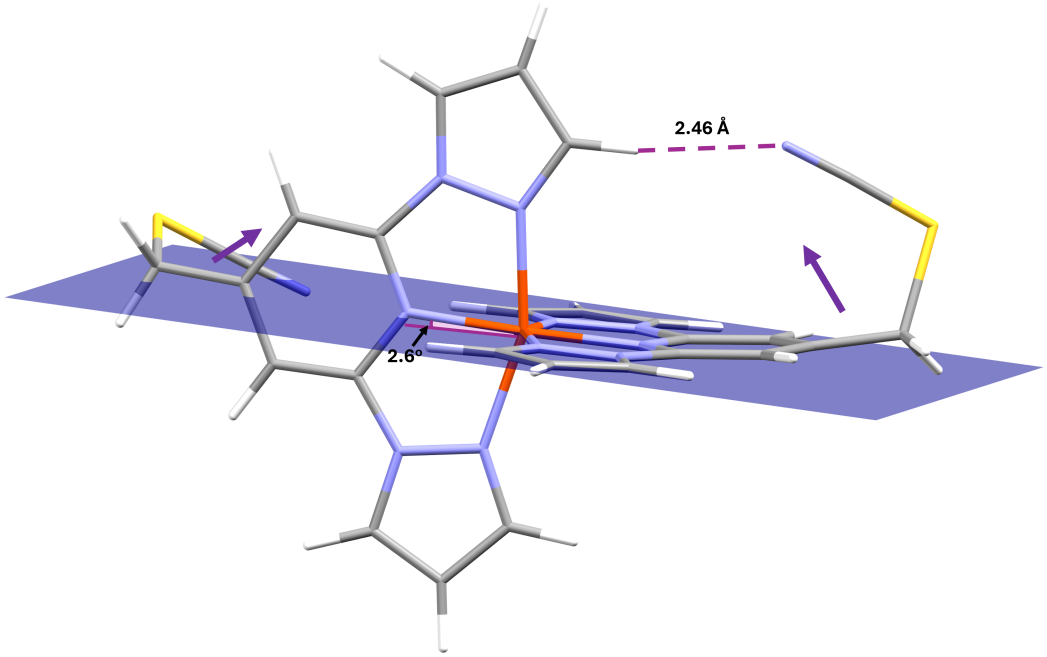

Figure S37: DFT optimised structure of HALC-3 (PBE0/def2-TZVP) showing the distortion causing the substituent to "fold back" towards the complex. The angle between the Fe-N(p_y) vector and the N(p_z)-Fe-N(p_z) plane (2.6°, blue) is also shown.

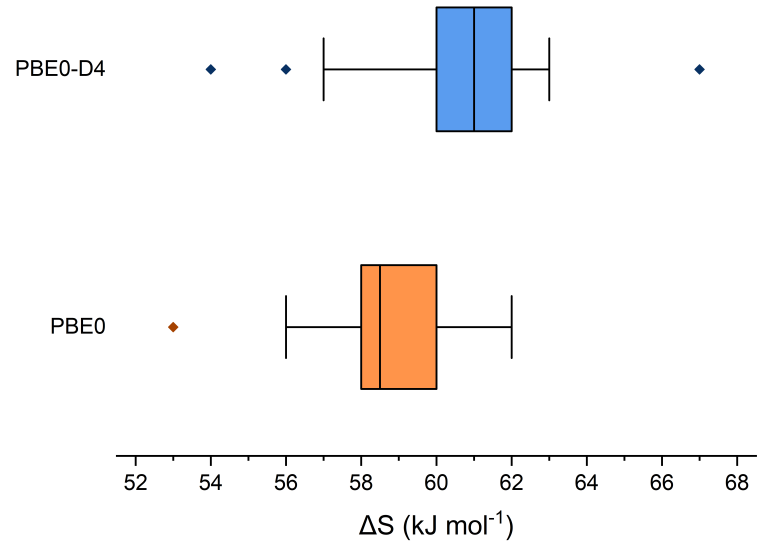

Figure S38: Box plot showing the variation in DFT-calculated entropy changes for PBE0 and PBE0-D4 structures. The data in this plot is taken from tables S42 and S43

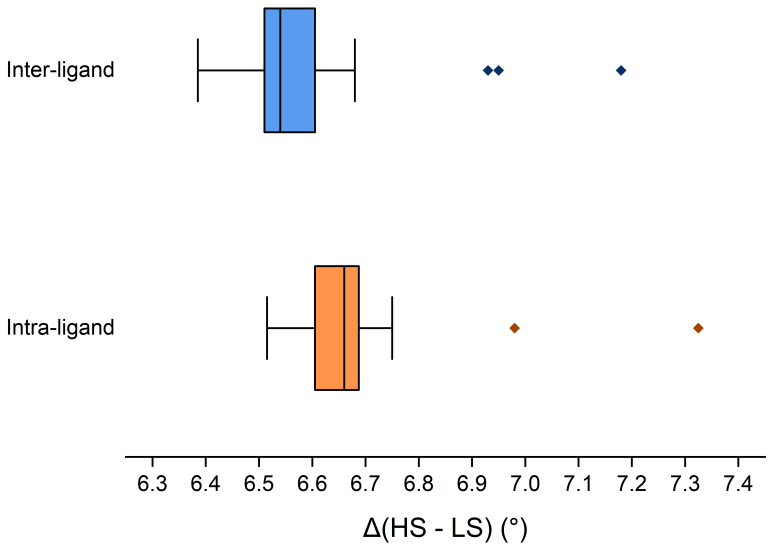

Figure S39: Box plot showing the variation in the difference between high-spin and low-spin bite angles for PBE0/def2-TZVP structures. The top box plot shows the difference for the inter-ligand bite angles and the bottom box plot the difference in intra-ligand bite angles.

4.4 Dependence of calculated T_{SCO} on e_σ parameter values

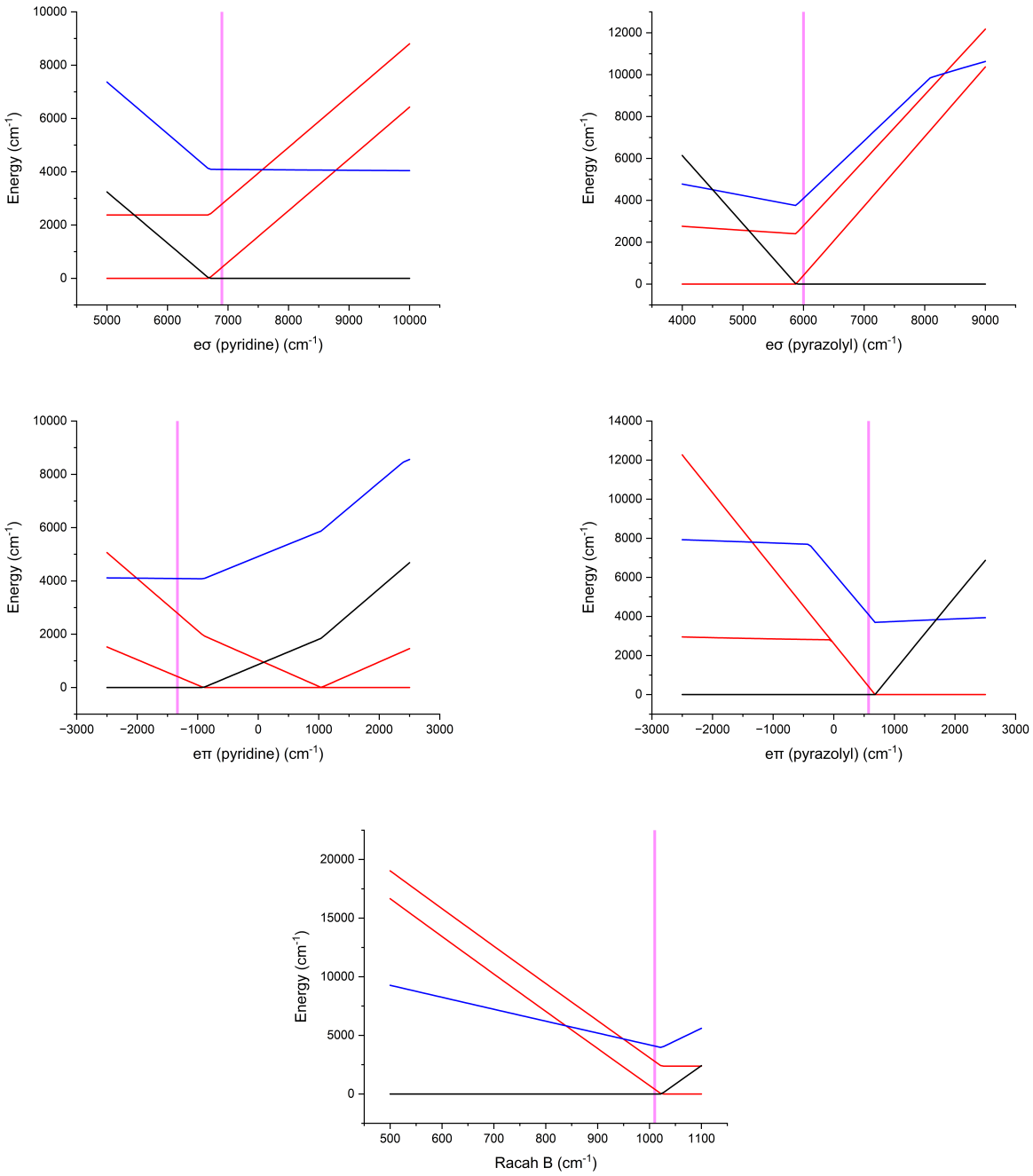

Figure S40: Tanabe-Sugano style variation diagram of the singlet (black), triplet (blue) and quintet (red) spin-state energies with variation of e and interelectronic repulsion parameters for HALC-1. From top left to bottom right, variation of p_y (e_σ), p_z (e_σ), p_y (e_π), p_z (e_π) and Racah B values. Parameter values used in calculations are highlighted by the pink lines.

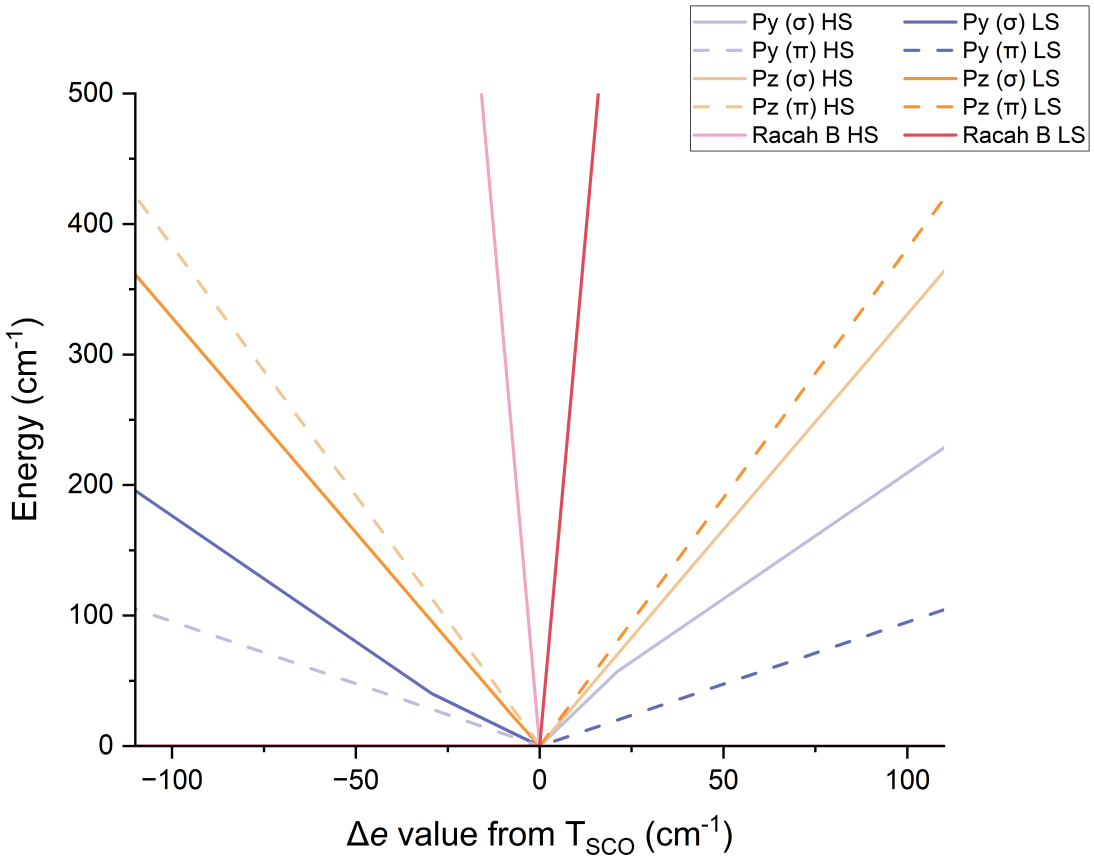

Figure S41: Superposition of Tanabe-Sugano style variation diagrams for each parameter value. Relative energies of the quintet state (light line) and singlet state (dark line) are given for variation of each parameter value above and below the parameter value at which SCO occurs.

4.4.1 Relationship between e_σ and Hammett (σ) values

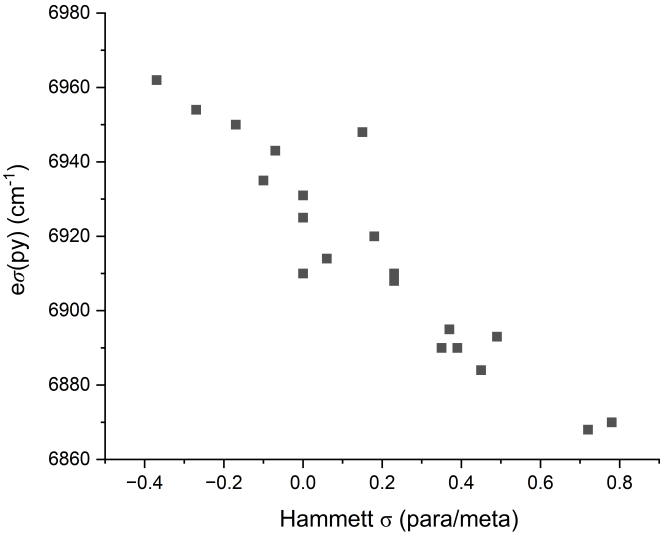

Figure S42: Variation of p_y (e_σ) with Hammett σ_p for -X substituents and Hammett σ_m for -Y substituents. A correlation of (e_σ) = 6930 - 85.H was determined (n = 20, R^2 = 0.87).

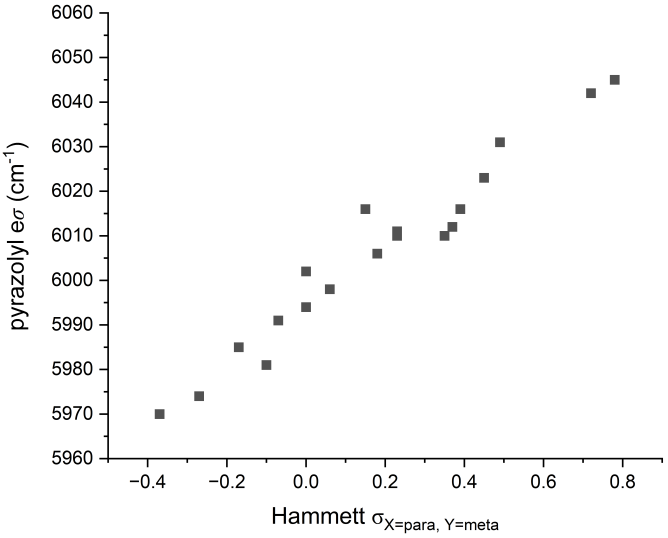

Figure S43: Variation of p_z (e_σ) with Hammett σ_p for -X substituents and Hammett σ_m for -Y substituents. A correlation of (e_σ) = 5995 + 65.H was determined (n = 20, R^2 = 0.95).

4.4.2 Calculated T_{SCO} with e parameters determined by Hammett (σ) values - PBE0/def2-TZVP optimised geoemtries

The variation diagrams in figure S40 show T_{SCO} to depend on the e values. We expect the precise nature of metal-ligand bonding to be dependent on the substituent attached to the pyridine (-X substituted) or pyrazolyl (-Y substituted) ring. The workflow below allows these differences to be quantified with reported Hammett parameters.[116]

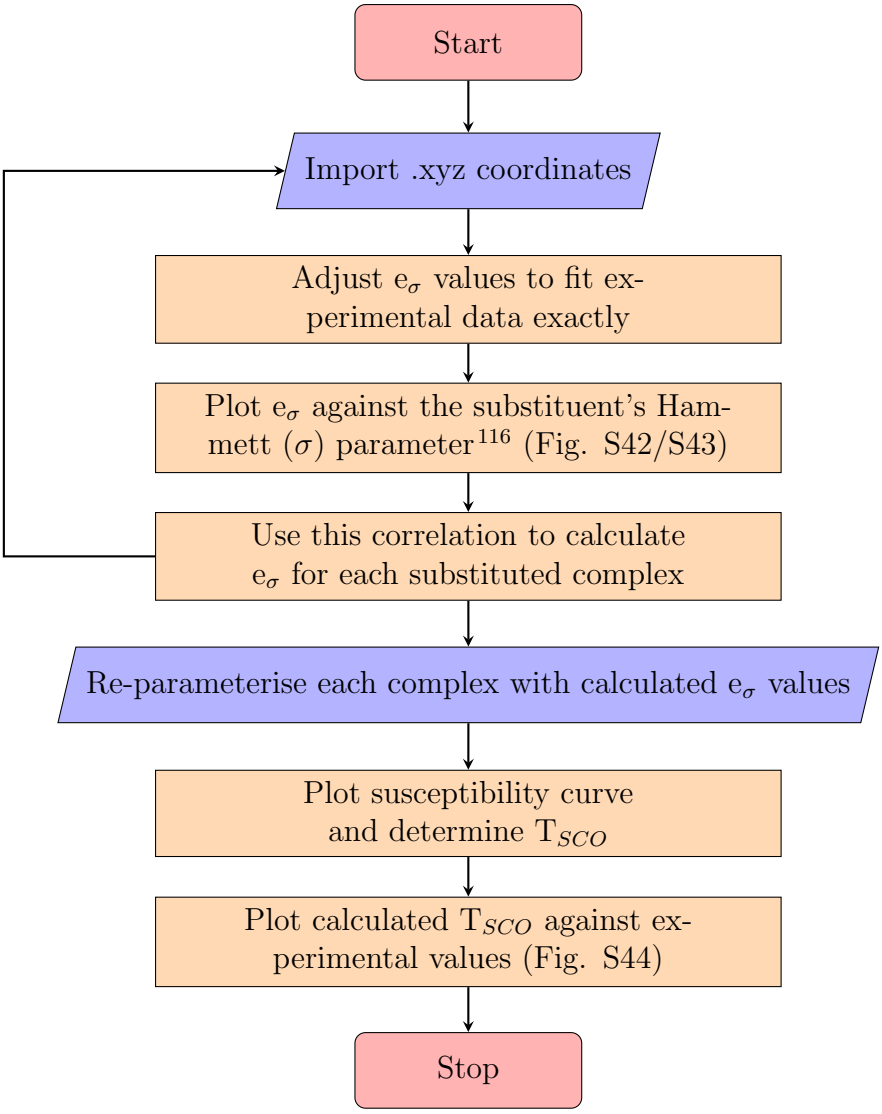

This approach can be extended to predict e values for novel substituents attached to this ligand scaffold, provided a Hammett parameter value is available.

Table S52: Tabulation of Experimental T_{SCO} from NMR studies by M. Halcrow,[116] *Kestrel*-calculated T_{SCO} and the energy gap between the singlet ground state and quintet state to which SCO occurs. DFT optimised geometries (PBE0/def2-TZVP) were used for each complex. Parameter values were varied for pyridine and pyrazole e_σ according to the Hammett σ_{para} parameter for each X substituent and Hammett σ_{meta} parameter for each Y substituent using the following correlations: $p_y(e_\sigma) = 6929 - 94.H$ and $p_z(e_\sigma) = 5995 + 70.H$.

Other parameter values were fixed at: $p_y(e_\pi)$ = -1335 cm^{-1}, $p_z(e_\pi)$ = 575 cm^{-1}, Racah B = 1010 cm^{-1}, Racah C = 3850 cm^{-1}, SOC = 450 cm^{-1}.

Complex	Hammett σ parameter*	pyridine e_σ (cm^{-1})	pyrazolyl e_σ (cm^{-1})	Experimental T_{SCO} (K)	*Kestrel* T_{SCO} (K)	LS-HS Energy gap (cm^{-1})
HALC-1	0	6929	5995	248	271	372
HALC-2	−0.17	6945	5983	216	206	265
HALC-4	0.45	6887	6027	281	291	404
HALC-5*	−0.66	6991	5949	<145	112	124
HALC-6*	−0.83	7007	5937	<190	79	79
HALC-7	0.78	6856	6050	309	303	422
HALC-8	0.05	6924	5999	215	170	210
HALC-9	−0.37	6964	5969	164	165	201
HALC-10	−0.27	6954	5976	158	162	196
HALC-11	0.06	6923	5999	215	227	299
HALC-12	0.23	6907	6011	226	227	298
HALC-13	0.23	6907	6011	234	230	304
HALC-14	0.18	6912	6008	236	231	305
HALC-15	0.15	6915	6006	246	188	237
HALC-16	0	6929	5995	194	178	221
HALC-17	0.49	6883	6029	284	269	366
HALC-18	0.72	6861	6045	294	291	397
HALC-19	−0.07	6936	5990	245	177	219
HALC-20	0.17	6913	6007	259	191	241
HALC-21	0.26	6905	6013	261	191	241
HALC-22	−0.07	6936	5990	273	263	356
HALC-23	0	6929	5995	259	265	362
HALC-24	−0.1	6938	5988	251	267	366
HALC-26	0.37	6894	6021	231	247	331
HALC-27	0.39	6892	6022	238	252	340
HALC-28	0.35	6896	6020	237	262	357

*For HALC-5 and HALC-6, Experimental T_{SCO} values were unavailable due to them remaining high spin over the liquid range of the solvent.

*Hammett σ_p and Hammett σ_m values were taken from a previous study by Kershaw Cook et al.[116]

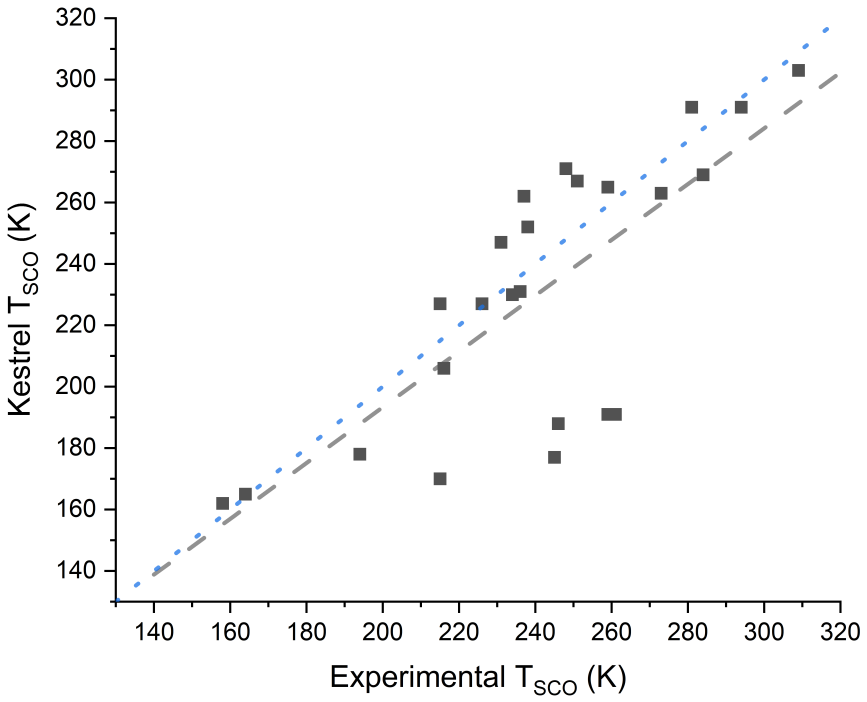

Figure S44: Experimental T_{SCO} against *Kestrel*-calculated T_{SCO} for HALCROW complexes optimised with PBE0/def2-TZVP and with HALC-8 and HALC-19-21 included (n = 24, R^2 = 0.56). Racah, SOC parameters and e parameters were taken from table S47. The dotted line (blue) shows the experimental trend ($y = x$).

4.4.3 Calculated T_{SCO} with e parameters determined by Hammett (σ) values - PBE0-D4/def2-TZVP optimised geoemtries

Table S53: Tabulation of Experimental T_{SCO} from NMR studies by M. Halcrow,[116] *Kestrel*-calculated T_{SCO} and the energy gap between the singlet ground state and quintet state to which SCO occurs. DFT optimised geometries (PBE0-D4/def2-TZVP) were used for each complex. Parameter values were varied for pyridine and pyrazole e_σ according to the Hammett σ_{para} parameter for each X substituent and Hammett σ_{meta} parameter for each Y substituent using the following correlations: $p_y(e_\sigma) = 6860 - 94.H$ and $p_z(e_\sigma) = 5980 + 70.H$.

Other parameter values were fixed at: $p_y(e_\pi)$ = -1335 cm^{-1}, $p_z(e_\pi)$ = 575 cm^{-1}, Racah B = 1010 cm^{-1}, Racah C = 3850 cm^{-1}, SOC = 450 cm^{-1}.

Complex	Hammett σ parameter*	pyridine e_σ (cm^{-1})	pyrazolyl e_σ (cm^{-1})	Experimental T_{SCO} (K)	Calculated T_{SCO} (K)	LS-HS Energy gap (cm^{-1})
HALC-1	0	6860	5980	248	266	361
HALC-2	−0.17	6876	5968	216	202	259
HALC-4	0.45	6818	6012	281	289	400
HALC-5*	−0.66	6922	5934	<145	109	119
HALC-6*	−0.83	6938	5922	<190	81	82
HALC-7	0.78	6787	6035	309	303	423
HALC-8	0.05	6855	5984	215	173	213
HALC-9	−0.37	6895	5954	164	164	199
HALC-10	−0.27	6885	5961	158	160	195
HALC-11	0.06	6854	5984	215	223	292
HALC-12	0.23	6838	5996	226	227	299
HALC-13	0.23	6838	5996	234	230	304
HALC-14	0.18	6843	5993	236	232	307
HALC-15	0.15	6846	5991	246	190	239
HALC-16	0	6860	5980	194	176	218
HALC-17	0.49	6814	6014	284	282	387
HALC-18	0.72	6792	6030	294	289	392
HALC-19	−0.07	6867	5975	245	202	256
HALC-20	0.17	6844	5992	259	218	282
HALC-21	0.26	6836	5998	261	217	281
HALC-22	−0.07	6867	5975	273	255	344
HALC-23	0	6860	5980	259	261	353
HALC-24	−0.1	6869	5973	251	268	366
HALC-26	0.37	6825	6006	231	246	330
HALC-27	0.39	6823	6007	238	252	339
HALC-28	0.35	6827	6005	237	260	353

*For HALC-5 and HALC-6, Experimental T_{SCO} values were unavailable due to them remaining high spin over the liquid range of the solvent.

*Hammett σ_p and Hammett σ_m values were taken from a previous study by Kershaw Cook et al.[116]

5 Prediction of spin states of catalytic intermediates with Kestrel

For each catalytic cycle, typical e values for each ligand were varied according to trends in bond lengths, nature of bonding and to fit to DFT spin state energies. In the case of disagreement with DFT, e parameters were freely varied to determine if any fit was possible using Tanabe-Sugano style diagrams. Their analysis allows any alternative parameter fits to be determined and assessed for their chemical feasibility.

5.1 Fe(II)-catalysed silylation

Table S54: Tabulation of ligand field parameters used to calculate the spin-state energies of TS1 and INT1 for the Fe^{II} silylation catalytic cycle. The ground state predicted by *Kestrel* is shown, with green coloured boxes denoting agreement with DFT [120] and red disagreement.

	X e_σ	X e_π	Silane e_σ	Alkene e_σ	Alkene e_π	Hydride e_σ	Racah B	Spin state
TS1	7800	−1500	5300	7250	−900	8500	875	5
INT1	7800	−1500	5300	6600	−750	6800	875	5

Racah C was fixed so that Racah C = 4 × Racah B.
X = 1,10-phenanthroline

5.1.1 TS1 parameter variation

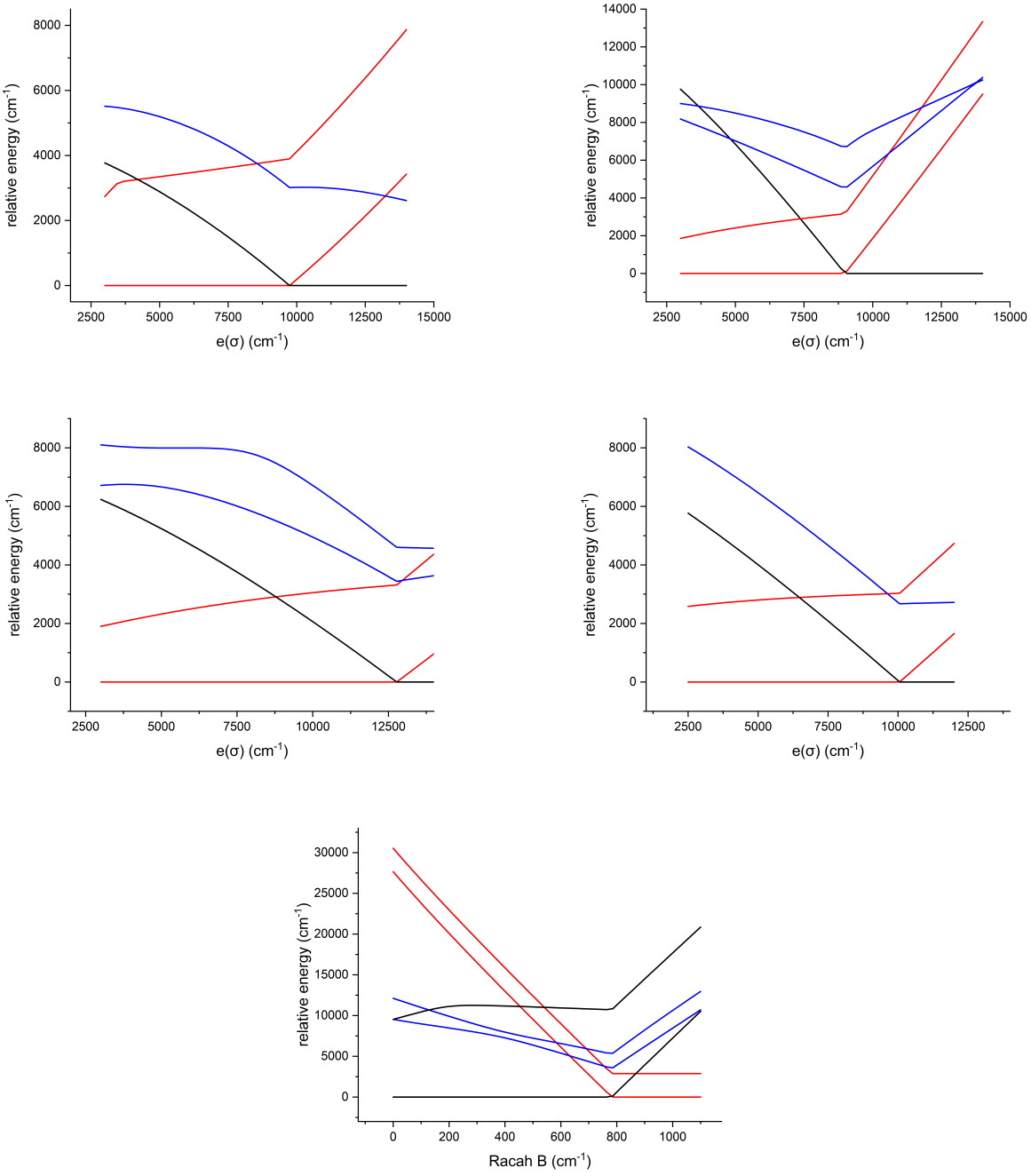

Figure S45: Tanabe-Sugano style diagrams showing how the energies of singlet (black), triplet (blue) and quintet (red) states change upon variation of e and interelectronic repulsion parameters for TS1. From top left to bottom right: alkene, phenanthroline, hydride, silyl (e_σ) and Racah B variation graphs. The DFT-predicted triplet ground state for TS1 is not observed at any parameter value.

5.2 Fe(III)-catalysed oxidation of styrenes - ligation of O_2

Table S55: Tabulation of ligand field parameters used to calculate the spin-state energies of RC2, TS2 and INT2 for the Fe(III) dioxygen ligation catalytic cycle. The ground state predicted by *Kestrel* is shown, with green coloured boxes denoting agreement with DFT[121] and red disagreement.

	O-O e_σ	O-O e_π	OTf e_σ	X-Py e_σ	X-Py e_π	X-NH e_σ	Racah B	Spin state
RC2	5900	600	7000	6400	−800	6200	925	6
TS2	5850	500	7300	6450	−820	6250	925	6
INT2	8200	−1200	7200	6300	−770	6400	925	6*

Racah C was fixed so that Racah C = 4 × Racah B.
X represents the PyBisulidine ligand coordinated to the Fe(III) centre.
*For INT2, Kestrel predicts significantly higher energies for the doublet and quartet state compared to DFT

5.2.1 INT2 parameter variation

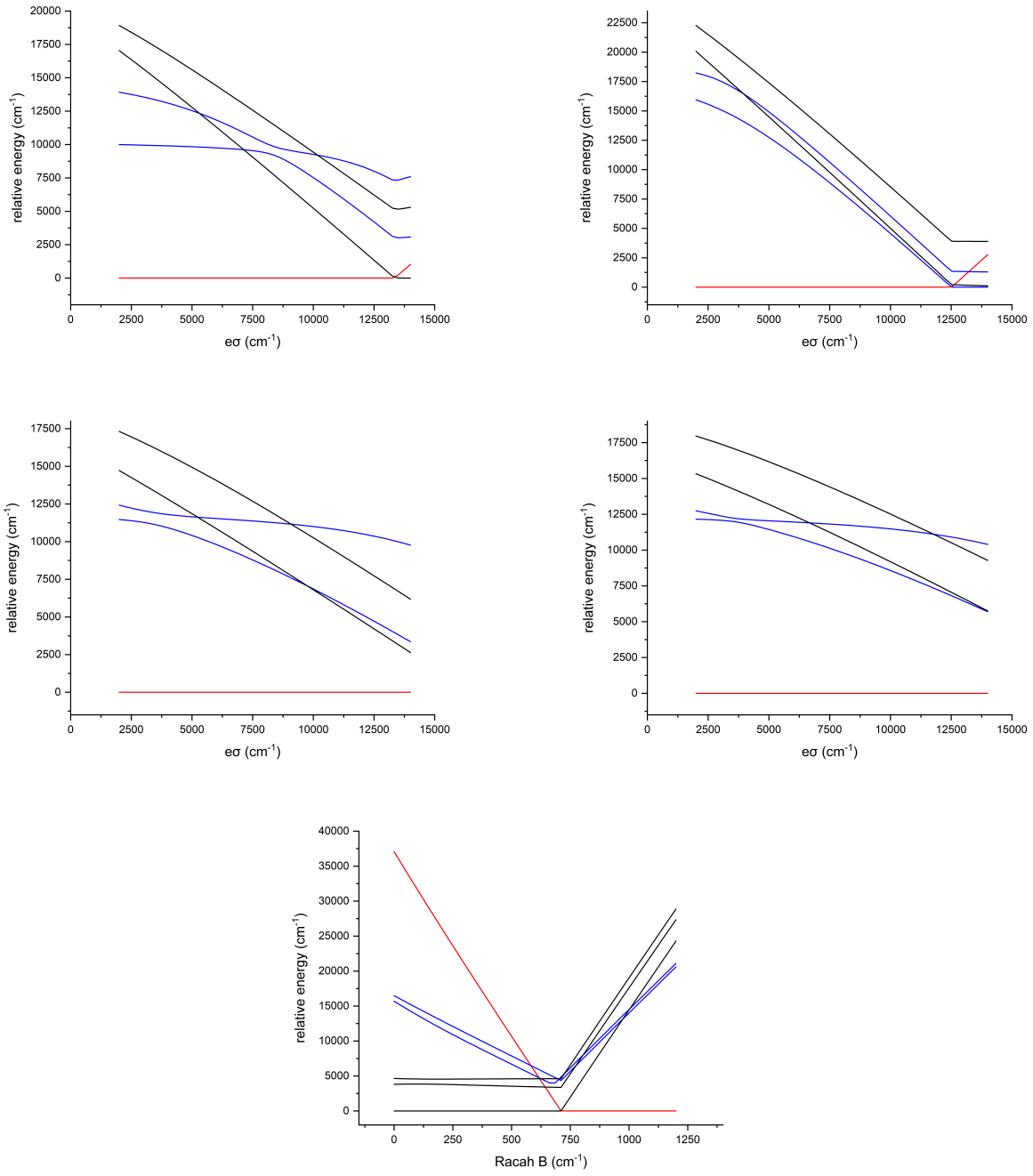

Figure S46: Tanabe-Sugano style diagrams showing how the energies of doublet (black), quartet (blue) and sextet (red) states change upon variation of e and interelectronic repulsion parameters for INT2. From top left to bottom right: bisulidine (NH), triflate, pyridine, oxygen (e_σ) and Racah B variation graphs. The sextet ground state and low lying quartet and doublet state predicted by DFT can only be achieved with a chemically unfeasible triflate e_σ parameter (11000 cm^{-1}).

5.3 Fe(III)–catalysed oxidation of styrene - ligation of olefin

Table S56: Tabulation of ligand field parameters used to calculate the spin-state energies of RC3, TS3 and INT3 for the Fe(III) olefin ligation catalytic cycle. The ground state predicted by *Kestrel* is shown, with green coloured boxes denoting agreement with DFT[121] and red disagreement.

	O-O e_σ	O-O e_π	OTf e_σ	X-Py e_σ	X-Py e_π	X-NH e_σ	L e_σ	L e_π	B	Spin
RC3	0	0	7400	7200	−1000	7200	6500	−750	875	6
TS3	6800	−700	7350	7500	−1250	7400	7000	−850	875	6
INT3	8300	−1000	7400	7000	−750	7000	6800	−800	875	6

Racah C was fixed so that Racah C = 4 × Racah B.
X represents the PyBisulidine ligand coordinated to the Fe(III) centre.
L represents the styrene ligand.

5.3.1 TS3 parameter variation

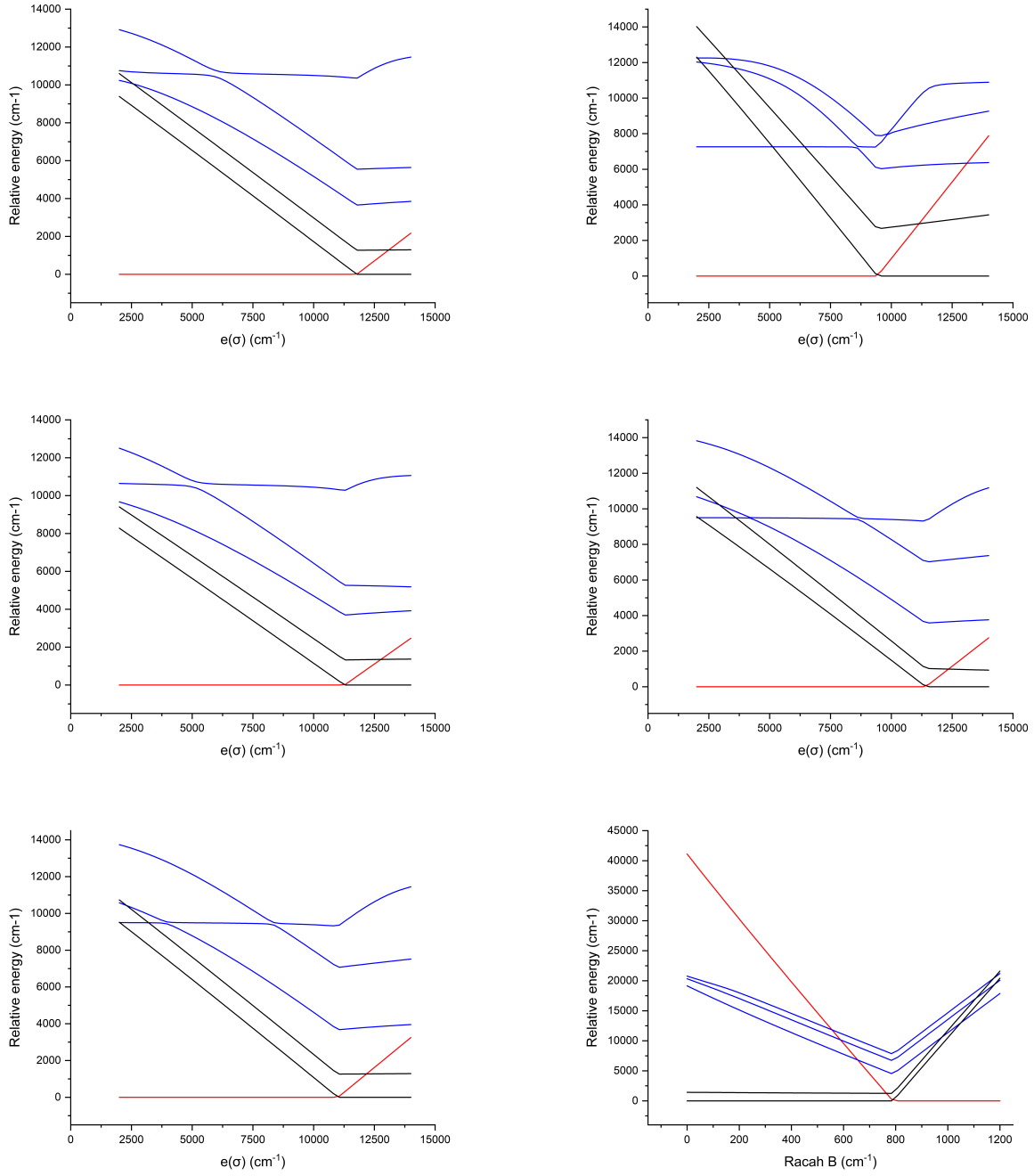

Figure S47: Tanabe-Sugano style diagrams showing how the energies of doublet (black), quartet (blue) and sextet (red) states change upon variation of e and interelectronic repulsion parameters for INT3. From top left to bottom right: triflate, bisulidine (NH), dioxygen, pyridine, styrene (e_σ) and Racah B variation graphs. The quartet ground state predicted by DFT is not observed at any parameter value.

5.3.2 INT3 parameter variation

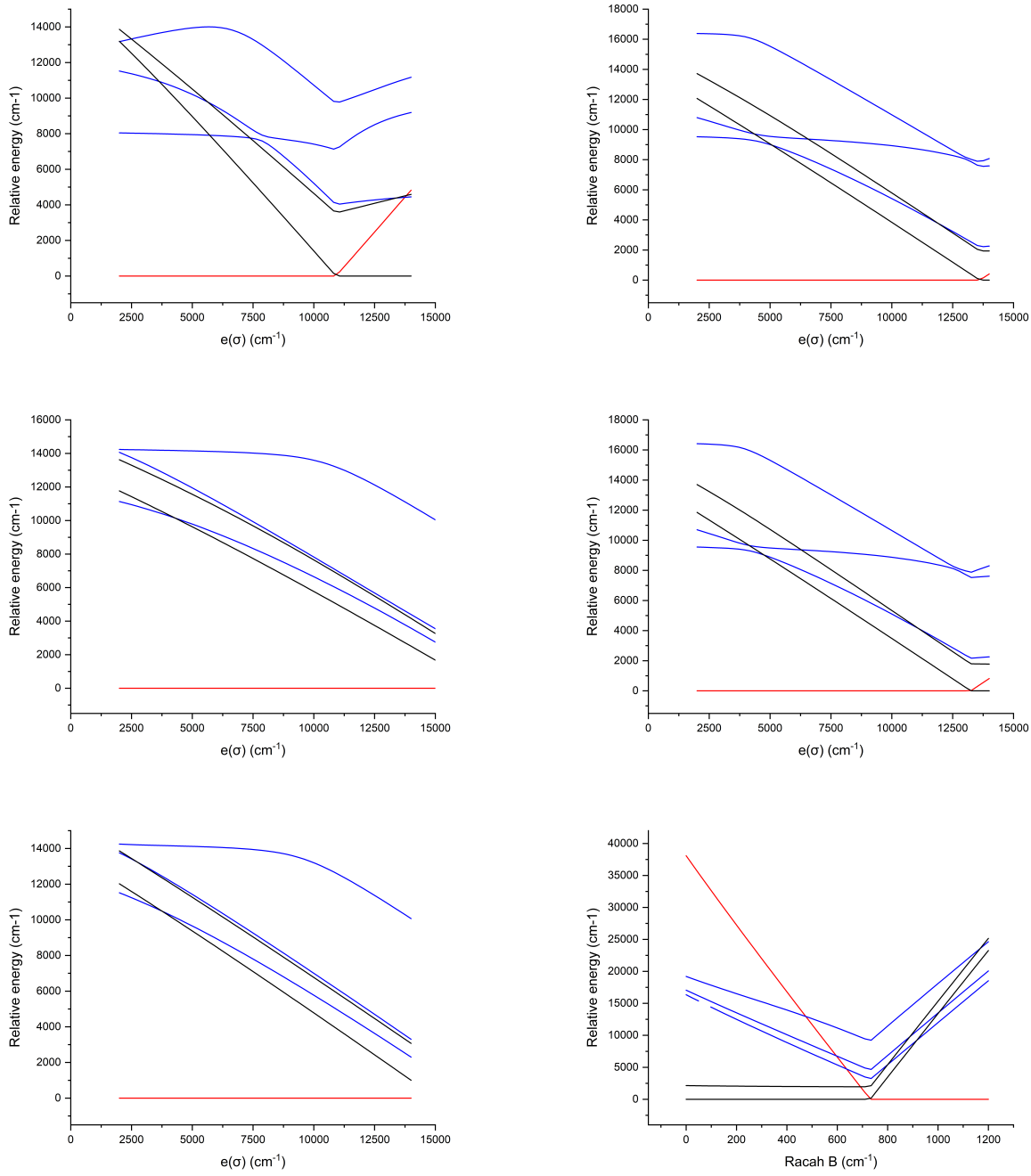

Figure S48: Tanabe-Sugano style diagrams showing how the energies of doublet (black), quartet (blue) and sextet (red) states change upon variation of e and interelectronic repulsion parameters for INT3. From top left to bottom right: bisulidine, styrene, dioxygen, pyridine, triflate (e_σ) and Racah B variation graphs. The quartet ground state predicted by DFT is not observed at any parameter value.

References

(1) Girolami, G. S.; Wilkinson, G.; Galas, A. M.; Thornton-Pett, M.; Hursthouse, M. B. Synthesis and properties of the divalent 1, 2-bis (dimethylphosphino) ethane (dmpe) complexes MCl 2 (dmpe) 2 and MMe 2 (dmpe) 2 (M= Ti, V, Cr, Mn, or Fe). X-Ray crystal structures of MCl 2 (dmpe) 2 (M= Ti, V, or Cr), MnBr 2 (dmpe) 2, TiMe 1.3 Cl 0.7 (dmpe) 2, and CrMe 2 (dmpe) 2. *Journal of the Chemical Society, Dalton Transactions* **1985**, 1339–1348.

(2) Broderick, W. E.; Pressprich, M. R.; Geiser, U.; Willett, R. D.; Legg, J. I. Characterization of an air-stable chromium (II) dinicotinate complex: trans-[Cr (II)(nic-N) 2 (H2O) 4]. *Inorganic Chemistry* **1986**, *25*, 3372–3377.

(3) Deng, Y.-F.; Han, T.; Wang, Z.; Ouyang, Z.; Yin, B.; Zheng, Z.; Krzystek, J.; Zheng, Y.-Z. Uniaxial magnetic anisotropy of square-planar chromium (II) complexes revealed by magnetic and HF-EPR studies. *Chemical communications* **2015**, *51*, 17688–17691.

(4) Ferreira, V.; Krause, R. A.; Larsen, S. Synthesis and structure of cis-dichlorobis (2-phenylazopyridine) chromium (II), an inert chromium (II) compound. *Inorganica chimica acta* **1988**, *145*, 29–38.

(5) Overby, J. S.; Schoell, N. J.; Hanusa, T. P. Synthesis and characterization of chromocenes containing bulky cyclopentadienyl ligands. *Journal of organometallic chemistry* **1998**, *560*, 15–19.

(6) Frazier, B. A.; Wolczanski, P. T.; Lobkovsky, E. B. Aryl-Containing Chelates and Amine Debenzylation to Afford 1, 3-Di-2-pyridyl-2-azaallyl (smif): Structures of {κ-C, N, Npy2-(2-pyridylmethyl) 2N (CH2 (4-tBu-phenyl-2-yl))} FeBr and (smif) CrN (TMS) 2. *Inorganic Chemistry* **2009**, *48*, 11576–11585.

(7) Jubb, J.; Larkworthy, L. F.; Leonard, G. A.; Povey, D. C.; Tucker, B. J. Stacked planar molecules in antiferromagnetic di-isothiocyanato-bis (thiourea) chromium (II), a new structural type for chromium (II). *Journal of the Chemical Society, Dalton Transactions* **1989**, 1631–1633.

(8) Desai, V.; König, E.; Kanellakopulos, B. Magnetic susceptibility and electron paramagnetic resonance of chromocene and 1, 1'-dimethyl-chromocene: Evidence for the dynamic Jahn–Teller effect. *The Journal of Chemical Physics* **1983**, *78*, 6299–6306.

(9) Zhai, Y.-Q.; Ge, N.; Li, Z.-H.; Chen, W.-P.; Han, T.; Ouyang, Z.-W.; Wang, Z.; Zheng, Y.-Z. Magnetic Anisotropy: Structural Correlation of a Series of Chromium (II)–Amidinate Complexes. *Inorganic Chemistry* **2021**, *60*, 1344–1351.

(10) Konarev, D. V.; Khasanov, S. S.; Kuzmin, A. V.; Shestakov, A. F.; Otsuka, A.; Yamochi, H.; Saito, G.; Lyubovskaya, R. N. cis-Conformation of indigo in the coordination complex (indigo-O, O)(Cp* Cr II Cl). *Dalton Transactions* **2016**, *45*, 17095–17099.

(11) Paolucci, G.; Ossola, F.; Bettinelli, M.; Sessoli, R.; Benetollo, F.; Bombieri, G. Bent Metallocenes Containing Ancillary Ligands in Ring-Bridging Chains. Synthesis, Spectroscopy, and X-ray Crystal Structure of [2, 6-Bis (methylenecyclopentadienyl) pyridine] chromium (II). *Organometallics* **1994**, *13*, 1746–1750.

(12) Boynton, J. N.; Merrill, W. A.; Reiff, W. M.; Fettinger, J. C.; Power, P. P. Two-Coordinate, Quasi-Two-Coordinate, and Distorted Three Coordinate, T-Shaped Chromium (II) Amido Complexes: Unusual Effects of Coordination Geometry on the Lowering of Ground State Magnetic Moments. *Inorganic Chemistry* **2012**, *51*, 3212–3219.

(13) Luo, Q.-C.; Ge, N.; Zhai, Y.-Q.; Wang, T.-B.; Sun, L.; Sun, Q.; Li, F.; Ouyang, Z.; Wang, Z.-X.; Zheng, Y.-Z. AC, S bonded quasi-two-coordinate chromium (ii) complex

showing field-induced slow magnetic relaxation behaviour. *Dalton Transactions* **2022**, *51*, 9218–9222.

(14) Jubb, J.; Larkworthy, L. F.; Oliver, L. F.; Povey, D. C.; Smith, G. W. Chromium (II) complexes of o-phenylenediamine. The crystal and molecular structures of bis (o-phenylenediamine-κ N)-bis (thiocyanato-κ N) chromium (II) and bis (o-phenylenediamine-κ 2 N, N') bis (o-phenylenediamine-κ N) chromium (II) trifluoromethanesulphonate. *Journal of the Chemical Society, Dalton Transactions* **1991**, 2045–2050.

(15) Schiwek, C. H.; Vasilenko, V.; Wadepohl, H.; Gade, L. H. The open d-shell enforces the active space in 3d metal catalysis: highly enantioselective chromium (ii) pincer catalysed hydrosilylation of ketones. *Chemical communications* **2018**, *54*, 9139–9142.

(16) Halepoto, D. M.; Holt, D. G.; Larkworthy, L. F.; Leigh, G. J.; Povey, D. C.; Smith, G. W. Spin crossover in chromium (II) complexes and the crystal and molecular structure of the high spin form of bis [1, 2-bis (diethylphosphino) ethane] diiodochromium (II). *Journal of the Chemical Society, Chemical Communications* **1989**, 1322–1323.

(17) O'Hare, D.; Murphy, V. J.; Kaltsoyannis, N. Synthesis and characterisation of permethylindenyl complexes of cobalt and chromium: crystal structures of [Cr (η 5-C 9 Me 7) 2],[Co (η 5-C 9 Me 7) 2][PF 6] and [Cr (η 5-C 9 Me 7) 2][PF 6]. *Journal of the Chemical Society, Dalton Transactions* **1993**, 383–392.

(18) Adams, R. D.; Miao, S.; Smith, M. D.; Farach, H.; Webster, C. E.; Manson, J.; Hall, M. B. Nickel- Manganese Sulfido Carbonyl Cluster Complexes. Synthesis, Structure, and Properties of the Unusual Paramagnetic Complexes Cp2Ni2Mn (CO) 3 (μ3-E) 2, E= S, Se. *Inorganic chemistry* **2004**, *43*, 2515–2525.

(19) Wu, J.-Z.; Bouwman, E.; Mills, A. M.; Spek, A. L.; Reedijk, J. Manganese (II) com-

plexes of a set of 2-aminomethylpyridine-derived ligands bearing a methoxyalkyl arm: syntheses, structures and magnetism. *Inorganica chimica acta* **2004**, *357*, 2694–2702.

(20) Lumme, P.; Mutikainen, I.; Lindell, E. x-ray Structure of Trans-tetrakis (pyrazole) bisisothiocyanatomanganese (II) and its Magnetic, Spectral and Thermal Properties. *Inorganica Chimica Acta* **1983**, *71*, 217–226.

(21) Walter, M. D.; Sofield, C. D.; Booth, C. H.; Andersen, R. A. Spin equilibria in monomeric manganocenes: solid-state magnetic and EXAFS studies. *Organometallics* **2009**, *28*, 2005–2019.

(22) Mueller, G.; Neugebauer, D.; Geike, W.; Koehler, F. H.; Pebler, J.; Schmidbaur, H. Bis [boranatobis (dimethylphosphoniumylidenemethylide)] complexes of manganese (II) and cobalt (II): stable, homoleptic tetraalkyls of paramagnetic transition-metal centers. *Organometallics* **1983**, *2*, 257–263.

(23) Howard, C. G.; Girolami, G. S.; Wilkinson, G.; Thornton-Pett, M.; Hursthouse, M. B. Tertiary phosphine adducts of manganese (II) dialkyls. Part 2. Synthesis, properties, and structures of monomeric complexes. *Journal of the Chemical Society, Dalton Transactions* **1983**, 2631–2637.

(24) Małecki, J.; Machura, B.; Świtlicka, A.; Groń, T.; Bałanda, M. Thiocyanate manganese (II) complexes with pyridine and its derivatives ligands. *Polyhedron* **2011**, *30*, 746–753.

(25) Hong, D.-M.; Wei, H.-H.; Chang, K.-H.; Lee, G.-H.; Wang, Y. Synthesis, crystal structure and magnetic properties of bis (1, 1, 1, 5, 5, 5-hexafluoropentane-2, 4-dionato) manganese (II) complexes with diazine ligands. *Polyhedron* **1998**, *17*, 3565–3573.

(26) Hubin, T. J.; McCormick, J. M.; Collinson, S. R.; Buchalova, M.; Perkins, C. M.; Alcock, N. W.; Kahol, P. K.; Raghunathan, A.; Busch, D. H. New iron (II) and

manganese (II) complexes of two ultra-rigid, cross-bridged tetraazamacrocycles for catalysis and biomimicry. *Journal of the American Chemical Society* **2000**, *122*, 2512–2522.

(27) Shen, L. Synthesis, crystal structure and magnetic property of a novel sheet-like polymer [Mn (bpd)(NCS) 2 (CH3OH) 2] n (bpd= 1, 4-bis (4-pyridyl)-2, 3-diaza-1, 3-butadiene). *Inorganic Chemistry Communications* **2003**, *6*, 1133–1136.

(28) Janczak, J.; Kubiak, R.; Śledź, M.; Borrmann, H.; Grin, Y. Synthesis, structural investigations and magnetic properties of dipyridinated manganese phthalocyanine, MnPc (py) 2. *Polyhedron* **2003**, *22*, 2689–2697.

(29) Yu, M.; Ward, M. B.; Franke, A.; Ambrose, S. L.; Whaley, Z. L.; Bradford, T. M.; Gorden, J. D.; Beyers, R. J.; Cattley, R. C.; Ivanovic-Burmazovic, I.; others Adding a second quinol to a redox-responsive MRI contrast agent improves its relaxivity response to H2O2. *Inorganic Chemistry* **2017**, *56*, 2812–2826.

(30) Deguenon, D.; Bernardinelli, G.; Tuchagues, J. P.; Castan, P. Molecular crystal structure and magnetic properties of (croconato)-and (oxalato) manganese (II) complexes. *Inorganic Chemistry* **1990**, *29*, 3031–3037.

(31) Figgis, B. N.; Kucharski, E. S.; Williams, G. A. Manganese 3 d and 4 s electron-density distribution in phthalocyaninatomanganese (II). *Journal of the Chemical Society, Dalton Transactions* **1980**, 1515–1525.

(32) Price, J. S.; Chadha, P.; Emslie, D. J. Base-free and bisphosphine ligand dialkylmanganese (II) complexes as precursors for manganese metal deposition. *Organometallics* **2016**, *35*, 168–180.

(33) Bellabarba, R. M.; Clancy, G. P.; Gomes, P. T.; Martins, A. M.; Rees, L. H.; Green, M. L. Synthesis of metallocenes of zirconium, hafnium, manganese, iron, tin,

lead and half-sandwich complexes of rhodium and iridium containing the ligands (η-C5R4CR' 2PMe2), where R and R' may be H or Me. *Journal of organometallic chemistry* **2001**, *640*, 93–112.

(34) Yu, L.; Shi, J.-M.; Zhang, Y.-Q.; Wang, Y.-Q.; Fan, Y.-N.; Zhang, G.-Q.; Shi, W.; Cheng, P. π–π Stacking and magnetic coupling mechanism on a mono-nuclear Mn (II) complex. *Journal of molecular structure* **2011**, *987*, 138–143.

(35) Uzelac, M.; Mastropierro, P.; de Tullio, M.; Borilovic, I.; Tarrés, M.; Kennedy, A. R.; Aromí, G.; Hevia, E. Tandem Mn–I exchange and homocoupling processes mediated by a synergistically operative lithium manganate. *Angewandte Chemie International Edition* **2021**, *60*, 3247–3253.

(36) MacáRory, P. P.; others Preparation, properties, and reactions with sulphur dioxide of triphenylphosphine oxide complexes of manganese (II) thiocyanate. Crystal structures of [{Mn (OPPh 3) 2 (NCS)(Á-NCS)} 2],[Mn (OPPh 3) 4 (NCS) 2], and (PPh 3 O)(PPh 3 OH)(HSO 4), a derivative of sulphuric acid formed under ambient air oxidation of sulphur dioxide. *Journal of the Chemical Society, Dalton Transactions* **1990**, 1243–1250.

(37) Karasawa, S.; Sano, Y.; Akita, T.; Koga, N.; Itoh, T.; Iwamura, H.; Rabu, P.; Drillon, M. Photochemical formation of ferrimagnetic chains from a pair of polymeric complexes made of octahedral bis (hexafluoroacetylacetonato) manganese (II) with diazodi (4-pyridyl) methane in the cis and trans configurations as repeating units. *Journal of the American Chemical Society* **1998**, *120*, 10080–10087.

(38) Beghidja, C.; Wesolek, M.; Welter, R. New manganese complexes with 2-salicyloylhydrazono-1, 3-dithiolane ligand and various coordination solvents. *Inorganica chimica acta* **2005**, *358*, 3881–3888.

(39) Ricciardi, G.; Bencini, A.; Bavoso, A.; Rosa, A.; Lelj, F. Crystal structure of high-spin

(S= 5/2) manganese (II) 2, 3, 7, 8, 12, 13, 17, 18-octakis (ethylsulfanyl)-5, 10, 15, 20-tetraazaporphyrinate. *Journal of the Chemical Society, Dalton Transactions* **1996**, 3243–3249.

(40) El-Azzouzi, N.; Hueso-Ureña, F.; Illán-Cabeza, N. A.; Moreno-Carretero, M. N. XRD structure of two heptacoordinated Mn (II) complexes containing 2, 9-dimethyl-1, 10-phenanthroline (phen), nitrato and nicotinato bidentate anions:[Mn (phen)(nicot)(NO3)(H2O)]· EtOH· H2O and [Mn (phen)(NO3) 2 (H2O)]. *Polyhedron* **2010**, *29*, 1405–1410.

(41) Shen, H.-Y.; Liao, D.-Z.; Jiang, Z.-H.; Yan, S.-P.; Sun, B.-W.; Wang, G.-L.; Yao, X.-K.; Wang, H.-G. A new one-dimensional 4, 4'-bipy-bridged compound [Mn (hfac) 2 (4, 4'-bipy)] n (hfac= hexafluoroacetetylacetonato; 4, 4'-bipy= 4, 4'-bipyridine). Synthesis, crystal structure and magnetic properties. *Polyhedron* **1998**, *17*, 1953–1957.

(42) Hays, M. L.; Burkey, D. J.; Overby, J. S.; Hanusa, T. P.; Sellers, S. P.; Yee, G. T.; Young, V. G. Steric influence on the structure, magnetic properties, and reactivity of hexa-and octaisopropylmanganocene. *Organometallics* **1998**, *17*, 5521–5527.

(43) King, E. R.; Betley, T. A. Unusual electronic structure of first row transition metal complexes featuring redox-active dipyrromethane ligands. *Journal of the American Chemical Society* **2009**, *131*, 14374–14380.

(44) Baldwin, M. J.; Kampf, J. W.; Kirk, M. L.; Pecoraro, V. L. Structural and magnetic Studies of Manganese (II) Complexes of the Imidazole-Containing Ligand 5-NO2-salimH [5-NO2-salimH2= 4-(2-((5-nitrosalicylidene) amino) ethyl) imidazole] with Varying Nuclearity. *Inorganic Chemistry* **1995**, *34*, 5252–5260.

(45) Phillippi, M. A.; Baenziger, N.; Goff, H. M. Preparation, solution properties, and structure of iron (III) porphyrin oxyanion complexes. Crystal and molecular stereo-

chemistry of a novel bidentate nitrato complex. *Inorganic Chemistry* **1981**, *20*, 3904–3911.

(46) Berry, K. J.; Clark, P. E.; Murray, K. S.; Raston, C. L.; White, A. H. Structure, magnetism, and Moessbauer spectrum of the five-coordinate complex chlorobis (N-methylbenzothiohydroxamato) iron (III). *Inorganic Chemistry* **1983**, *22*, 3928–3934.

(47) Glockner, A.; Bannenberg, T.; Ibrom, K.; Daniliuc, C. G.; Freytag, M.; Jones, P. G.; Walter, M. D.; Tamm, M. Flexibility of an Open Indenyl Ligand in Iron (II) Complexes. *Organometallics* **2012**, *31*, 4480–4494.

(48) Yahsi, Y.; Kara, H.; Sorace, L.; Buyukgungor, O. Mono-and dinuclear Fe (III) complexes with the N2O2 donor 5-chlorosalicylideneimine ligands; synthesis, X-ray structural characterization and magnetic properties. *Inorganica Chimica Acta* **2011**, *366*, 191–197.

(49) Martins, N. M.; Mahmudov, K. T.; da Silva, M. F. C. G.; Martins, L. M.; Pombeiro, A. J. Copper (II) and iron (III) complexes with arylhydrazone of ethyl 2-cyanoacetate or formazan ligands as catalysts for oxidation of alcohols. *New Journal of Chemistry* **2016**, *40*, 10071–10083.

(50) Diaz-Acosta, I.; Baker, J.; Cordes, W.; Pulay, P. Calculated and experimental geometries and infrared spectra of metal tris-acetylacetonates: vibrational spectroscopy as a probe of molecular structure for ionic complexes. Part I. *The journal of physical chemistry a* **2001**, *105*, 238–244.

(51) Masárová, P.; Zoufalỳ, P.; Moncol, J.; Nemec, I.; Pavlik, J.; Gembickỳ, M.; Trávníček, Z.; Boča, R.; Šalitroš, I. Spin crossover and high spin electroneutral mononuclear iron (III) Schiff base complexes involving terminal pseudohalido ligands. *New Journal of Chemistry* **2015**, *39*, 508–519.

(52) Abdol Abadi, B. E.; Palmer, R. A.; Fitzsimmons, B. W. Crystal structure of form 1, magnetic properties and polymorphism of bis (NN-di-(n-propyl) dithiocarbamato iron (III) iodide. *Journal of crystallographic and spectroscopic research* **1988**, *18*, 35–53.

(53) Grande, L. M.; Noll, B. C.; Oliver, A. G.; Scheidt, W. R. Dynamics of NO motion in solid-state [Co (tetraphenylporphinato)(NO)]. *Inorganic chemistry* **2010**, *49*, 6552–6557.

(54) Shedbalkar, V.; Dugad, L.; Mazumdar, S.; Mitra, S. Electronic structure of synthetic iron (III) porphyrins in pyridine and pyridinewater solutions: A proton magnetic resonance study. *Inorganica chimica acta* **1988**, *148*, 17–20.

(55) Dunbar, K. R.; Haefner, S. C.; Quillevéré, A. Synthesis and characterization of [{2, 4, 6-(CH3O) 3C6H2} 3P O] FeCl3: A four-coordinate phosphine oxide adduct of FeCl3. *Polyhedron* **1990**, *9*, 1695–1702.

(56) Harriman, K. L.; Leitch, A. A.; Stoian, S. A.; Habib, F.; Kneebone, J. L.; Gorelsky, S. I.; Korobkov, I.; Desgreniers, S.; Neidig, M. L.; Hill, S.; others Ambivalent binding between a radical-based pincer ligand and iron. *Dalton Transactions* **2015**, *44*, 10516–10523.

(57) Kooijman, H.; Spek, A. L.; Hoogenraad, M.; Bouwman, E.; Haasnoot, J. G.; Reedijk, J. Tris [2-(2-oxazolin-2-yl) phenolato] iron (III). *Acta Crystallographica Section C: Crystal Structure Communications* **2002**, *58*, m390–m392.

(58) Masuda, H.; Taga, T.; Osaki, K.; Sugimoto, H.; Yoshida, Z.; Ogoshi, H. Crystal and molecular structure of (octaethylporphinato) iron (III) perchlorate. Anomalous magnetic properties and structural aspects. *Inorganic Chemistry* **1980**, *19*, 950–955.

(59) Palamarciuc, O. V.; Bourosh, P. N.; Revenco, M. D.; Lipkowski, J.; Simonov, Y. A.; Clérac, R. Synthesis, crystal structure and characterizations of iron (III) and copper

(II) complexes with the hydrazone ligand obtained from 2-formyl-pyridine and Girard's T reagent. *Inorganica Chimica Acta* **2010**, *363*, 2561–2566.

(60) Huxel, T.; Leone, S.; Lan, Y.; Demeshko, S.; Klingele, J. 2-Amino-4-(2-pyridyl) thiazole as Chelating Ligand: A Dinuclear Oxido-Bridged Ferric Complex and Mononuclear 3d Metal Complexes. *European Journal of Inorganic Chemistry* **2014**, *2014*, 3114–3124.

(61) Pascualini, M. E.; Di Russo, N. V.; Quintero, P. A.; Thuijs, A. E.; Pinkowicz, D.; Abboud, K. A.; Dunbar, K. R.; Christou, G.; Meisel, M. W.; Veige, A. S. Synthesis, Characterization, and Reactivity of Iron (III) Complexes Supported by a Trianionic ONO3–Pincer Ligand. *Inorganic Chemistry* **2014**, *53*, 13078–13088.

(62) Walker, J. D.; Poli, R. Trichloroiron (FeCl3)-phosphine adducts with trigonal-bipyramidal geometry. Influence of the phosphine on the spin state. *Inorganic Chemistry* **1989**, *28*, 1793–1801.

(63) Kopf, M.-A.; Varech, D.; Tuchagues, J.-P.; Mansuy, D.; Artaud, I. New intermediate-spin chloroiron (III) complex with a mixed nitrogen–sulfur co-ordination sphere. *Journal of the Chemical Society, Dalton Transactions* **1998**, 991–998.

(64) Slep, L. D.; Calvo, R.; Nascimento, O. R.; Baggio, R.; Garland, M. T.; Peña, O.; Perec, M. A seven-coordinate FeIII compound:[Fe {O (CH2CO2) 2}(H2O) 2 (NO3)]. Preparation, structure and magnetic properties. *Inorganica chimica acta* **2007**, *360*, 2911–2916.

(65) Ricciardi, G.; Bavoso, A.; Bencini, A.; Rosa, A.; Lelj, F.; Bonosi, F. Synthesis, structure, magnetic, spectroscopic and electrochemical behaviour of chloro-iron (III) andmanganese (III) complexes of 2, 3, 7, 8, 12, 13, 17, 18-octakis (ethylsulfanyl)-5, 10, 15, 20-tetraazaporphyrin. *Journal of the Chemical Society, Dalton Transactions* **1996**, 2799–2807.

(66) Butsch, K.; Haseloer, A.; Schmitz, S.; Ott, I.; Schur, J.; Klein, A. FeIII, CuII and ZnII complexes of the rigid 9-oxido-phenalenone ligand—Spectroscopy, electrochemistry, and cytotoxic properties. *International journal of molecular sciences* **2021**, *22*, 3976.

(67) Rajnák, C.; Mičová, R.; Moncol', J.; Dlháň, L.; Krüger, C.; Renz, F.; Boča, R. Spin-crossover in an iron (iii) complex showing a broad thermal hysteresis. *Dalton Transactions* **2021**, *50*, 472–475.

(68) Šalitroš, I.; Boča, R.; Dlháň, L.; Gembickỳ, M.; Kožíšek, J.; Linares, J.; Moncol', J.; Nemec, I.; Perašínová, L.; Renz, F.; others Unconventional spin crossover in dinuclear and trinuclear iron (III) complexes with cyanido and metallacyanido bridges. 2009.

(69) Sarwar, M.; Madalan, A. M.; Lloret, F.; Julve, M.; Andruh, M. Mononuclear Fe (III) and tetranuclear [Fe (III) Gd (III)] 2 complexes with a Schiff-base ligand derived from the o-vanillin: Synthesis, crystal structures and magnetic properties. *Polyhedron* **2011**, *30*, 2414–2420.

(70) Mikuriya, M.; Kushida, K.; Nakayama, H.; Mori, W.; Kishita, M. A unique mononuclear iron (III) complex with the binucleating ligand 2, 6-bis [N-(2-pyridylethyl) iminomethyl]-4-methylphenol. *Inorganica chimica acta* **1989**, *165*, 35–36.

(71) Cotton, F. A.; Luck, R. L.; Son, K.-A. New polynuclear compounds of iron (II) chloride with oxygen donor ligands Part I. Fe4Cl8 (THF) 6: Synthesis and a single crystal X-ray structure determination. *Inorganica chimica acta* **1991**, *179*, 11–15.

(72) Tyagi, N.; Chakraborty, A.; Singh, U. P.; Roy, P.; Ghosh, K. Mononuclear iron (III) complexes of tridentate ligands with efficient nuclease activity and studies of their cytotoxicity. *Organic & Biomolecular Chemistry* **2015**, *13*, 11445–11458.

(73) Oliver, J.; Mullica, D.; Hutchinson, B.; Milligan, W. Iron-nitrogen bond lengths in low-spin and high-spin iron (II) complexes with poly (pyrazolyl) borate ligands. *Inorganic Chemistry* **1980**, *19*, 165–169.

(74) Marchivie, M.; Guionneau, P.; Howard, J. A.; Chastanet, G.; Létard, J.-F.; Goeta, A. E.; Chasseau, D. Structural characterization of a photoinduced molecular switch. *Journal of the American Chemical Society* **2002**, *124*, 194–195.

(75) Campbell, C. J.; Muetterties, A. T.; Chan, B. C.; Reisner, B. A. New polymorphs of hydrotris (1, 2, 4-triazolyl) borate complexes with M2+ cations (M= Fe, Co, Ni, Zn). *Inorganica Chimica Acta* **2018**, *473*, 275–281.

(76) Thompson, A. L.; Goeta, A. E.; Real, J. A.; Galet, A.; Muñoz, M. C. Thermal and light induced polymorphism in iron (II) spin crossover compounds. *Chemical communications* **2004**, 1390–1391.

(77) Li, B.; Wei, R.-J.; Tao, J.; Huang, R.-B.; Zheng, L.-S. Pressure effects on a spin-crossover monomeric compound [Fe (pmea)(SCN) 2](pmea= bis [(2-pyridyl) methyl]-2-(2-pyridyl) ethylamine). *Inorganic chemistry* **2010**, *49*, 745–751.

(78) Long, G. J.; Galeazzi, G.; Russo, U.; Valle, G.; Calogero, S. A Moessbauer, magnetic, and single-crystal x-ray structural study of trans-bis (4-acetylpyridine) diaquabis (isothiocyanato) iron (II). *Inorganic Chemistry* **1983**, *22*, 507–510.

(79) Taylor, R. A.; Lough, A. J.; Seda, T.; Poddutoori, P. K.; Lemaire, M. T. Di-and trivalent iron complexes with redox-active 1-(2-pyridylazo)-2-phenanthrol (papl). *Polyhedron* **2017**, *123*, 462–469.

(80) Das, O.; Chatterjee, S.; Paine, T. K. Functional models of α-keto acid dependent non-heme iron oxygenases: synthesis and reactivity of biomimetic iron (II) benzoylformate complexes supported by a 2, 9-dimethyl-1, 10-phenanthroline ligand. *JBIC Journal of Biological Inorganic Chemistry* **2013**, *18*, 401–410.

(81) Strauss, S. H.; Silver, M. E.; Long, K. M.; Thompson, R. G.; Hudgens, R. A.; Spartalian, K.; Ibers, J. A. Comparison of the molecular and electronic structures of (2,

3, 7, 8, 12, 13, 17, 18-octaethylporphyrinato) iron (II) and (trans-7, 8-dihydro-2, 3, 7, 8, 12, 13, 17, 18-octaethylporphyrinato) iron (II). *Journal of the American Chemical Society* **1985**, *107*, 4207–4215.

(82) Lin, C.-Y.; Guo, J.-D.; Fettinger, J. C.; Nagase, S.; Grandjean, F.; Long, G. J.; Chilton, N. F.; Power, P. P. Dispersion force stabilized two-coordinate transition metal–amido complexes of the- N (SiMe3) Dipp (Dipp= C6H3-2, 6-Pri2) ligand: Structural, spectroscopic, magnetic, and computational studies. *Inorganic Chemistry* **2013**, *52*, 13584–13593.

(83) Konarev, D. V.; Ishikawa, M.; Khasanov, S. S.; Otsuka, A.; Yamochi, H.; Saito, G.; Lyubovskaya, R. N. Synthesis, Structural and Magnetic Properties of Ternary Complexes of (Me4P+)·{[Fe (I) Pc (- 2)]-}· Triptycene and (Me4P+)·{[Fe (I) Pc (- 2)]-}·(N, N, N', N'-Tetrabenzyl-p-phenylenediamine) 0.5 with Iron (I) Phthalocyanine Anions. *Inorganic Chemistry* **2013**, *52*, 3851–3859.

(84) Nachtigallová, D.; Antalík, A.; Lo, R.; Sedlák, R.; Manna, D.; Tuček, J.; Ugolotti, J.; Veis, L.; Legeza, Ö.; Pittner, J.; others An Isolated Molecule of Iron (II) Phthalocyanin Exhibits Quintet Ground-State: A Nexus between Theory and Experiment. *Chemistry–A European Journal* **2018**, *24*, 13413–13417.

(85) Liu, Y.-Z.; Wang, J.; Zhao, Y.; Chen, L.; Chen, X.-T.; Xue, Z.-L. Four-coordinate Co (ii) and Fe (ii) complexes with bis (N-heterocyclic carbene) borate and their magnetic properties. *Dalton Transactions* **2015**, *44*, 908–911.

(86) Cook, B. J.; Polezhaev, A. V.; Chen, C.-H.; Pink, M.; Caulton, K. G. Deprotonation, Chloride Abstraction, and Dehydrohalogenation as Synthetic Routes to Bis-Pyrazolate Pyridyl Iron (II) Complexes. *European Journal of Inorganic Chemistry* **2017**, *2017*, 3999–4012.

(87) Sheu, C.-F.; Pillet, S.; Lin, Y.-C.; Chen, S.-M.; Hsu, I.-J.; Lecomte, C.; Wang, Y.

Magnetostructural relationship in the spin-crossover complex t-{Fe (abpt) 2 [N (CN) 2] 2}: Polymorphism and disorder phenomenon. *Inorganic chemistry* **2008**, *47*, 10866–10874.

(88) Supej, M. J.; Volkov, A.; Darko, L.; West, R. A.; Darmon, J. M.; Schulz, C. E.; Wheeler, K. A.; Hoyt, H. M. Aryl-substituted BIAN complexes of iron dibromide: Synthesis, X-ray and electronic structure, and catalytic hydrosilylation activity. *Polyhedron* **2016**, *114*, 403–414.

(89) Ott, J. C.; Wadepohl, H.; Enders, M.; Gade, L. H. Taking solution proton NMR to its extreme: prediction and detection of a hydride resonance in an intermediate-spin iron complex. *Journal of the American Chemical Society* **2018**, *140*, 17413–17417.

(90) Sheu, C.-F.; Shih, C.-H.; Sugimoto, K.; Cheng, B.-M.; Takata, M.; Wang, Y. A long-lived photo-induced metastable state of linkage isomerization accompanied with a spin transition. *Chemical communications* **2012**, *48*, 5715–5717.

(91) Weber, B.; Jäger, E.-G. Magnetic Ordering in Iron (II) Complexes due to a 2D Network of Hydrogen Bonds. *Zeitschrift für anorganische und allgemeine Chemie* **2009**, *635*, 130–133.

(92) Irwin, M.; Jenkins, R. K.; Denning, M. S.; Kramer, T.; Grandjean, F.; Long, G. J.; Herchel, R.; McGrady, J. E.; Goicoechea, J. M. Experimental and computational study of the structural and electronic properties of FeII (2, 2'-bipyridine)(mes) 2 and [FeII (2, 2'-bipyridine)(mes) 2]-, a complex containing a 2, 2'-bipyridyl radical anion. *Inorganic chemistry* **2010**, *49*, 6160–6171.

(93) Lin, P.-H.; Smythe, N. C.; Gorelsky, S. I.; Maguire, S.; Henson, N. J.; Korobkov, I.; Scott, B. L.; Gordon, J. C.; Baker, R. T.; Murugesu, M. Importance of out-of-state spin–orbit coupling for slow magnetic relaxation in mononuclear FeII complexes. *Journal of the American Chemical Society* **2011**, *133*, 15806–15809.

(94) Dub, P. A.; Scott, B. L.; Gordon, J. C. First-row transition metal complexes of ENENES ligands: the ability of the thioether donor to impact the coordination chemistry. *Dalton Transactions* **2016**, *45*, 1560–1571.

(95) Musgrave, R. A.; Turbervill, R. S.; Irwin, M.; Herchel, R.; Goicoechea, J. M. Iron (II) complexes of ditopic carbanionic carbenes. *Dalton Transactions* **2014**, *43*, 4335–4344.

(96) Leung, W.-P.; Lee, H. K.; Weng, L.-H.; Luo, B.-S.; Zhou, Z.-Y.; Mak, T. C. Synthesis and Structures of Iron (II) Alkyl and Thiolate Compounds Containing Sterically Hindered N-Functionalized Alkyl Ligands. *Organometallics* **1996**, *15*, 1785–1792.

(97) Yang, F.; Zhou, Q.; Zhang, Y.; Zeng, G.; Li, G.; Shi, Z.; Wang, B.; Feng, S. Inspiration from old molecules: field-induced slow magnetic relaxation in three air-stable tetrahedral cobalt (II) compounds. *Chemical communications* **2013**, *49*, 5289–5291.

(98) Titiš, J.; Miklovič, J.; Boča, R. Magnetostructural study of tetracoordinate cobalt (II) complexes. *Inorganic Chemistry Communications* **2013**, *35*, 72–75.

(99) Shapiro, I. R.; Jenkins, D. M.; Thomas, J. C.; Day, M. W.; Peters, J. C. A homoleptic phosphine adduct of Tl (i) Electronic supplementary information (ESI) available: 31P and 205Tl NMR spectra of [PhBP3] Tl in C6D6. See http://www. rsc. org/suppdata/cc/b1/b104447h. *Chemical Communications* **2001**, 2152–2153.

(100) Mondal, A. K.; Sundararajan, M.; Konar, S. A new series of tetrahedral Co (ii) complexes [CoLX 2](X= NCS, Cl, Br, I) manifesting single-ion magnet features. *Dalton Transactions* **2018**, *47*, 3745–3754.

(101) Habib, F.; Luca, O. R.; Vieru, V.; Shiddiq, M.; Korobkov, I.; Gorelsky, S. I.; Takase, M. K.; Chibotaru, L. F.; Hill, S.; Crabtree, R. H.; others Influence of the ligand field on slow magnetization relaxation versus spin crossover in mononuclear cobalt complexes. *Angewandte Chemie International Edition* **2013**, *52*, 11290–11293.

(102) Li, J.-X.; Du, Z.-X.; Wang, L.-Z.; Huang, W.-P. Cobalt and cadmium complexes with N-heterocyclic dicarboxylic acid ligands: syntheses, structures, magnetic and fluorescent properties. *Inorganica Chimica Acta* **2011**, *376*, 479–485.

(103) Idešicová, M.; Dlháň, L.; Moncol', J.; Titiš, J.; Boča, R. Zero-field splitting in tetracoordinate Co (II) complexes. *Polyhedron* **2012**, *36*, 79–84.

(104) Titiš, J.; Hudák, J.; Kožíšek, J.; Krutošíková, A.; Moncol, J.; Tarabová, D.; Boča, R. Structural, spectral and magnetic properties of carboxylato cobalt (II) complexes with heterocyclic N-donor ligands: Reconstruction of magnetic parameters from electronic spectra. *Inorganica Chimica Acta* **2012**, *388*, 106–113.

(105) Lee, H.; Mak, T. W.; others Synthesis and structural characterisation of mono-and bi-nuclear cobalt (II) alkyls. *Journal of the Chemical Society, Dalton Transactions* **1997**, 779–784.

(106) Sokolov, F. D.; Zabirov, N. G.; Yamalieva, L. N.; Shtyrlin, V. G.; Garipov, R. R.; Brusko, V. V.; Verat, A. Y.; Baranov, S. V.; Mlynarz, P.; Glowiak, T.; others Coordination diversity of N-phosphoryl-N'-phenylthiourea (LH) towards CoII, NiII and PdII cations: Crystal structure of ML2-N, S and ML2-O, S chelates. *Inorganica chimica acta* **2006**, *359*, 2087–2096.

(107) Safin, D. A.; Mlynarz, P.; Hahn, F. E.; Babashkina, M. G.; Sokolov, F. D.; Zabirov, N. G.; Galezowska, J.; Kozlowski, H. Cobalt (II) Complexes with N-Thioacylamidophosphates and 2, 2'-Bipyridyl and 1, 10-Phenathroline. Crystal Structures, Solution 1H NMR Spectral and Magnetic Properties. *Zeitschrift für anorganische und allgemeine Chemie* **2007**, *633*, 1472–1479.

(108) Khrizanforova, V. V.; Fayzullin, R. R.; Bogomyakov, A. S.; Morozov, V. I.; Batulin, R. G.; Gerasimova, T. P.; Islamov, D. R.; Budnikova, Y. H. Cobalt (ii) coordi-

nation to an N 4-acenaphthene-based ligand and its sodium complex. *Dalton Transactions* **2023**, *52*, 7876–7884.

(109) Krest, A.; Sandleben, A.; Valldor, M.; Werker, M.; Ruschewitz, U.; Klein, A. Heteroleptic Complexes of the Tridentate Pyridine-2, 6-di-tetrazolate Ligand. *ChemistrySelect* **2017**, *2*, 5849–5859.

(110) Stevens, E. D. Electronic structure of metalloporphyrins. 1. Experimental electron density distribution of (meso-tetraphenylporphinato) cobalt (II). *Journal of the American Chemical Society* **1981**, *103*, 5087–5095.

(111) Mamardashvili, G.; Kaigorodova, E.; Simonova, O.; Mamardashvili, N. Influence of the macrocycle structure on the ability of Co (II)-porphyrins to oxidize in the presence of organic bases. *Journal of Coordination Chemistry* **2018**, *71*, 4194–4209.

(112) Smith, M. E.; Andersen, R. A. Me5C5Ni (acac): a monomeric, paramagnetic, 18-electron, spin-equilibrium molecule. *Journal of the American Chemical Society* **1996**, *118*, 11119–11128.

(113) Zhu, D.; Janssen, F. F.; Budzelaar, P. H. (Py) 2Co (CH2SiMe3) 2 As an Easily Accessible Source of "CoR2". *Organometallics* **2010**, *29*, 1897–1908.

(114) Żurowska, B.; Brzuszkiewicz, A. Co (II)-promoted transformation of diethyl (quinolin-2-ylmethyl) phosphonate to quinoline-2-carboxylate (2-qca): Synthetic, structural and magnetic studies of [Co (2-qca) 2 (EtOH) 2]. *Polyhedron* **2008**, *27*, 1623–1630.

(115) Legrand, Y.-M.; van der Lee, A.; Masquelez, N.; Rabu, P.; Barboiu, M. Temperature induced single-crystal-to-single-crystal transformations and structure directed effects on magnetic properties. *Inorganic chemistry* **2007**, *46*, 9083–9089.

(116) Kershaw Cook, L. J.; Kulmaczewski, R.; Mohammed, R.; Dudley, S.; Barrett, S. A.; Little, M. A.; Deeth, R. J.; Halcrow, M. A. A unified treatment of the relationship be-

tween ligand substituents and spin state in a family of iron (II) complexes. *Angewandte Chemie* **2016**, *128*, 4399–4403.

(117) Scarborough, C. C.; Sproules, S.; Doonan, C. J.; Hagen, K. S.; Weyhermuller, T.; Wieghardt, K. Scrutinizing low-spin Cr (II) complexes. *Inorganic Chemistry* **2012**, *51*, 6969–6982.

(118) Addison, A. W.; Rao, T. N.; Reedijk, J.; van Rijn, J.; Verschoor, G. C. Synthesis, structure, and spectroscopic properties of copper (II) compounds containing nitrogen–sulphur donor ligands; the crystal and molecular structure of aqua [1, 7-bis (N-methylbenzimidazol-2-yl)-2, 6-dithiaheptane] copper (II) perchlorate. *Journal of the Chemical Society, Dalton Transactions* **1984**, 1349–1356.

(119) Alessandro Bencini, D. G., Cristiano Benelli The angular overlap model for the description of the paramagnetic properties of transition metal complexes. *Coordination Chemistry Reviews* **1984**, *60*, 131–169.

(120) Peng He, M.-Y. H. Y.-J. Z. M.-Y. H., Mu-Han Guan; Zhu, S.-F. Iron-Catalyzed Allylic C(sp3) H Silylation: Spin-CrossoverEfficiency-Determined Chemoselectivity. *Angewandte Chemie* **2024**, *63*.

(121) Yafei Jiang, Q. M.-H. T. X. L. G. C., Xiaotong Zhang; Jia, Z. A theoretical study on oxidative cleavage of olefins to carbonyls catalysed by Fe(III)-PyBisulidine. *Dalton Transactions* **2017**, *46*, 3825–3832.